Test no.	Vertical stress σ'_V (kPa)	Horiz. stress σ'_H (kPa)	Maximum vertical stress σ'_{Vmax} (kPa)	Maximum Horiz. stress σ'_{Hmax} (kPa)	Stress ratio K	$R=\frac{p'_{max}}{p'}$
1. OC	200	200	200	200	1.0	1
2. OCD	450	450	450	450	1.0	1
3. OCDC	200	200	450	450	1.0	2.25
4. OA	273	164	273	200	0.6	1
5. OAB	614	368	614	450	0.6	1
6. OABA	273	164	614	450	0.6	2.25
7. OE	120	240	200	240	2.0	1
8. OEF	270	540	450	540	2.0	1
9. OCDX	80	80	450	450	1.0	5.63

Table 1.1 Nominal test stress states in clay testing programme.

Clay Bed	σ'_V (kPa)	σ'_H (kPa)	u_0 (kPa)	$\sigma'_{V\max}$ (kPa)	$\sigma'_{H\max}$ (kPa)	$R = \frac{p'_{\max}}{p'}$	w_c %	$s_{u\ vane}$ (kN/m²)	P_0 (kPa)	P_1 (kPa)	P_2 (kPa)	P_D (kN)
OC	197	199	2	197	199	1.0	45.4	23.0	343	374	231	1.30
	198	199	3	198	199	1.0	45.5	22.3	332	359	254	1.25
	198	199	4	198	199	1.0	45.6	25.2	359	394	239	1.15
	199	199	5	199	199	1.0	45.3	22.4	340	380	235	1.10
	200	199	6	200	199	1.0	45.3	22.2	314	355	232	1.02
OCD	455	461	6	455	461	1.0	40.6	61.4	691	790	435	-
	455	460	8	455	460	1.0	40.7	62.2	711	833	408	-
	455	460	9	455	460	1.0	40.6	55.2	696	793	443	-
	456	459	10	456	459	1.0	40.6	59.8	729	840	436	-
	457	460	11	457	460	1.0	40.2	57.6	719	816	459	-
OCDC	190	200	2	449	452	2.3	42.3	46.9	493	600	220	2.85
	191	200	3	449	452	2.3	41.7	49.2	545	670	209	3.22
	192	200	4	450	452	2.3	41.8	50.1	539	669	198	3.35
	192	200	5	451	452	2.3	41.7	52.6	534	677	205	3.47
	193	200	6	451	452	2.3	42.0	50.2	512	625	211	3.47

Table 5.1 Summary of dilatometer tests in clay

Clay Bed	σ'_V (kPa)	σ'_H (kPa)	u_0 (kPa)	$\sigma'_{V\max}$ (kPa)	$\sigma'_{H\max}$ (kPa)	$R = \frac{p'_{\max}}{p'}$	w_c %	$s_{u\ vane}$ (kN/m²)	P_0 (kPa)	P_1 (kPa)	P_2 (kPa)	P_D (kN)
OCDX	82	83	3	454	460	5.6	42.9	39.1	292	347	139	1.72
	82	83	4	455	460	5.5	43.3	39.0	290	350	132	1.95
	83	83	5	456	460	5.5	42.4	41.9	309	389	129	2.02
	84	83	6	457	460	5.5	42.8	40.5	305	376	134	2.02
	85	83	7	457	460	5.5	43.0	38.1	315	414	112	2.03
OA	268	158	4	268	219	1.0	44.3	29.5	364	405	241	1.39
	269	157	6	269	219	1.0	44.0	30.1	359	394	246	1.49
	270	157	7	270	219	1.0	43.4	30.4	373	418	254	1.36
	270	157	8	270	219	1.0	43.6	30.0	373	434	230	1.39
	271	157	9	271	219	1.0	43.3	31.4	387	463	214	1.51
OAB	609	379	6	609	451	1.0	36.9	105.0	920	1114	456	3.73
	609	378	7	609	451	1.0	37.6	106.1	880	1094	409	4.76
	609	378	8	609	451	1.0	36.6	108.8	896	1104	431	5.07
	610	378	9	610	451	1.0	36.6	104.8	874	1125	385	5.07
	611	378	10	611	451	1.0	36.4	105.7	969	1149	409	5.53

Table 5.1 continued

Clay Bed	σ'_V (kPa)	σ'_H (kPa)	u_0 (kPa)	$\sigma'_{V\max}$ (kPa)	$\sigma'_{H\max}$ (kPa)	$R = \frac{p'_{\max}}{p'}$	w_c %	$s_{u\ vane}$ (kN/m²)	P_0 (kPa)	P_1 (kPa)	P_2 (kPa)	P_D (kN)
OABA	271	165	3	614	451	2.3	40.0	52.8	477	612	214	2.78
	272	165	4	615	451	2.3	40.5	58.1	560	697	242	3.18
	273	165	5	616	451	2.3	40.6	58.6	493	608	246	2.87
	274	165	6	616	451	2.3	40.5	60.6	517	655	218	3.16
	274	165	7	617	451	2.3	40.8	61.0	599	753	229	3.35
OE	122	243	3	202	243	1.0	44.6	27.2	390	439	240	1.61
	122	243	4	203	243	1.0	44.1	27.6	400	447	268	1.74
	123	243	5	204	243	1.0	43.7	30.4	439	501	266	1.70
	124	243	6	204	243	1.0	43.5	29.9	421	474	279	1.66
	124	243	7	205	243	1.0	43.5	29.6	411	464	266	1.66
OEF	270	538	3	450	538	1.0	39.1	77.4	825	971	433	3.39
	271	538	4	450	538	1.0	38.3	82.2	891	1076	471	4.04
	271	538	5	450	538	1.0	38.0	84.7	912	1077	529	4.34
	272	538	6	451	538	1.0	37.7	83.4	920	1119	525	4.48
	273	538	7	452	538	1.0	37.9	83.9	946	1128	539	4.49

Table 5.1 continued

Parameter	Description	Relationship	Typical Value	Range of Value	Source
ϕ	Friction angle	-	25°	20-25°	Muir Wood (1990)
K_{0nc}	Stress ratio during one-dimensional compression	$K_{0nc} = 1 - \sin\phi$	0.58	0.66-0.58	Muir Wood (1990) after Jaky (1944)
a	Exponent in Eqn 5.13	$1.2 \sin\phi$	0.51	0.41-0.51	Schmidt (1967) & Schmertmann (1985)
m	Exponent in Eqn 5.14	$m = \Lambda = (\lambda - \kappa)/\lambda$	0.8	0.7-0.9	Wroth (1984)
$(s_u/\sigma'_V)_{nc}$	Normalised undrained strength of normally consolidated clay	$(s_u/\sigma'_V)_{nc} = \frac{s(3-2s)}{(3-s)}\left(\frac{(3-s)^2}{8(3-2s)^2} + \frac{1}{2}\right)^{\Lambda}$ where $s = \sin\phi$	0.259	0.206-0.269	Houlsby (1993)
N_D	Dilatometer factor	$N_D = \frac{P_0 - \sigma_H}{s_u}$	5.18	4.05-6.97	Figure 5.10

Table 5.2 Some typical geotechnical properties for clays

Property	Symbol	Value	Source
Liquid limit	LL	69 %	Steenfelt et al (1981)
Plastic limit	PL	38 %	Steenfelt et al (1981)
Plasticity index	PI	31 %	Steenfelt et al (1981)
Specific gravity of solids	G_s	2.61	Steenfelt et al (1981)
Slope in e : $\ln p'$ of consolidation lines	λ	0.187	Al-Tabbaa (1987)
Slope in e : $\ln p'$ of swelling lines	κ	0.028	Al-Tabbaa (1987)
Slope in p' : q of critical state line	M	0.9 (ϕ=23°)	Al-Tabbaa (1987)
Void ratio at p' = 1 kPa			
$q/p'=0$	e_{is}	2.20	Al-Tabbaa (1987)
$q/p'=\frac{3(1-K_0)}{(1+2K_0)}$	e_{1-d}	2.13	"
$q/p'=M$	e_{cs}	2.00	"
$q/p'=0.545$	$e_{K=0.6}$	2.14	Modified Cam-clay
$q/p'=-0.6$	$e_{K=2.0}$	2.10	"
Stress ratio for one-dimensional compression	K_0	0.69	Al-Tabbaa (1987)
Permeability	k	$0.5e^{3.25}\cdot10^{-9}$ m/s	Al-Tabbaa (1987)
Coefficient of consolidation	c_v	0.5 mm²/s	Steenfelt et al (1981)
swelling	c_{vs}	1.0 mm²/s	"
Shear strength (one-dimensional consolidation)	$(s_u/\sigma'_v)_{nc}$	0.21	Steenfelt et al (1981)

Table 3.1 Mechanical and consolidation properties of speswhite kaolin.

Clay bed	Radial. strain ε_r %	Vert. strain ε_z %	Vol. strain ε_v %
OC	2.4	2.9	7.7
OCD	3.5	2.4	9.4
OCDC	3.8	3.4	11.0
OCDX	3.3	2.9	9.5
OA	1.9	5.3	9.1
OAB	1.1	9.7	11.9
OABA	*	2.9	*
OE	7.5	1.9	16.9
OEF	6.6	0.5	13.7

* No measurement taken

Table 3.2 Radial, vertical and volumetric strains for clay beds.

TEST	σ'_V (kPa)	σ'_H (kPa)	σ'_{Vmax} (kPa)	σ'_{Hmax} (kPa)	P_0 (kPa)	P_1 (kPa)	P_D (kN)	R_d %
DENSE SAND								
DMT3	59.5	36.1	61.3	36.5	262	1558	20.4	83
	61.1	37.3	62.9	37.5	314	1587	20.7	83
	62.3	39.5	64.6	39.5	352	1636	20.8	83
DMT2	149.1	80.2	149.1	80.8	669	2406	41.5	83
	151.7	82.5	151.7	82.5	689	2416	44.6	83
	154.3	84.7	154.3	84.7	677	2327	41.8	83
DMT4	62.4	33.8	147.4	78.9	274	1450	17.6	83
	62.6	35.6	149.1	79.9	285	1450	17.9	83
	64.0	38.4	150.8	80.9	334	1499	18.3	83
DMT10	19.2	56.7	20.4	57.1	526	1937	31.1	83
	20.8	57.9	22.1	58.1	470	1957	32.3	83
	22.4	59.5	23.9	59.5	524	1957	32.1	83
DMT12	53.6	135.0	58.4	135.0	1309	3353	63.3	83
	59.9	137.1	60.2	137.1	1380	3392	70.7	83
	65.3	138.0	65.3	138.1	1352	3245	65.8	83
DMT13	20.3	58.0	52.8	126.6	634	2044	36.6	83
	22.5	57.9	54.4	127.6	618	1995	32.8	83
	23.7	59.0	56.2	128.6	616	2015	33.0	83
DMT5	23.5	58.9	146.4	80.4	489	1980	32.8	83
	25.2	63.4	148.1	81.3	512	1970	36.2	83
	27.0	64.9	149.8	82.3	584	2009	35.3	83
DMT9	41.0	47.3	41.0	51.0	434	1783	25.1	83
	42.7	47.5	42.7	52.0	397	1823	25.8	83
	44.4	48.6	44.4	53.0	433	1891	25.0	83
DMT7	97.6	104.9	116.1	105.2	974	2833	46.9	83
	98.2	106.7	117.8	106.7	1010	2902	52.3	83
	99.8	109.8	119.6	109.8	955	2804	55.5	83

Table 6.1 Results of dilatometer tests in dense, medium and loose sand.

TEST	σ'_V (kPa)	σ'_H (kPa)	σ'_{Vmax} (kPa)	σ'_{Hmax} (kPa)	P_0 (kPa)	P_1 (kPa)	P_D (kN)	R_d %
DMT6	42.4	44.8	107.7	113.7	340	1538	18.9	83
	43.1	46.0	109.4	114.7	390	1577	19.0	83
	44.7	47.9	111.1	115.6	411	1489	20.2	83
DMT1	96.5	38.9	99.7	46.6	390	1759	25.2	83
	102.9	53.2	102.9	53.2	485	1886	28.8	83
	104.1	62.8	104.5	62.8	421	1975	32.6	83
DMT8	12.6	53.5	13.4	54.7	494	1937	32.8	83
	14.4	54.9	15.1	55.7	504	1937	32.5	83
	15.8	55.9	16.8	56.7	466	1888	31.5	83
DMT11	50.0	122.5	50.3	122.9	1355	3557	-	83
	51.7	123.4	52.0	123.9	1379	3645	-	83
	53.5	124.4	53.8	124.9	1196	3420	-	83
MEDIUM SAND								
DMT14	55.7	37.0	55.7	37.6	256	1440	15.3	64
	57.1	38.9	57.3	38.9	361	1479	14.8	64
	58.7	41.2	58.9	41.2	422	1411	13.8	64
DMT20	149.6	77.0	149.6	77.0	453	1782	26.3	53
	151.1	77.7	151.2	77.9	594	1890	27.3	53
	152.7	79.0	152.8	79.0	582	1802	26.6	53
DMT17	53.3	36.1	142.8	81.7	182	1221	13.6	62
	54.6	37.3	144.4	82.6	266	1241	13.8	62
	55.1	38.3	146.1	83.6	296	1270	13.9	62
DMT16	16.8	54.4	17.3	54.5	302	1608	21.0	59
	18.5	55.4	18.9	55.5	343	1627	21.9	59
	20.2	56.6	20.6	56.6	389	1706	22.7	59
DMT29	58.7	120.1	59.1	120.4	741	2278	38.3	56
	60.3	121.0	60.6	121.3	772	2396	39.5	56
	61.9	122.5	62.2	122.5	835	2415	39.0	56

Table 6.1 continued.

TEST	σ'_V (kPa)	σ'_H (kPa)	σ'_{Vmax} (kPa)	σ'_{Hmax} (kPa)	P_0 (kPa)	P_1 (kPa)	P_D (kN)	R_d %
DMT19	25.3	50.4	62.3	120.5	402	1644	23.9	59
	26.9	50.3	63.9	121.5	406	1605	23.0	59
	28.4	51.4	65.6	122.5	379	1556	22.3	59
DMT21	24.7	49.6	147.8	75.9	336	1550	21.0	60
	26.2	50.6	149.4	76.9	413	1638	21.6	60
	27.7	51.8	151.0	77.8	435	1638	22.0	60
DMT15	33.6	43.7	33.6	45.0	174	1322	14.6	59
	36.0	45.0	36.0	46.0	273	1420	15.5	59
	39.3	46.2	39.3	47.0	305	1420	14.4	59
DMT22	100.8	97.9	104.4	98.7	698	2219	31.5	58
	100.2	100.4	106.0	100.4	731	2219	34.3	58
	102.3	102.1	107.5	102.1	727	2258	34.1	58
DMT18	42.1	39.7	105.4	104.9	254	1314	15.7	57
	42.2	41.5	107.0	105.9	337	1353	17.5	57
	43.6	43.1	108.6	106.9	342	1412	18.0	57
DMT23	74.8	150.5	75.4	151.1	1057	2965	50.4	59
	76.2	151.8	77.0	152.1	1045	2974	52.9	59
	77.8	153.2	78.7	153.2	1044	2984	53.7	59
DMT27	36.9	74.8	38.2	75.1	555	1885	28.9	59
	38.6	75.8	39.8	76.1	551	1925	28.7	59
	40.1	77.1	41.3	77.1	533	1895	29.5	59
DMT24	60.4	123.0	60.6	123.4	1006	2826	53.3	72
	61.9	123.9	62.2	124.3	989	2934	53.7	72
	63.2	124.9	63.7	125.2	1021	2944	53.7	72
DMT28	-	-	-	-	863	2562	-	-
	-	-	-	-	946	2592	-	-
	-	-	-	-	953	2523	-	-

Table 6.1 continued.

TEST	σ'_V (kPa)	σ'_H (kPa)	σ'_{Vmax} (kPa)	σ'_{Hmax} (kPa)	P_0 (kPa)	P_1 (kPa)	P_D (kN)	R_d %
LOOSE SAND								
DMT25	149.0	76.2	149.4	76.8	122	767	9.2	29
	150.4	76.9	150.9	77.8	188	865	10.8	29
	151.7	77.6	152.2	78.7	216	904	11.6	29
DMT30	59.9	117.5	60.0	120.1	277	1042	11.8	32
	61.5	118.4	61.5	121.1	306	1071	12.5	32
	62.9	120.1	62.9	122.0	343	1130	13.6	32
DMT26	101.1	99.5	101.1	101.3	203	895	9.7	30
	102.5	99.5	102.7	102.3	219	954	10.2	30
	104.2	100.1	104.2	103.3	278	1003	10.4	30
DMT31	148.5	148.1	148.5	150.0	395	1239	14.0	25
	150.1	147.5	150.1	151.0	422	1288	13.9	25
	151.4	148.1	151.4	151.9	429	1327	14.4	25

Table 6.1 continued.

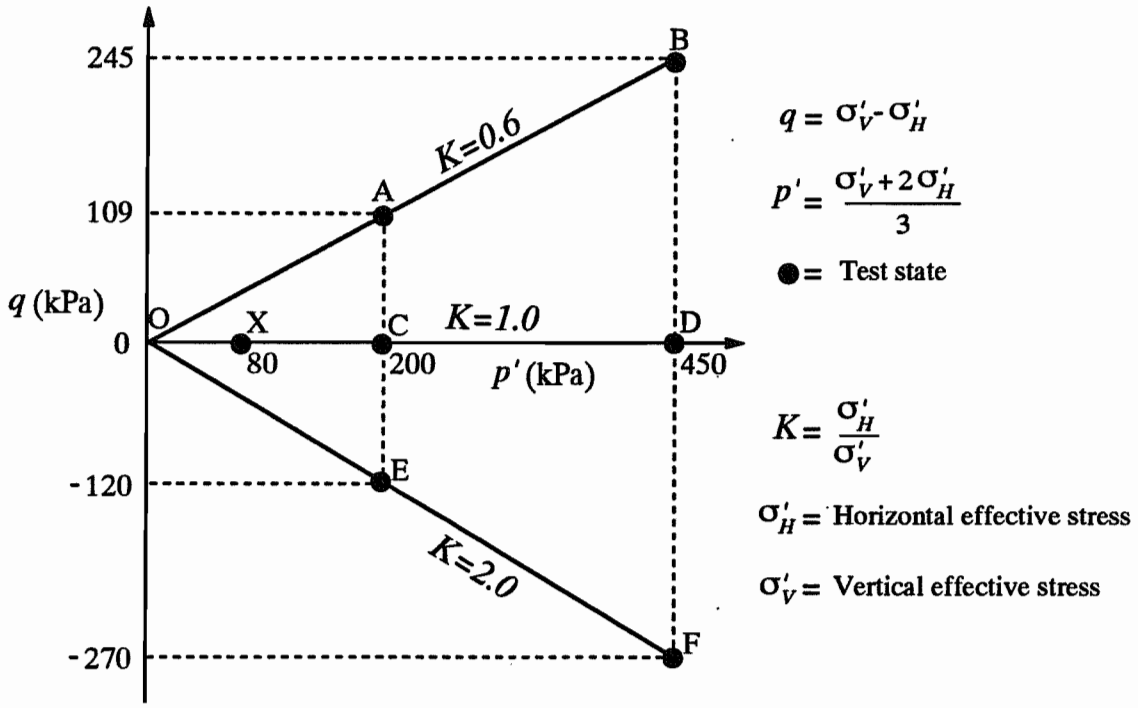


Figure 1.1 Nominal test states for clay beds.

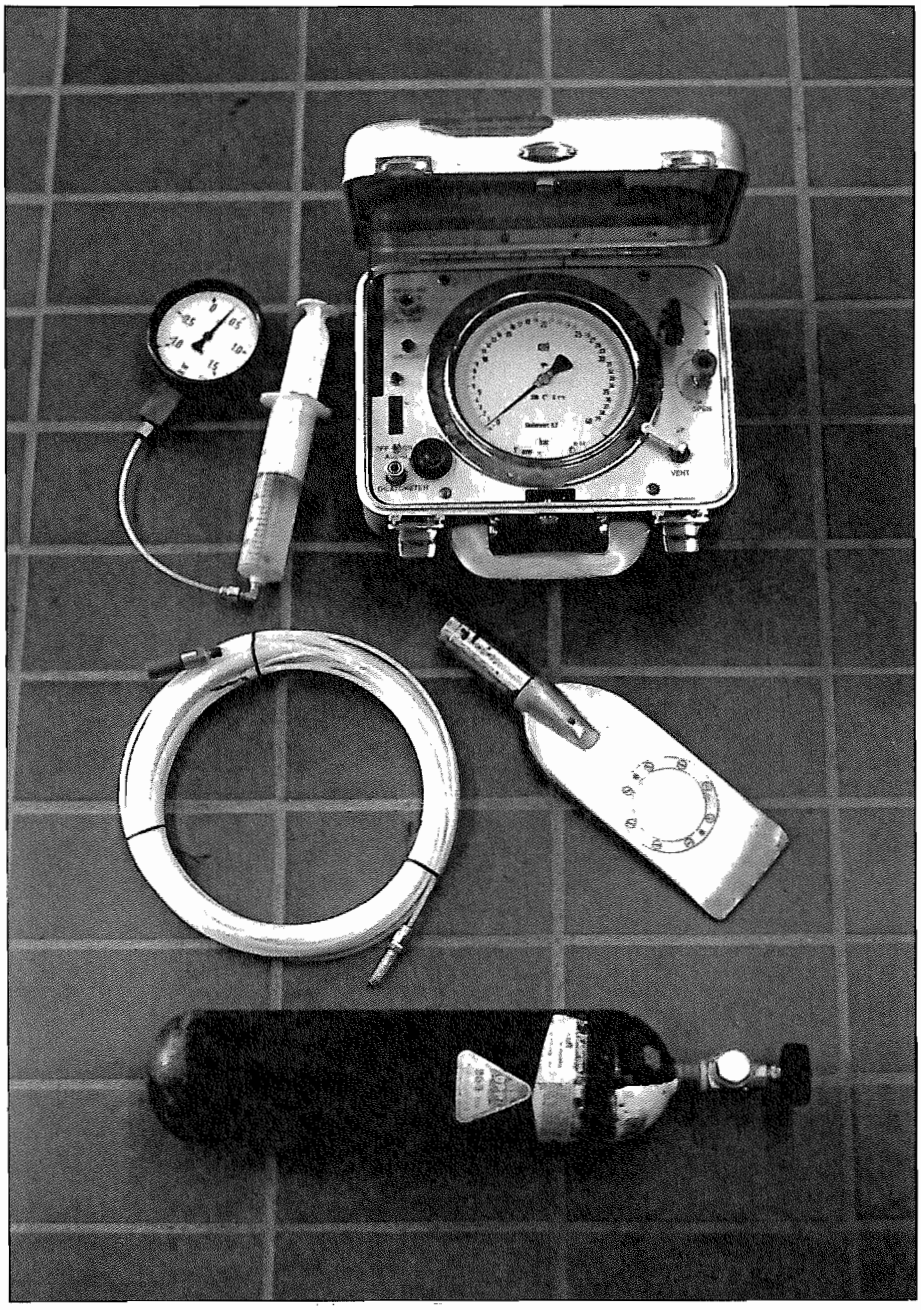


Figure 2.1 Components of the Marchetti dilatometer test.

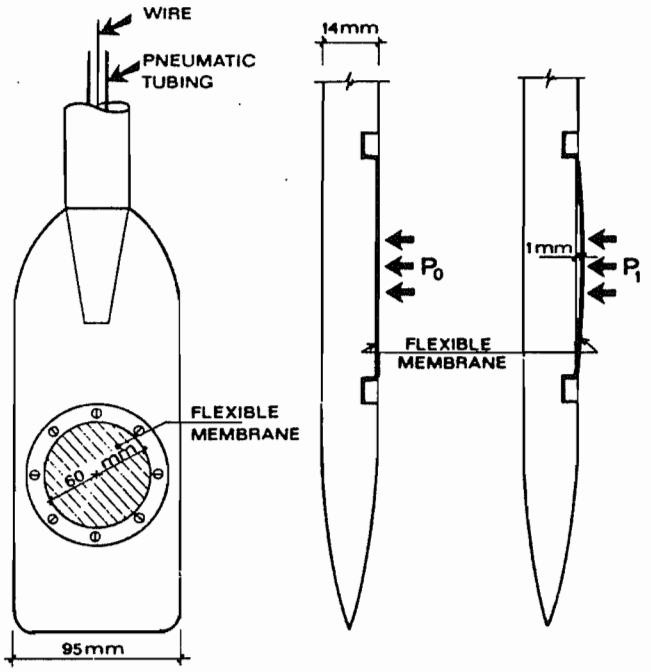


Figure 2.2 Dimensions and geometry of the dilatometer blade.

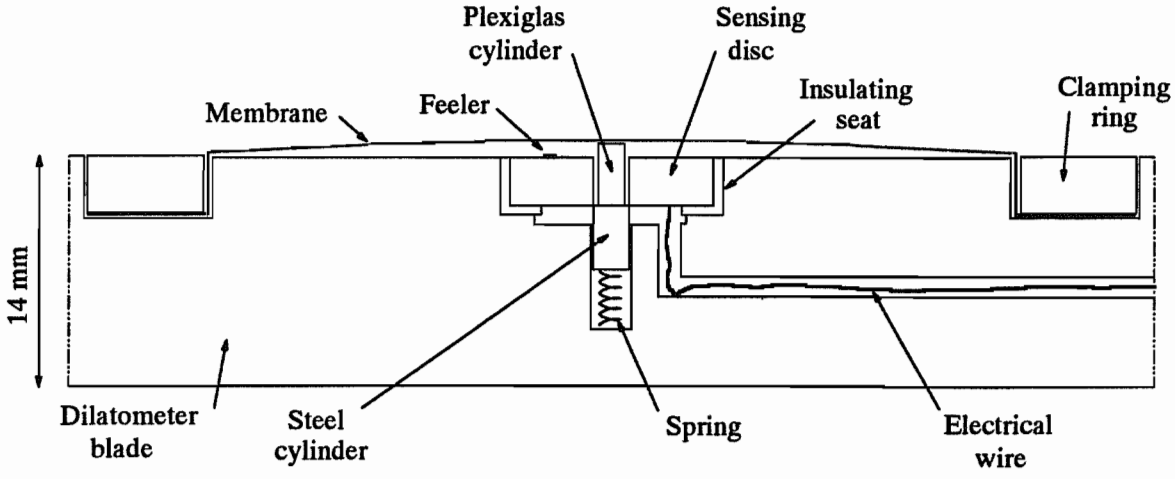


Figure 2.3 Cross-section through the dilatometer blade and membrane.

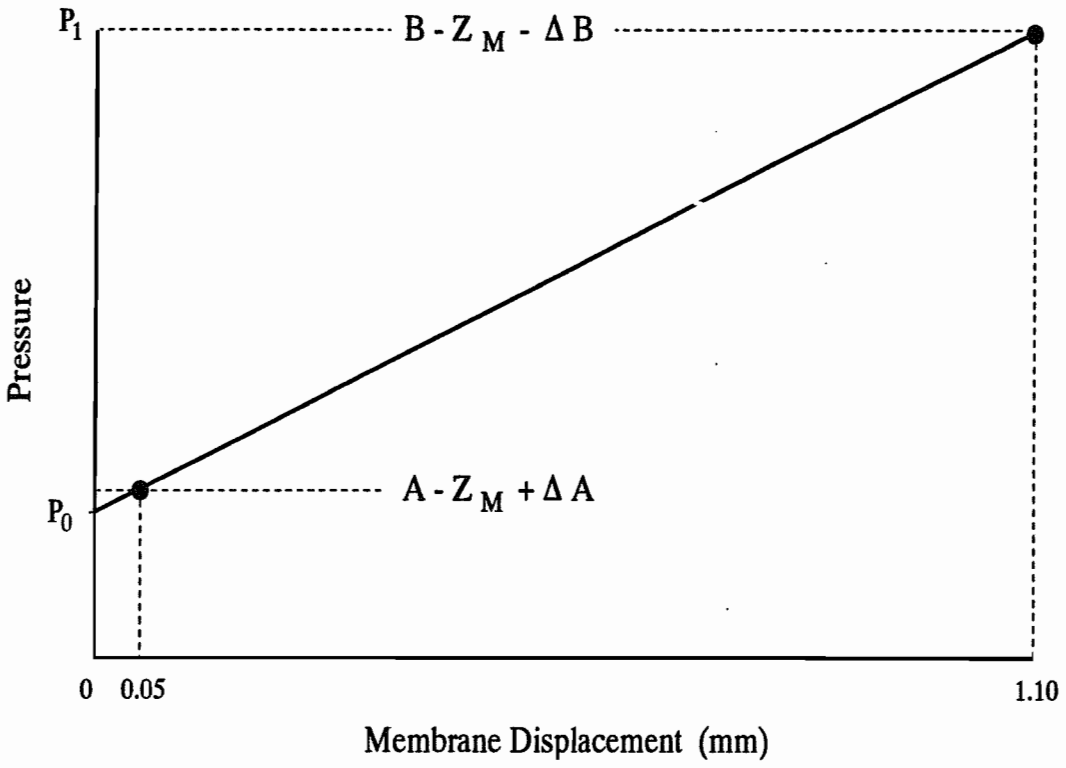


Figure 2.4 Linear extrapolation to find P_0.

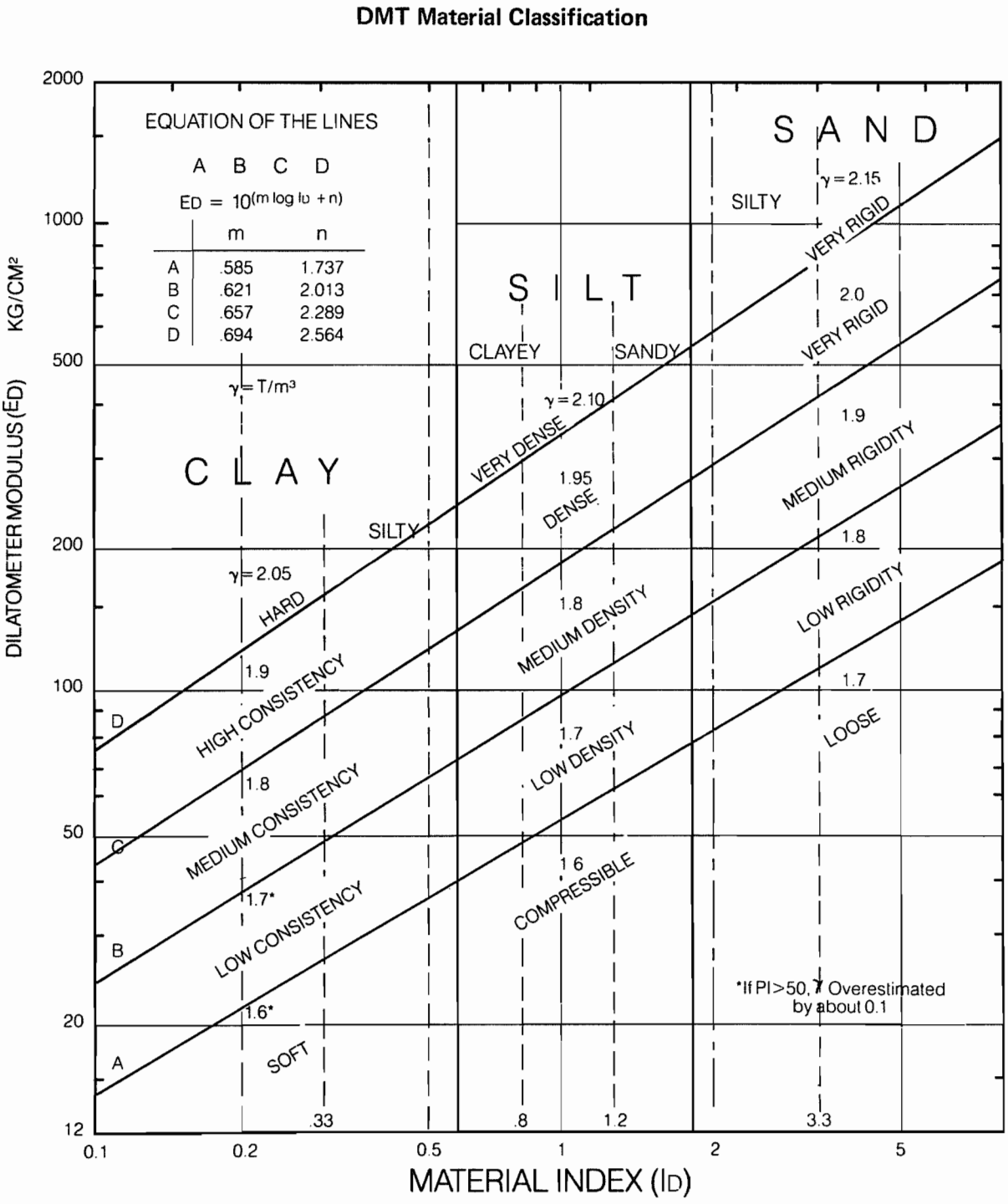


Figure 2.5 Dilatometer chart for material description, Marchetti & Crapps (1981).

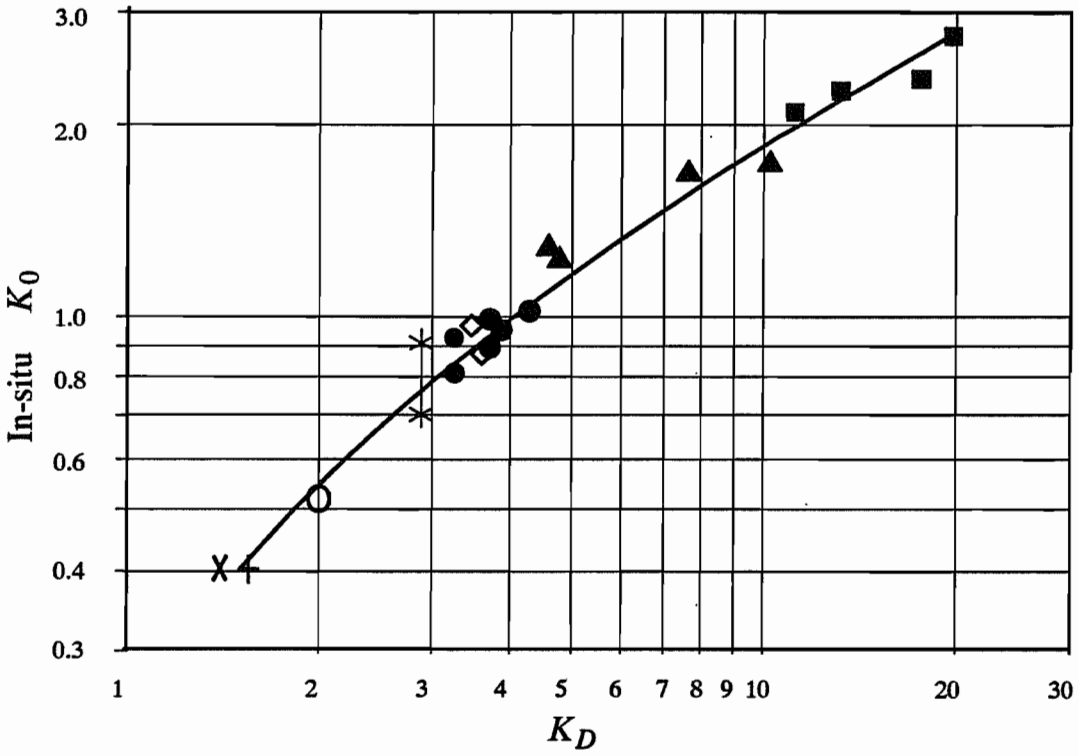


Figure 2.6 Correlation between K_0 and K_D, Marchetti (1980).

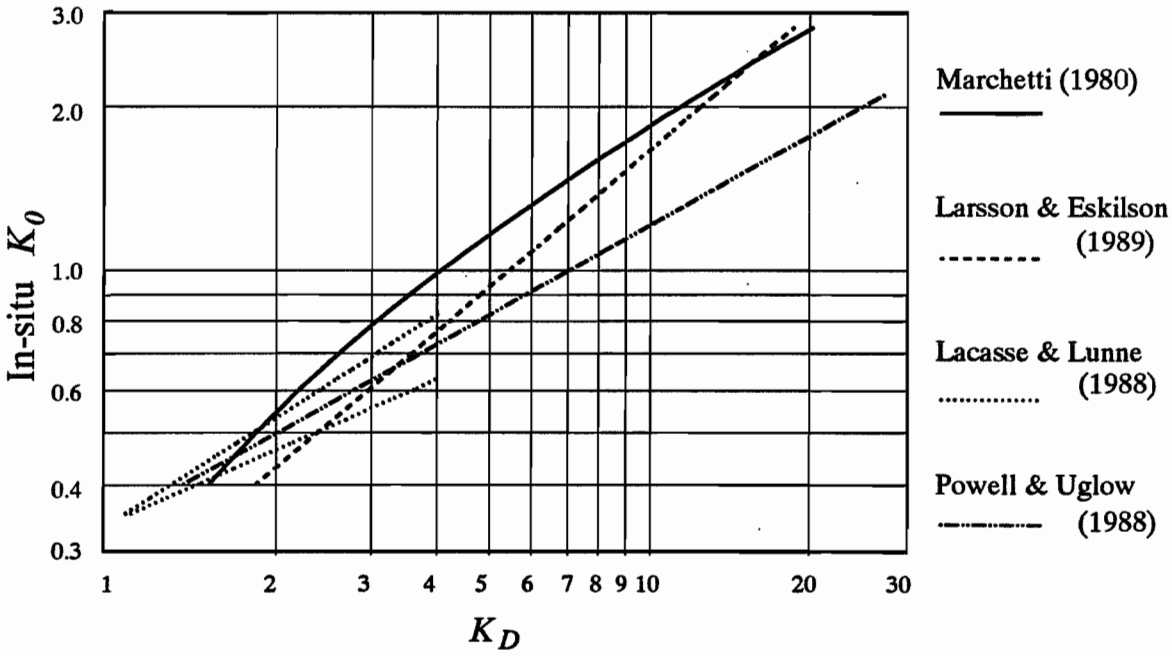


Figure 2.7 Various K_0 : K_D correlations.

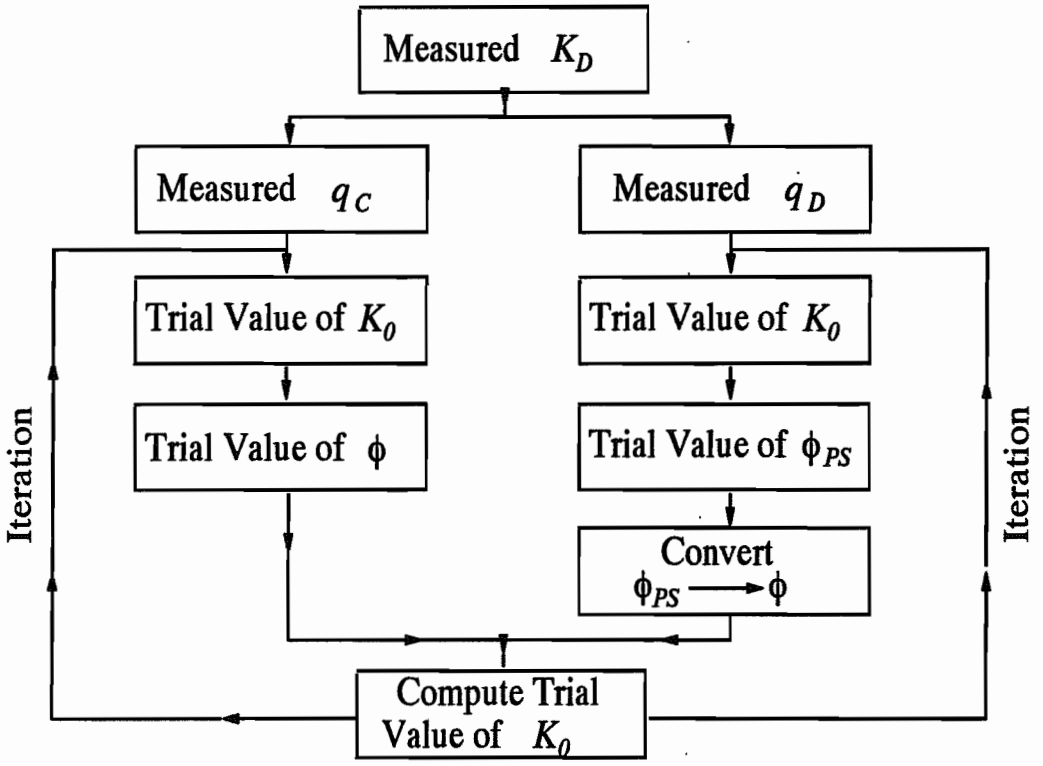


Figure 2.8 Summary of iterative procedure used by Schmertmann (1983) to evaluate K_0 in sands.

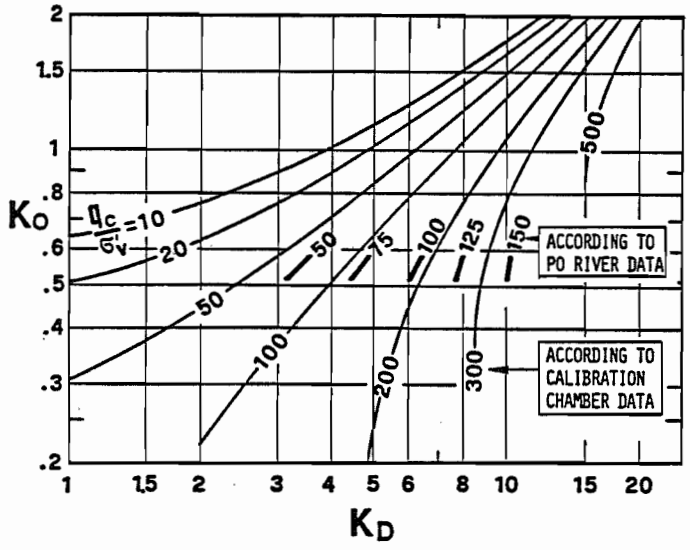


Figure 2.9 Chart for interpreting K_0 from K_D and q_c, Marchetti (1985).

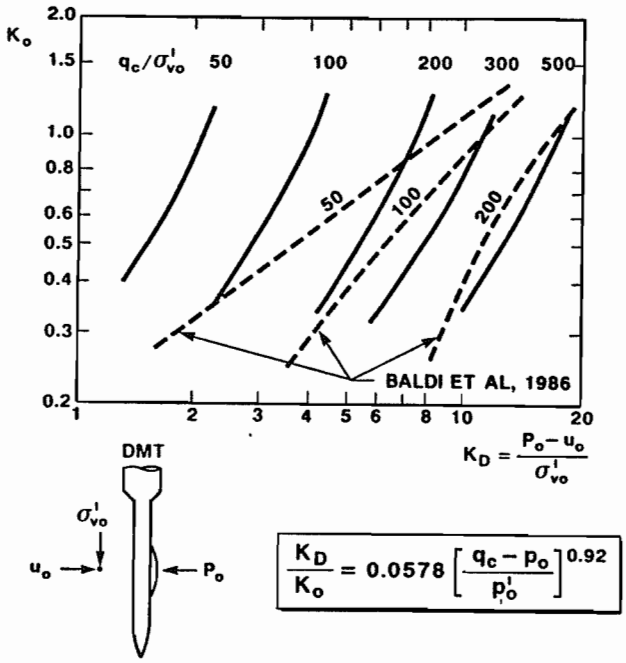


Figure 2.10 Relationships between K_D, q_c and K_0 proposed by Baldi et al. (1986), and Jamiolkowski & Robertson (1988).

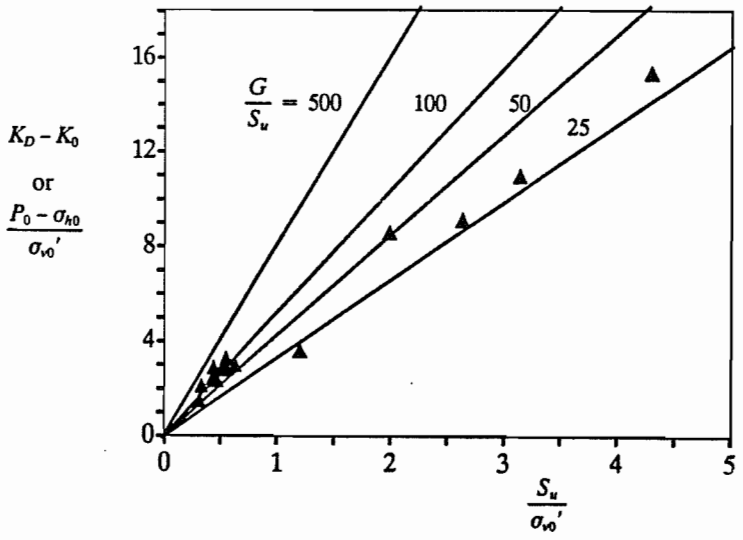


Figure 2.11 Correlation between the total horizontal stress, P_0 and the undrained strength, Yu et al. (1992).

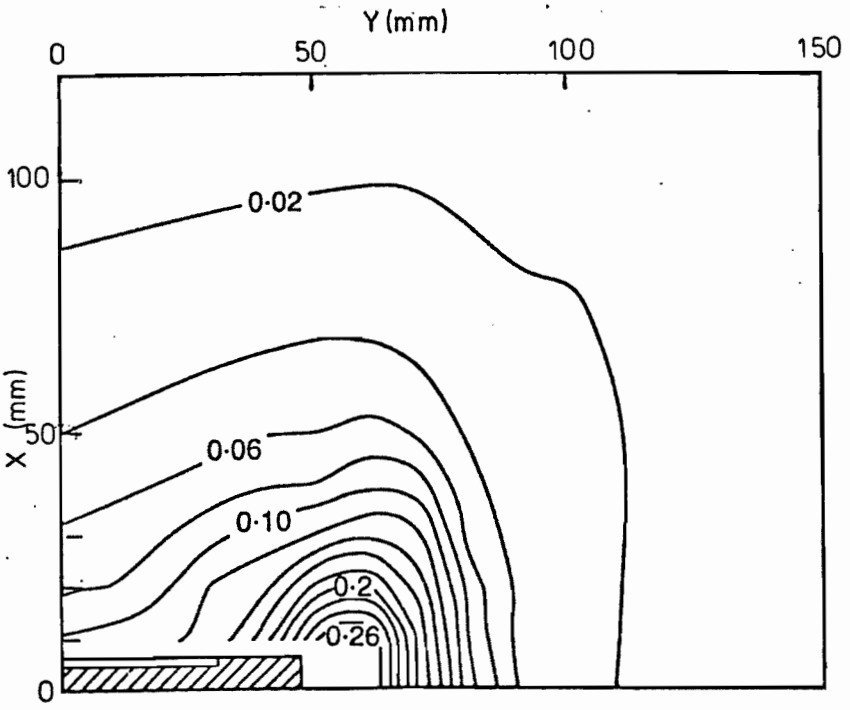


Figure 2.12 Numerical prediction of the octahedral shear strain pattern around the dilatometer, Finno (1993).

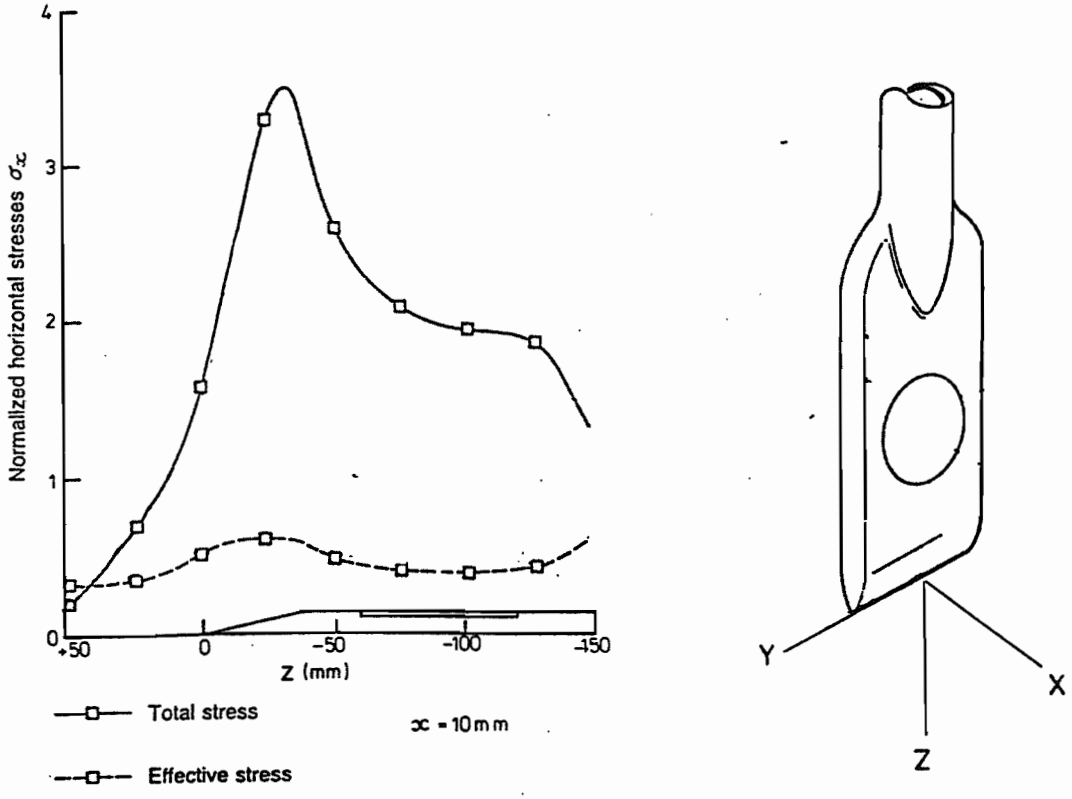


Figure 2.13 Numerical prediction of the stresses against the dilatometer blade normalised by the vertical stress, Finno (1993).

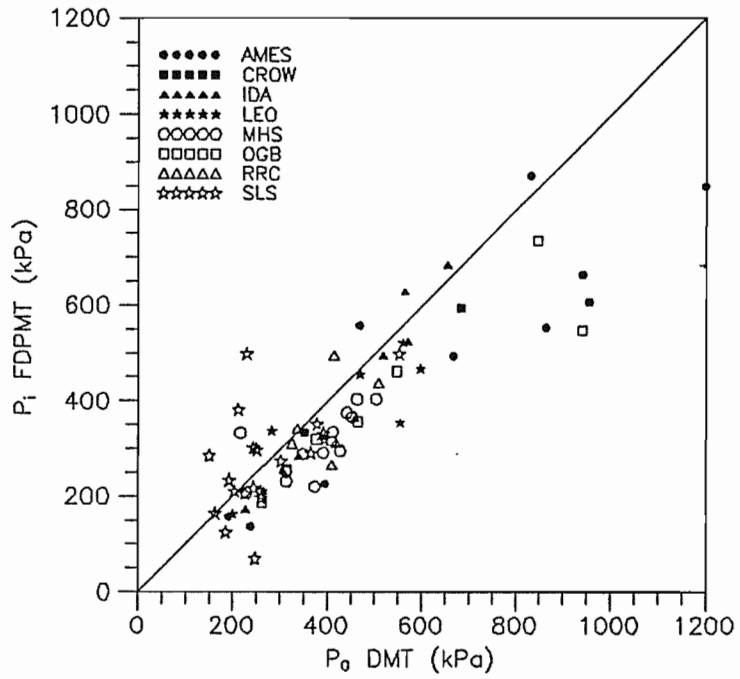


Figure 2.14 Comparison of cone-pressuremeter P_i and dilatometer P_0 Lutenegger & Blanchard (1990).

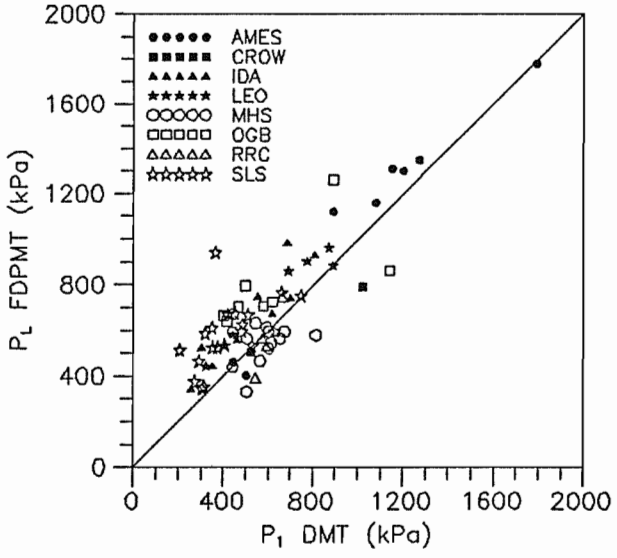
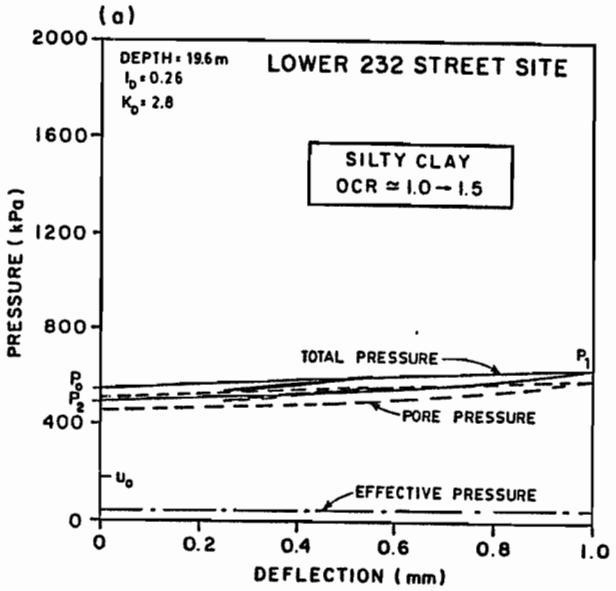
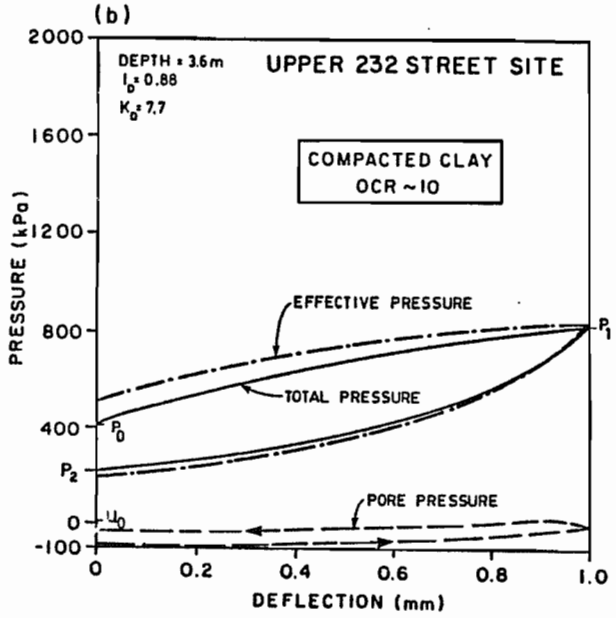


Figure 2.15 Comparison of cone-pressuremeter P_L and dilatometer P_1 Lutenegger & Blanchard (1990).

a)



b)



c)

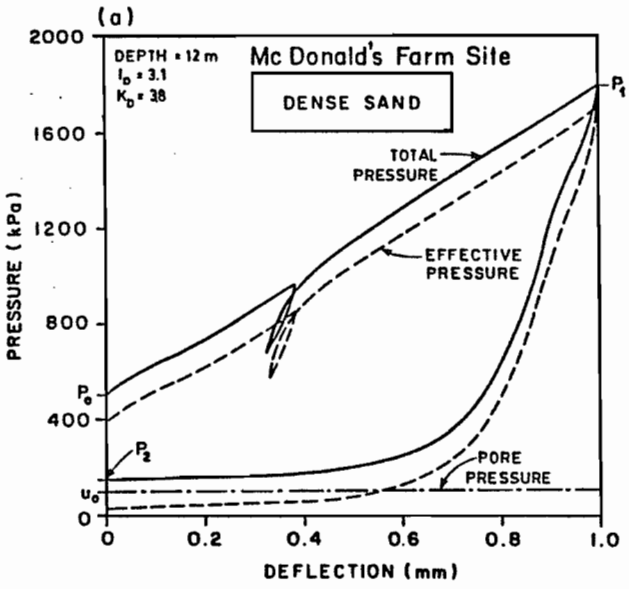


Figure 2.16 Typical results from an instrumented diatometer in a) soft clay, b) stiff clay, and c) sand, Campanella & Robertson (1991).

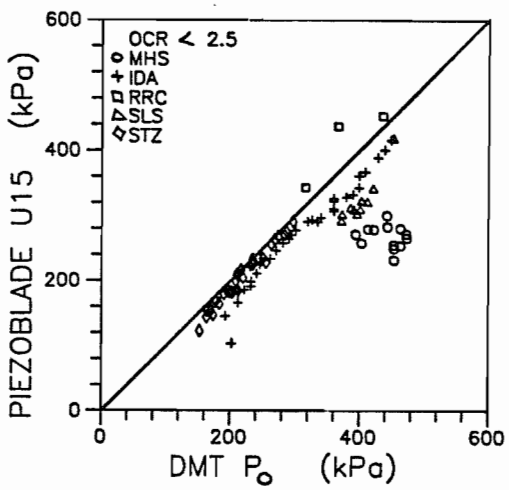


Figure 2.17 Comparison of dilatometer P_0 reading and pore pressure from piezoblade, in normally consolidated and lightly overconsolidated clays, Lutenegger (1988).

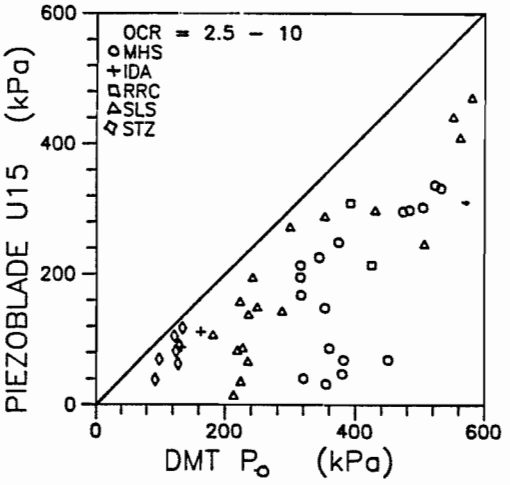


Figure 2.18 Comparison of dilatometer P_0 reading and pore pressure from piezoblade, in overconsolidated clays, Lutenegger (1988).

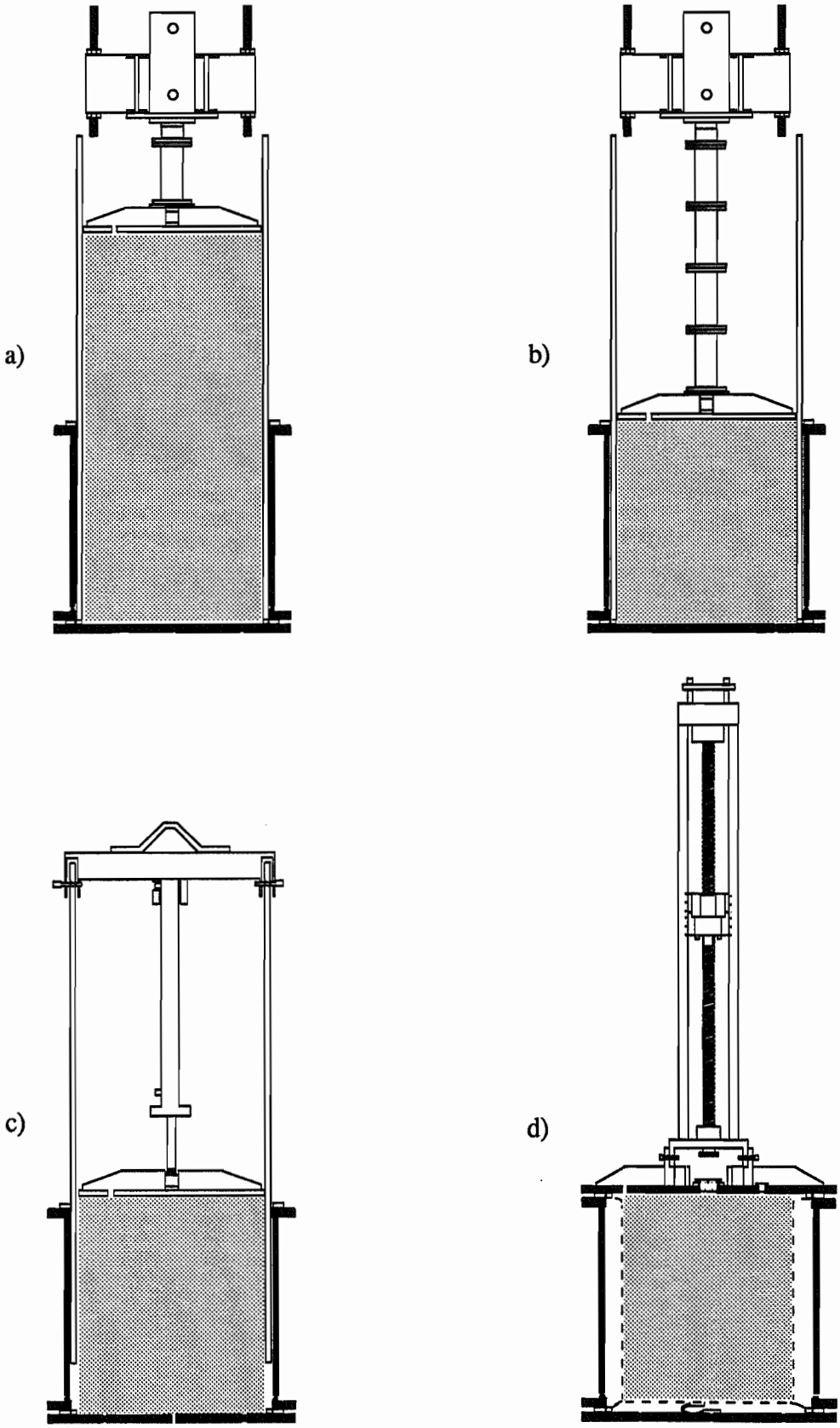
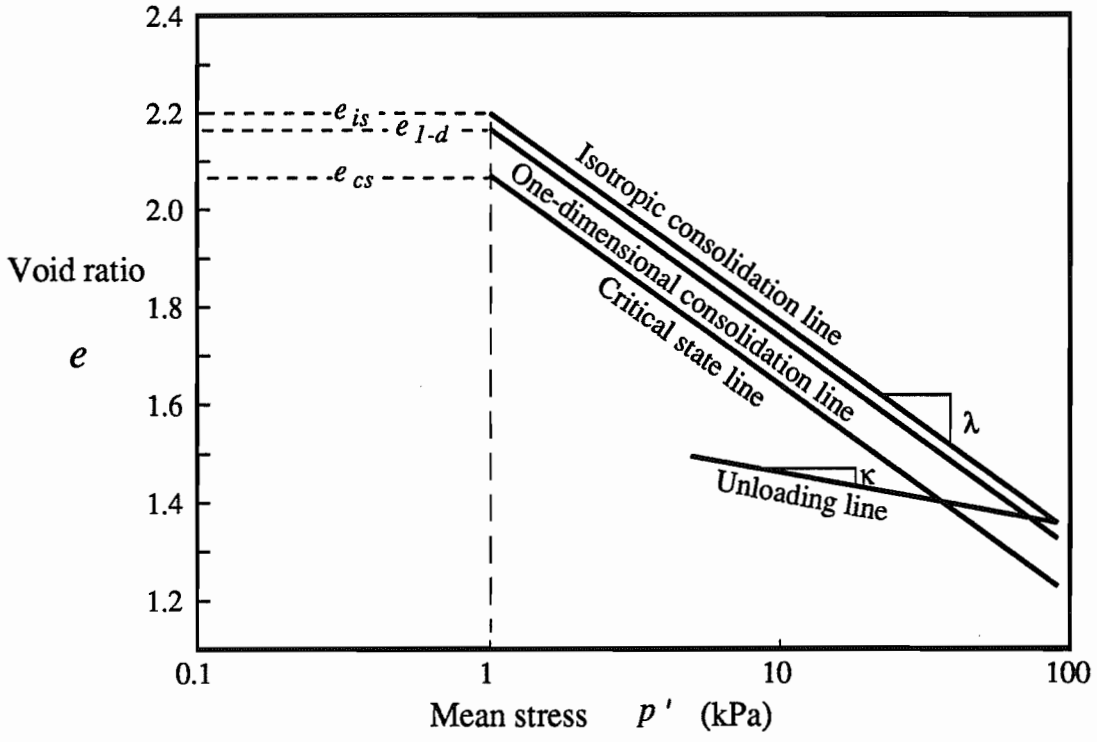
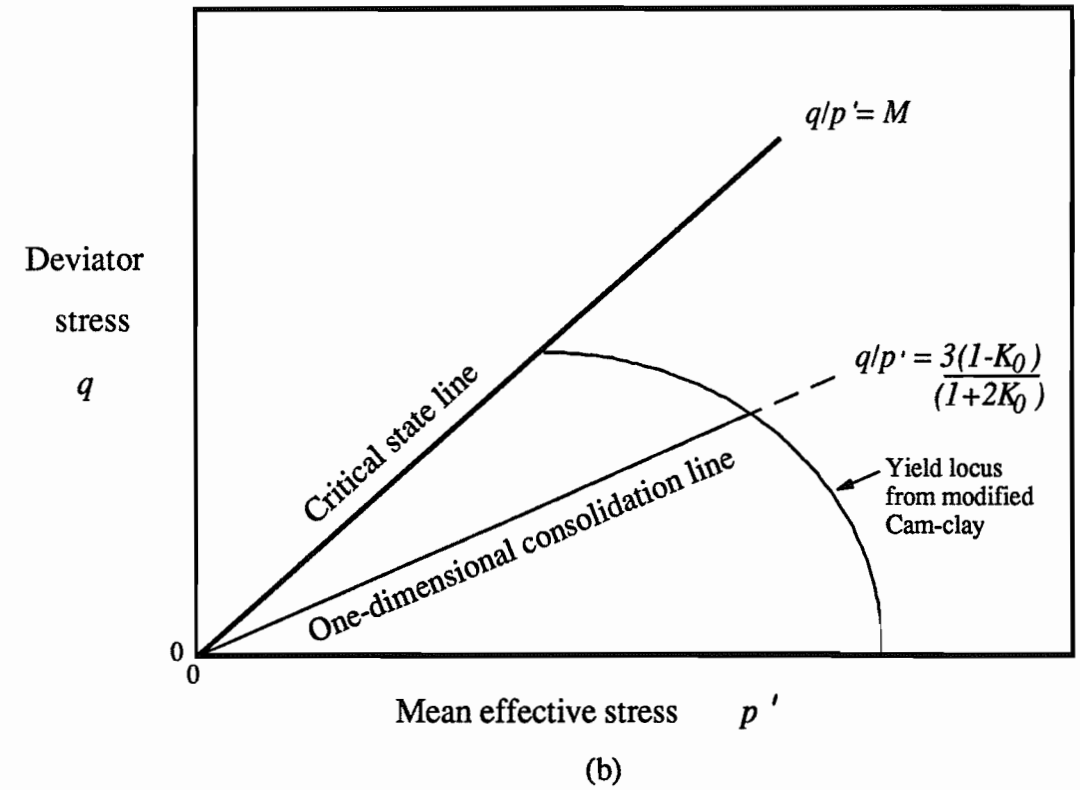


Figure 3.1 Stages in the preparation of a clay bed: a) & b) one-dimensional consolidation, c) extrusion, and d) triaxial consolidation.



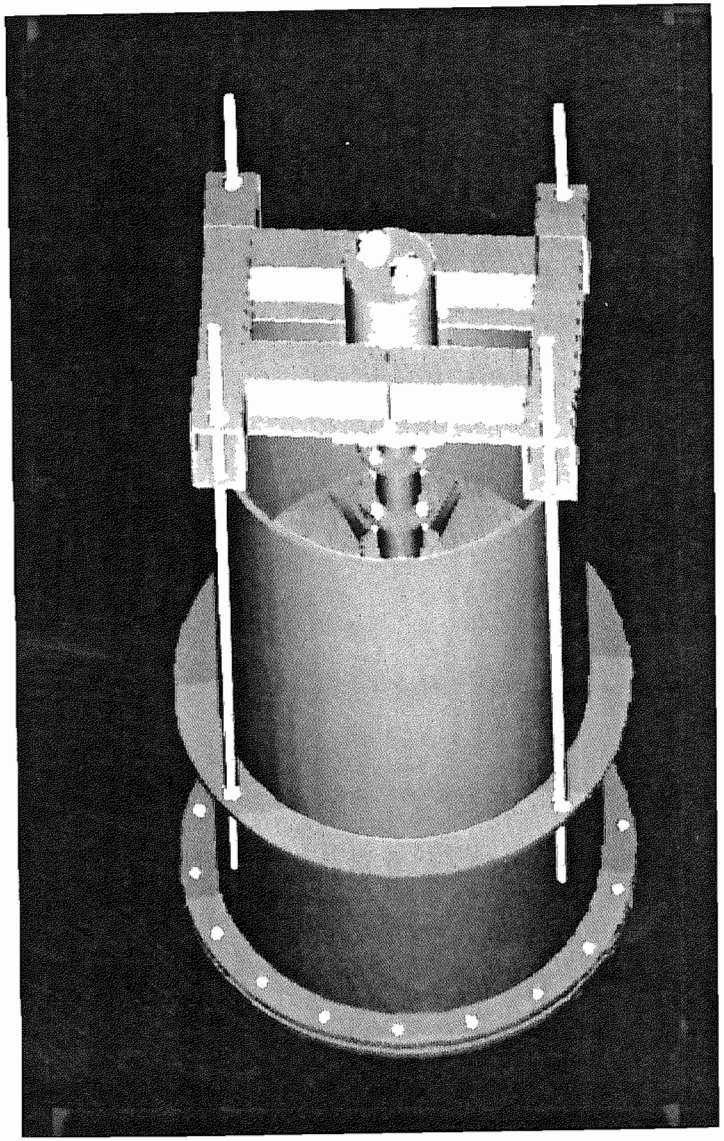
(a)



(b)

Figure 3.2 Relationships between the void ratio and mean stress (a); and between the deviator stress and mean stress (b) according to the framework of modified Cam-clay.

a)



b)

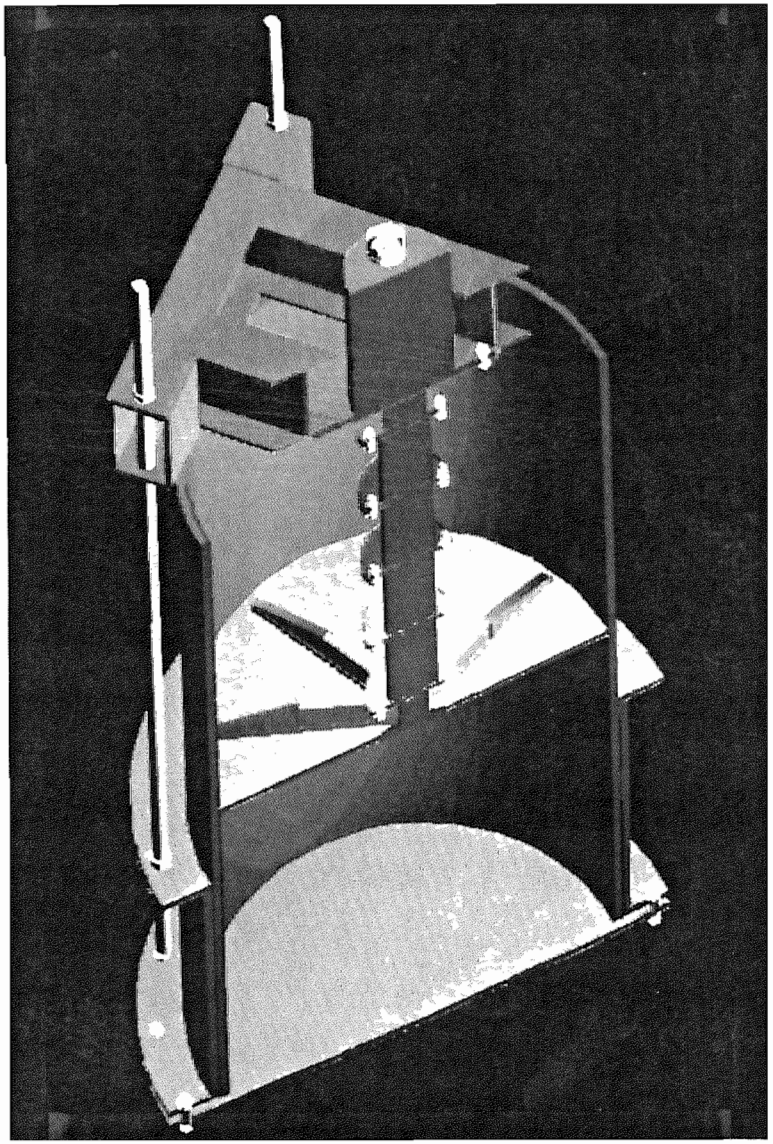


Figure 3.3 Computer generated images of the one-dimensional consolidation apparatus a) general view, b) cut away view.

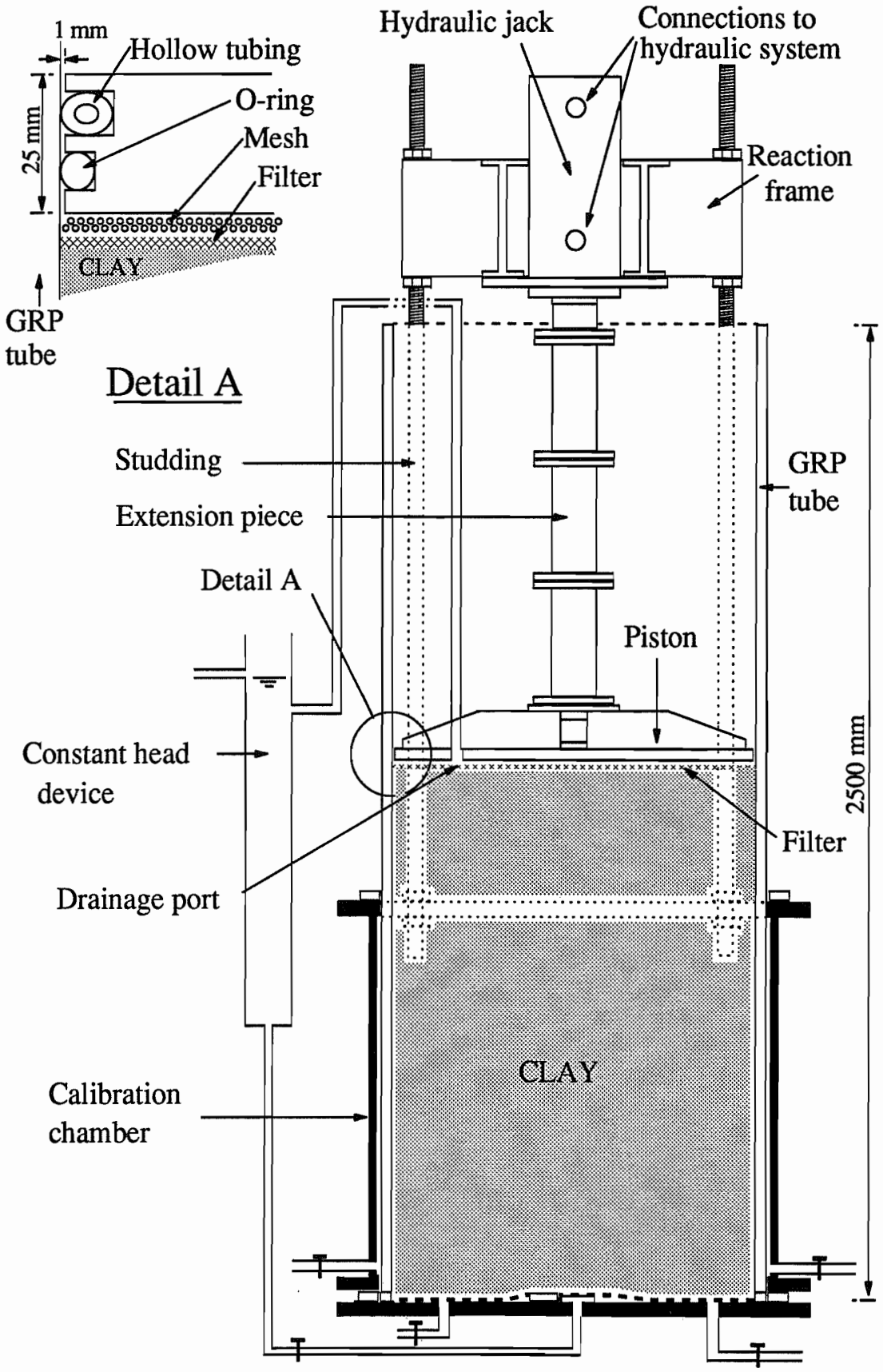


Figure 3.4 One-dimensional consolidation apparatus.

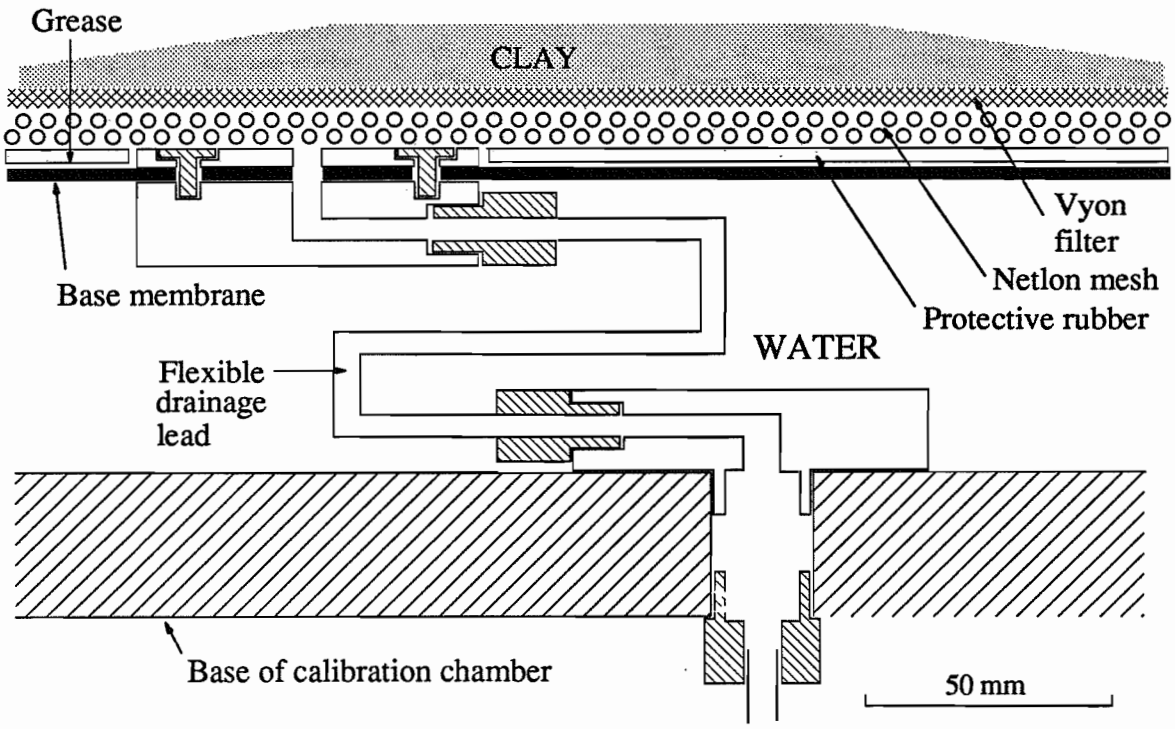


Figure 3.5 Detail of base drainage during second-stage consolidation.

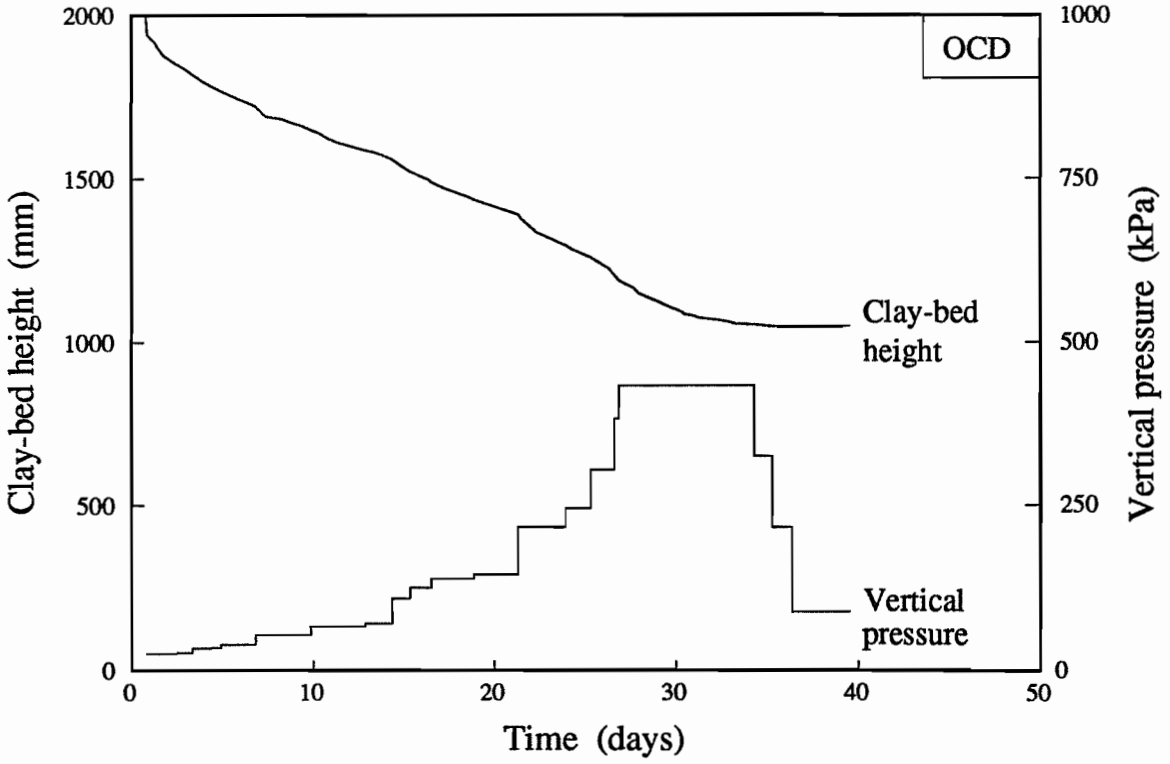


Figure 3.6 Settlement-time plot for clay bed OCD.

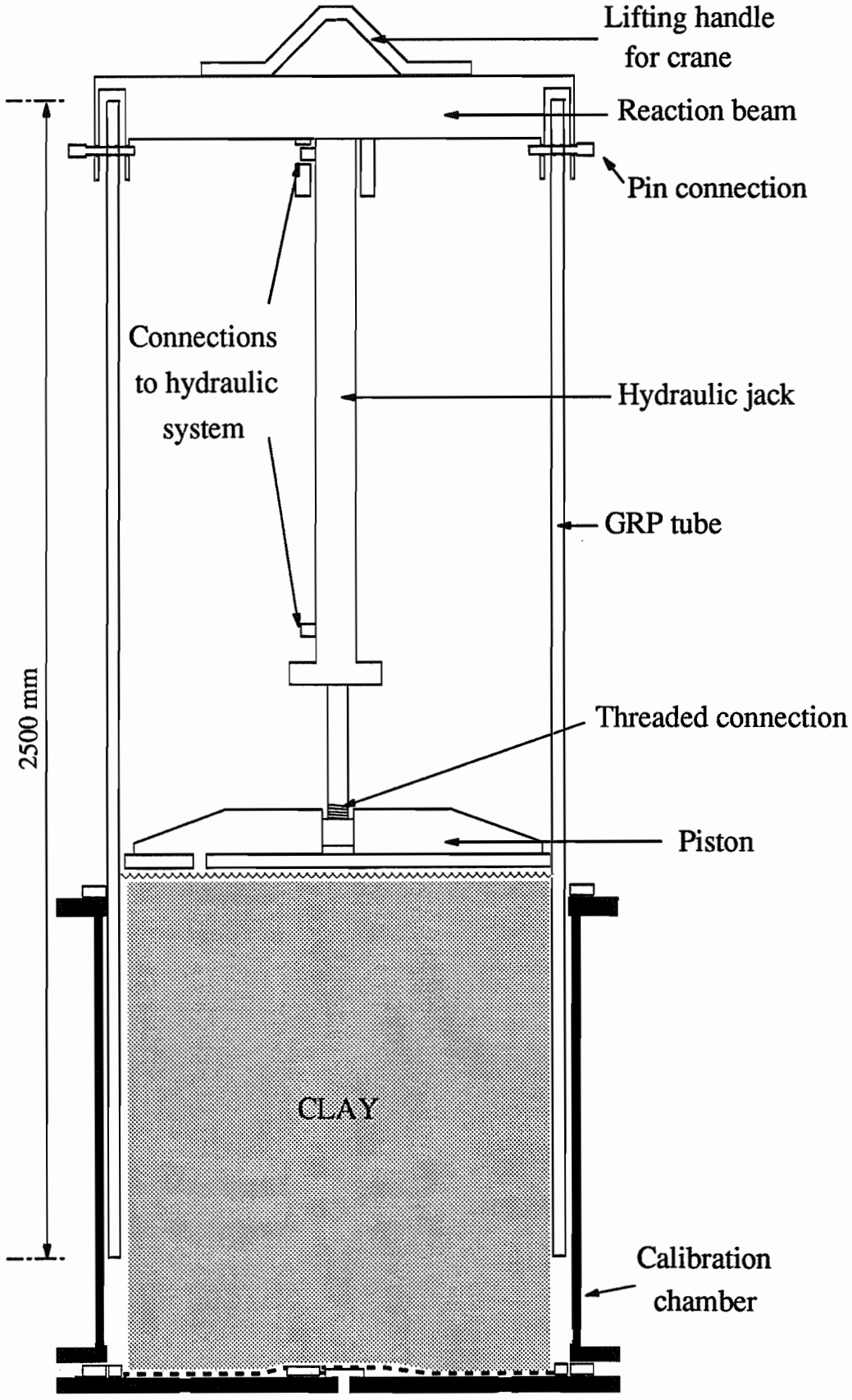


Figure 3.7 Extrusion assembly

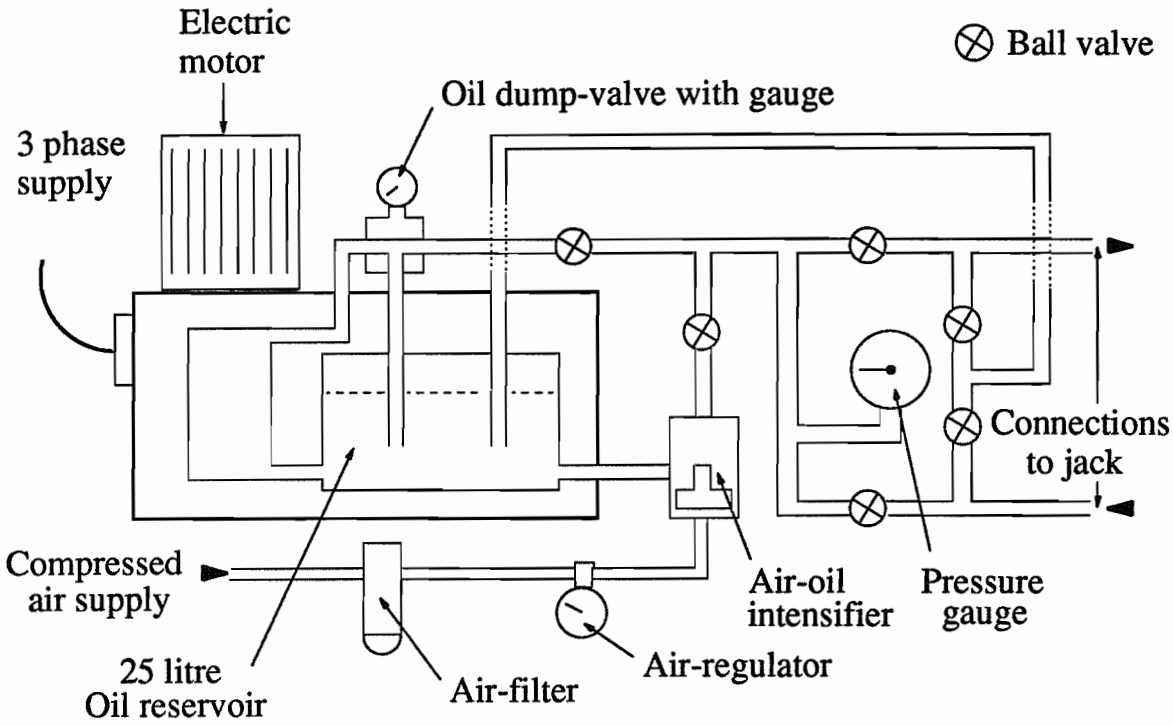


Figure 3.8 Hydraulic system.

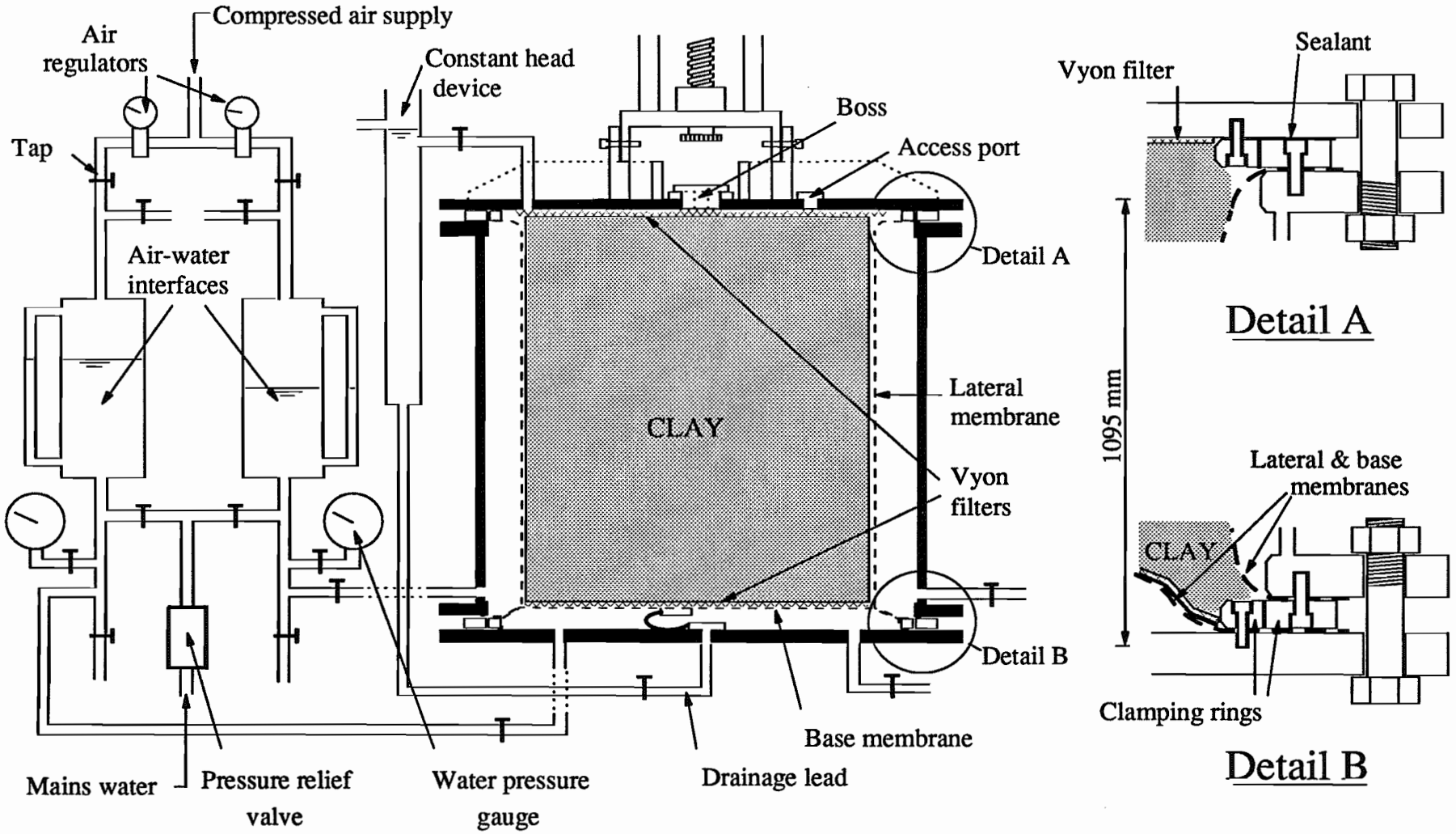


Figure 3.9 Section through the calibration chamber and pressurization system

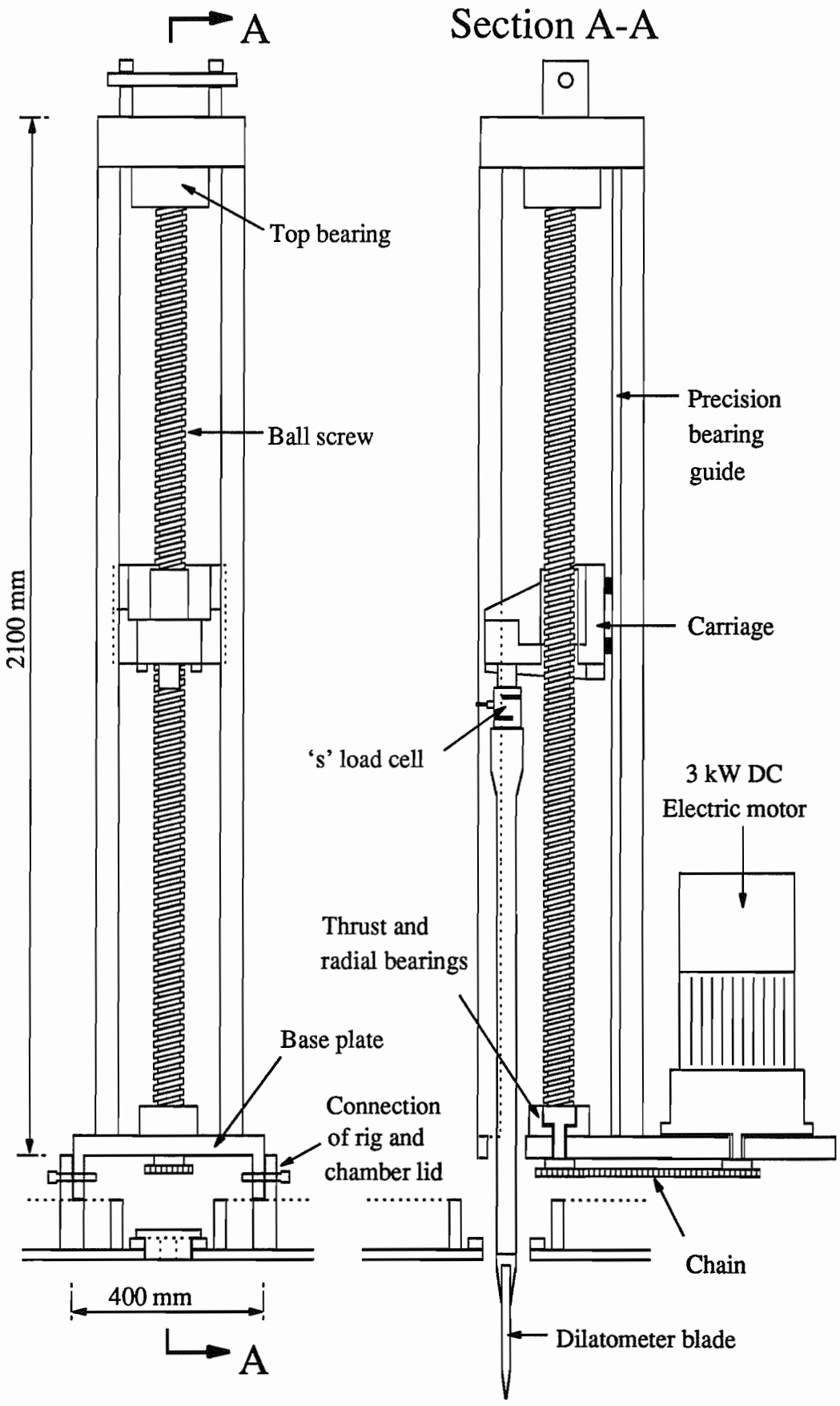


Figure 3.10 Driving Mechanism

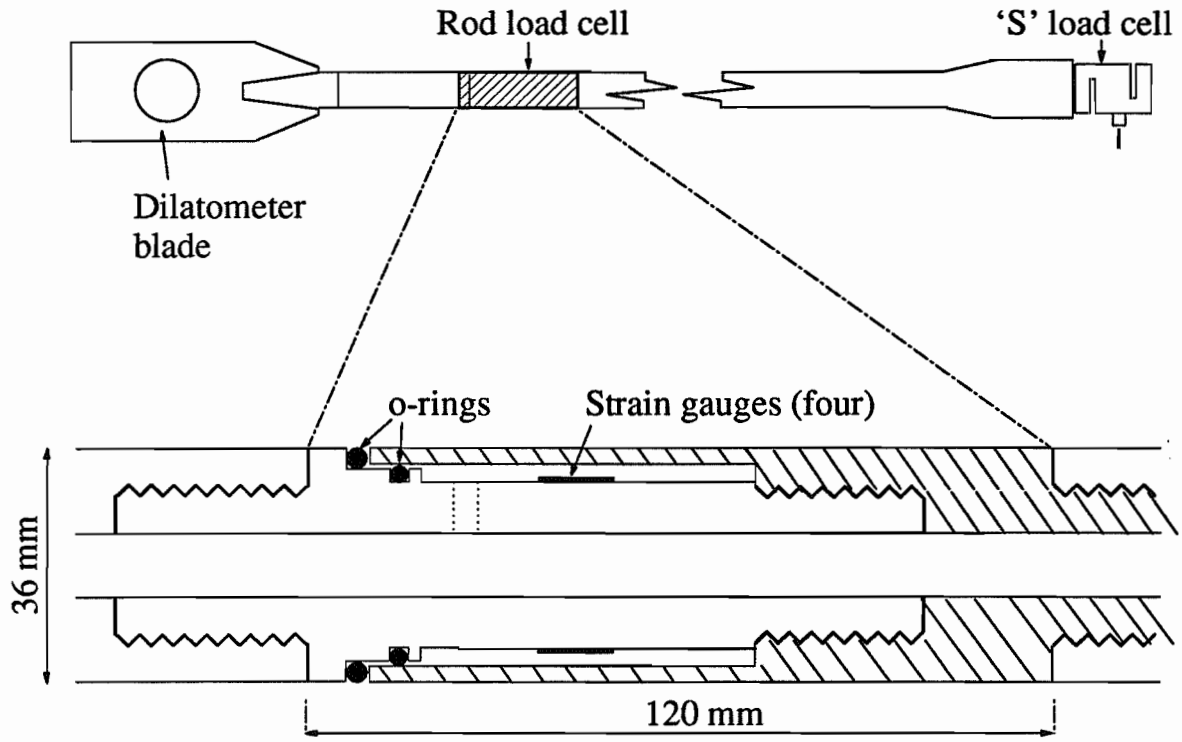


Figure 3.11 Detail of dilatometer rod load cell.

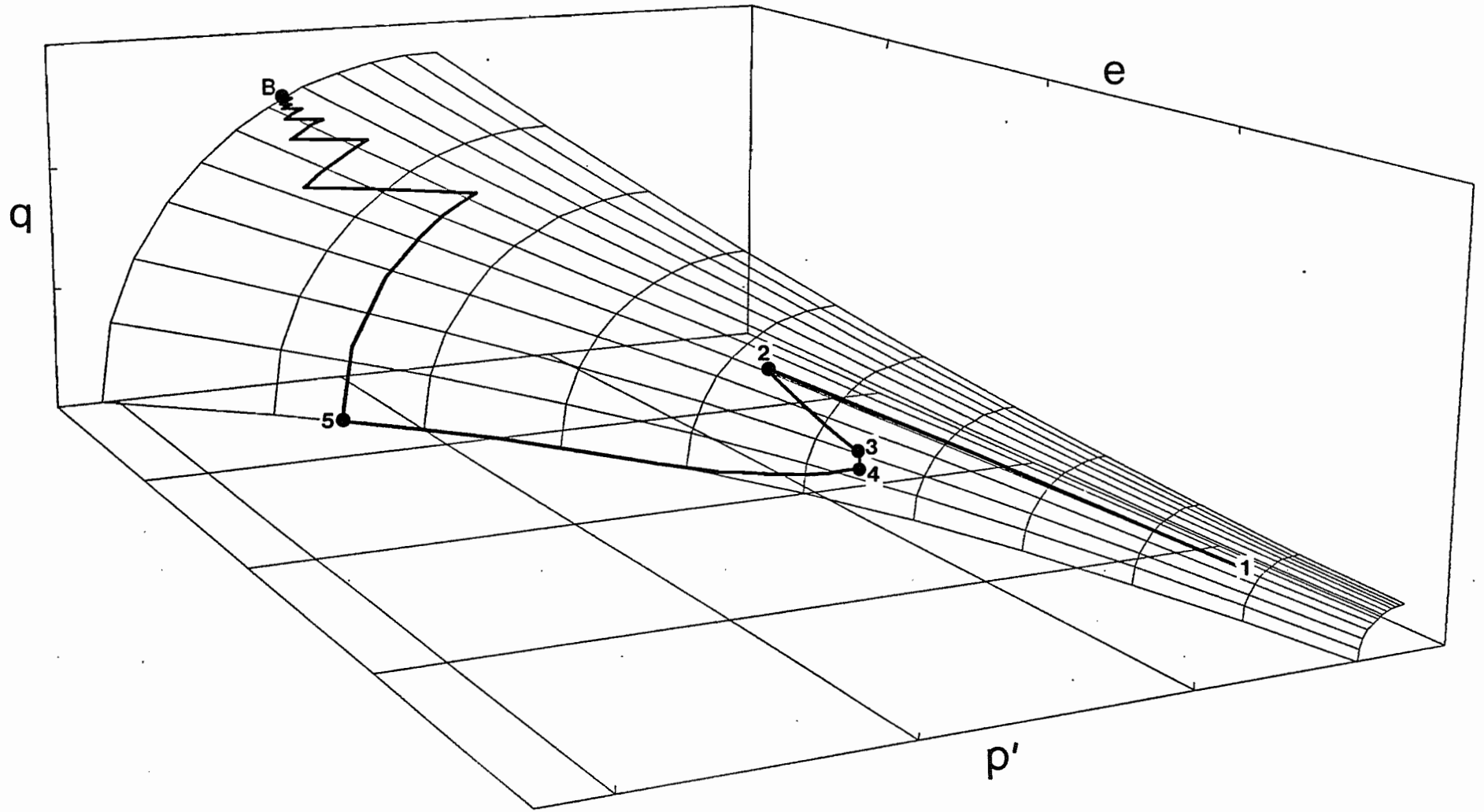


Figure 3.12 Preparation stress path for clay bed OAB in p': q: e space.

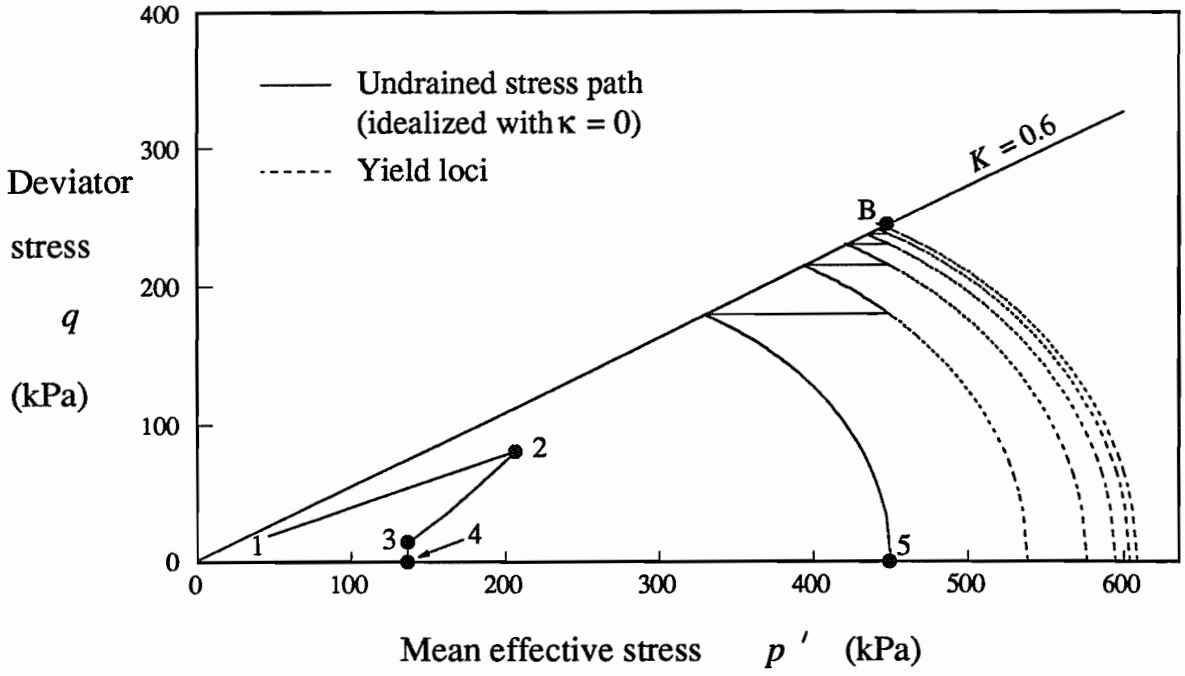


Figure 3.13 Preparation stress path for sample OAB.

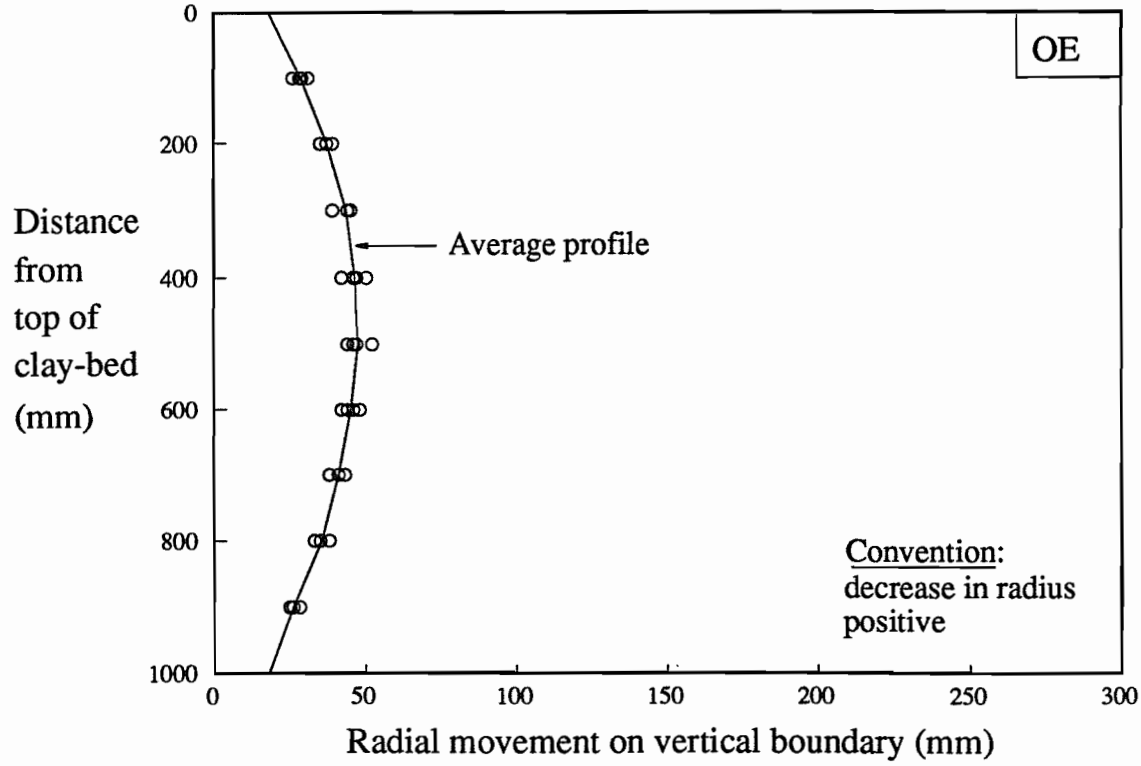


Figure 3.14 Radial movement during second-stage consolidation for clay bed OE.

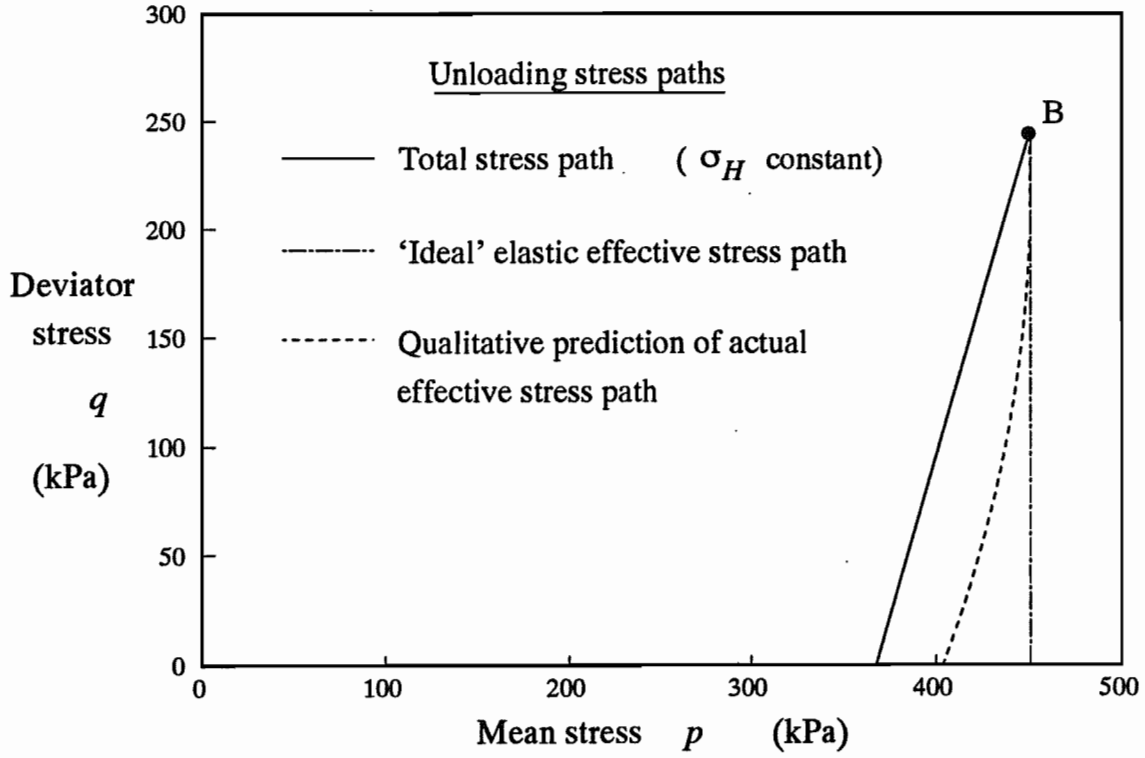


Figure 4.1 Total and effective stress paths during destressing of clay bed OAB.

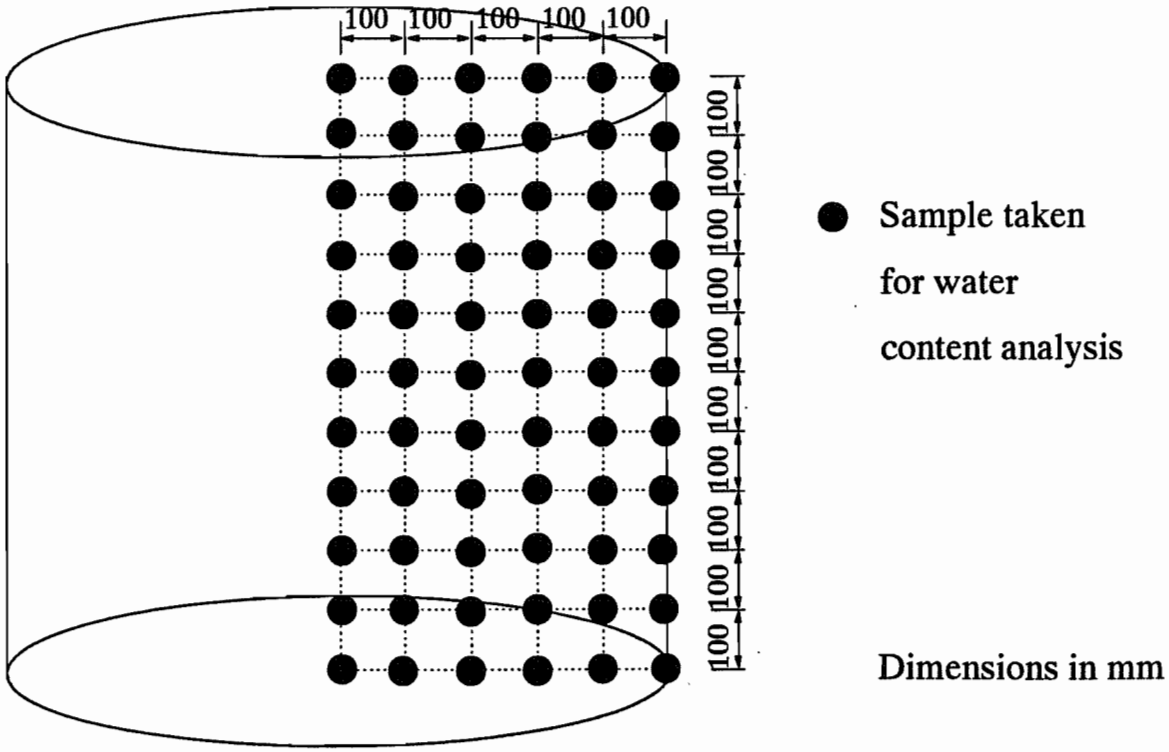
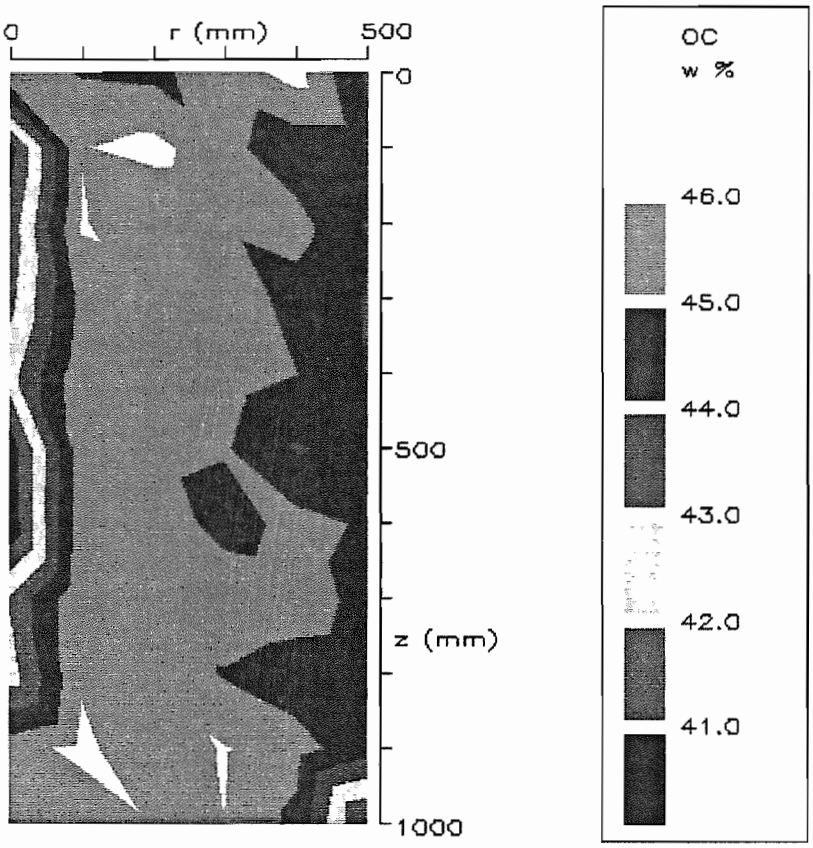


Figure 4.2 Positions of water content samples in typical clay bed.

a)



b)

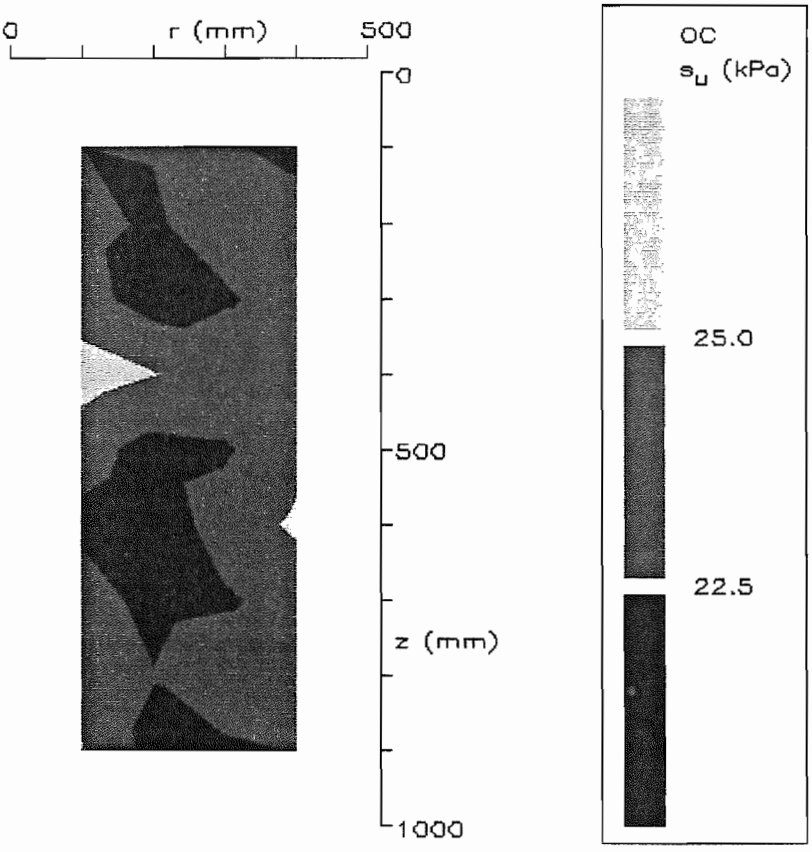
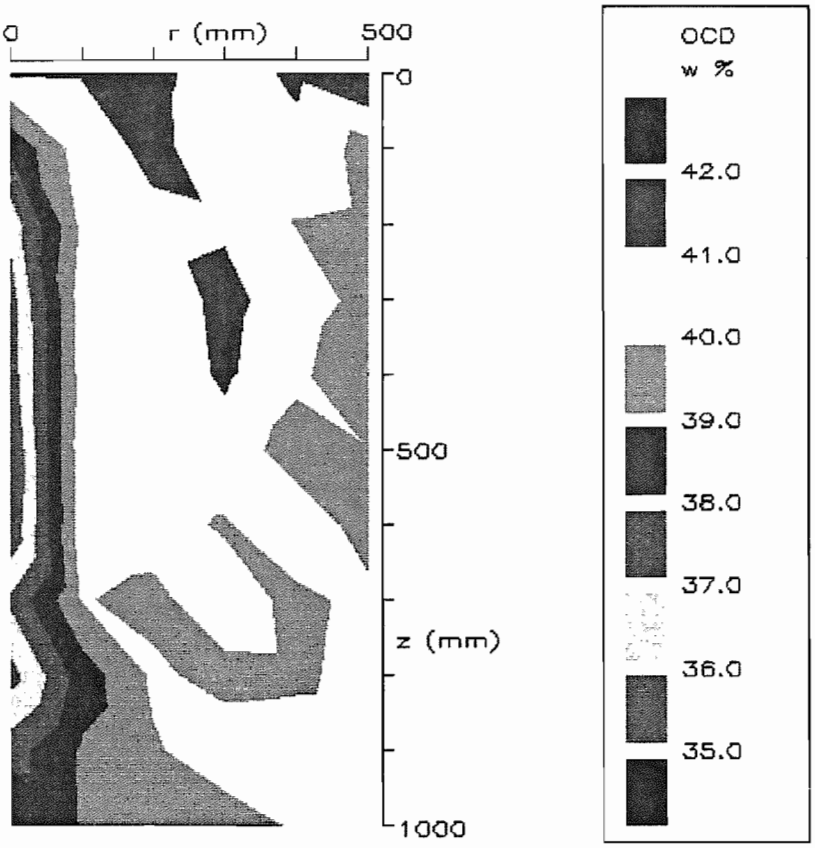


Figure 4.3 Sample OC a) Water content contour plot, and
b) Vane undrained strength contour plot.

a)



b)

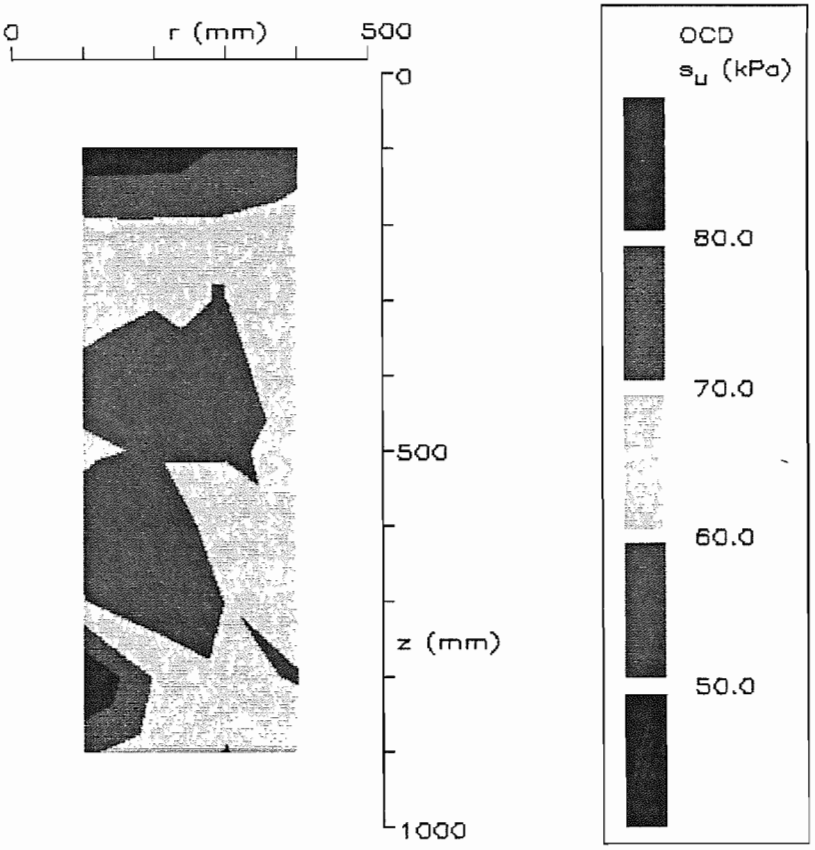
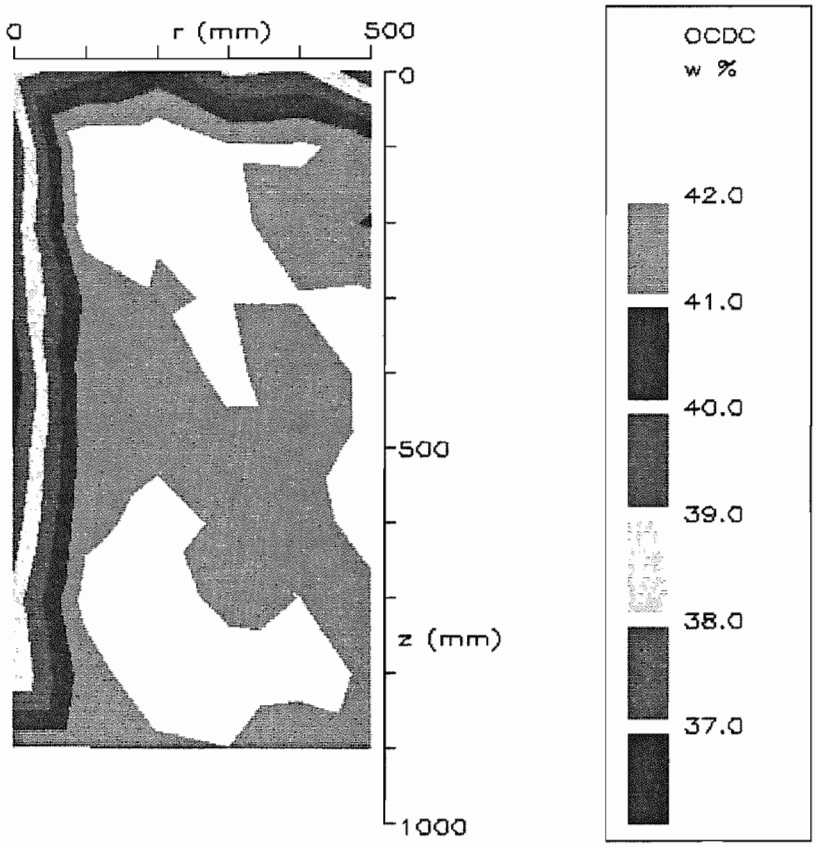


Figure 4.4 Sample OCD a) Water content contour plot, and b) Vane undrained strength contour plot.

a)



b)

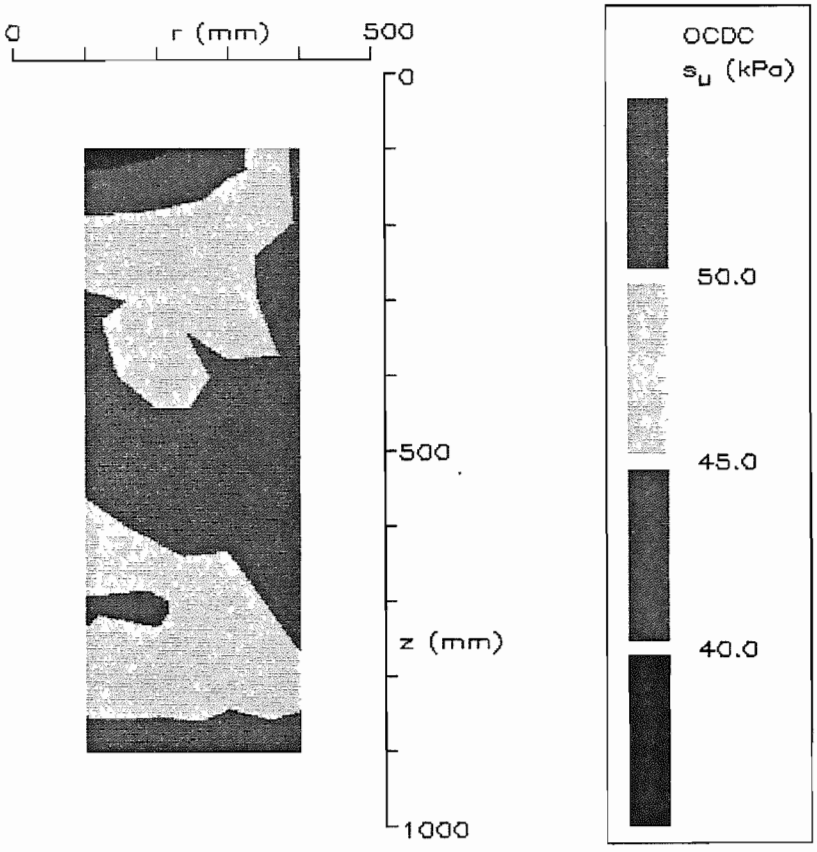
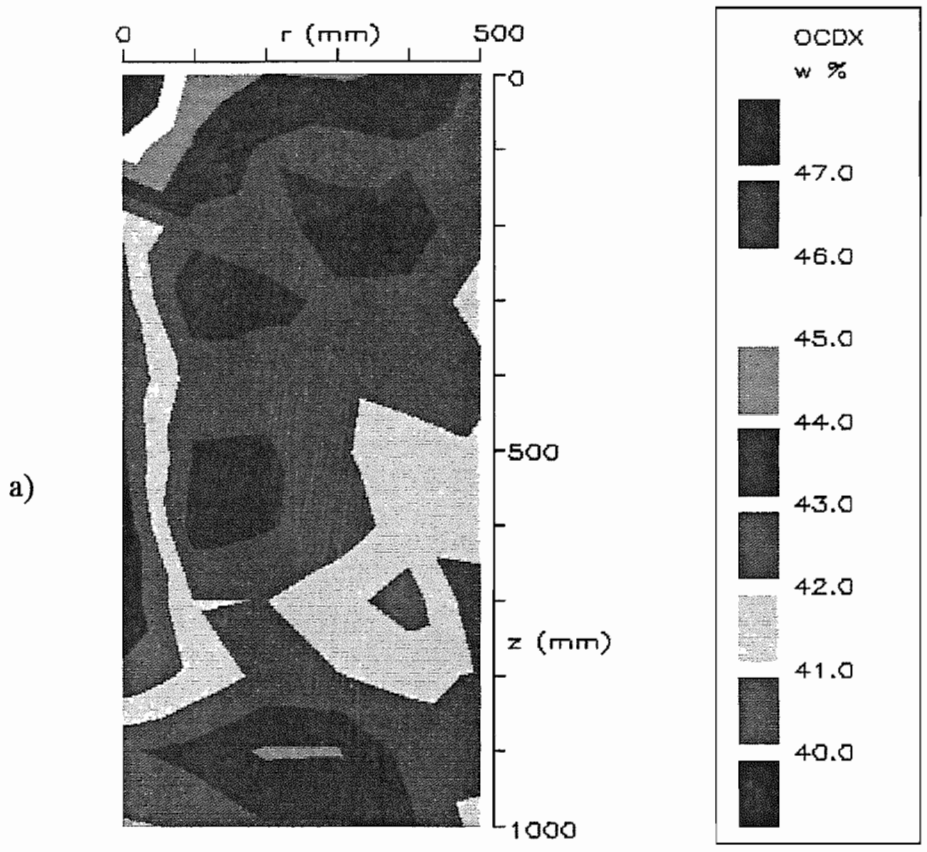


Figure 4.5 Sample OCDC a) Water content contour plot, and b) Vane undrained strength contour plot.



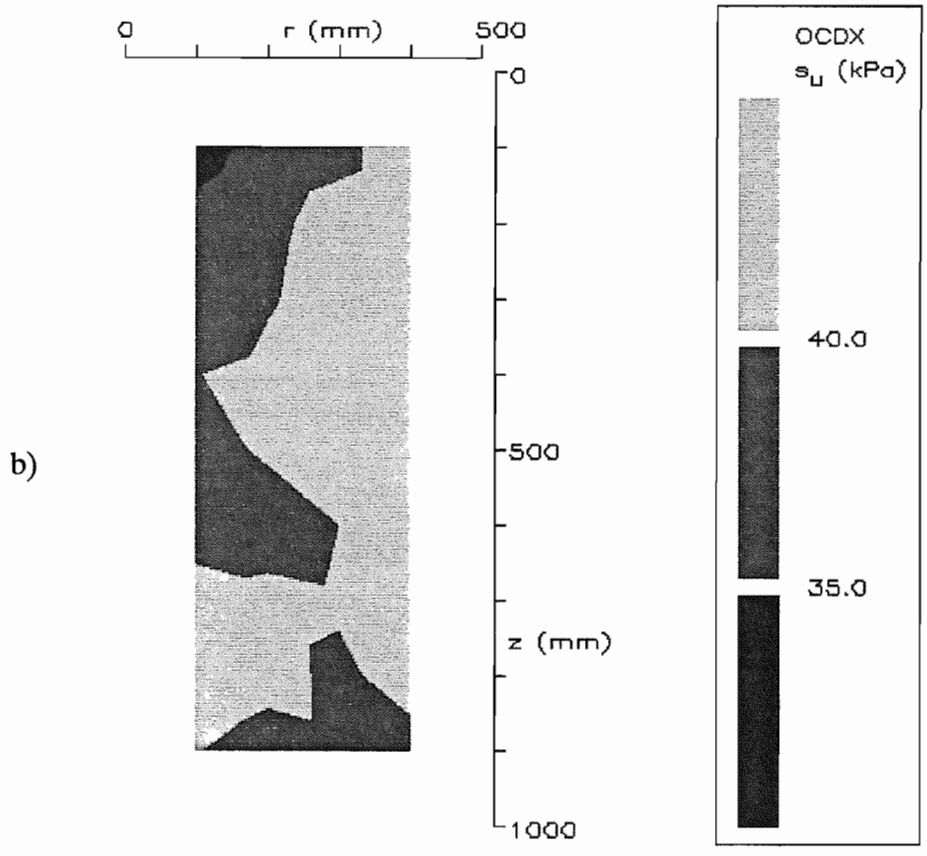
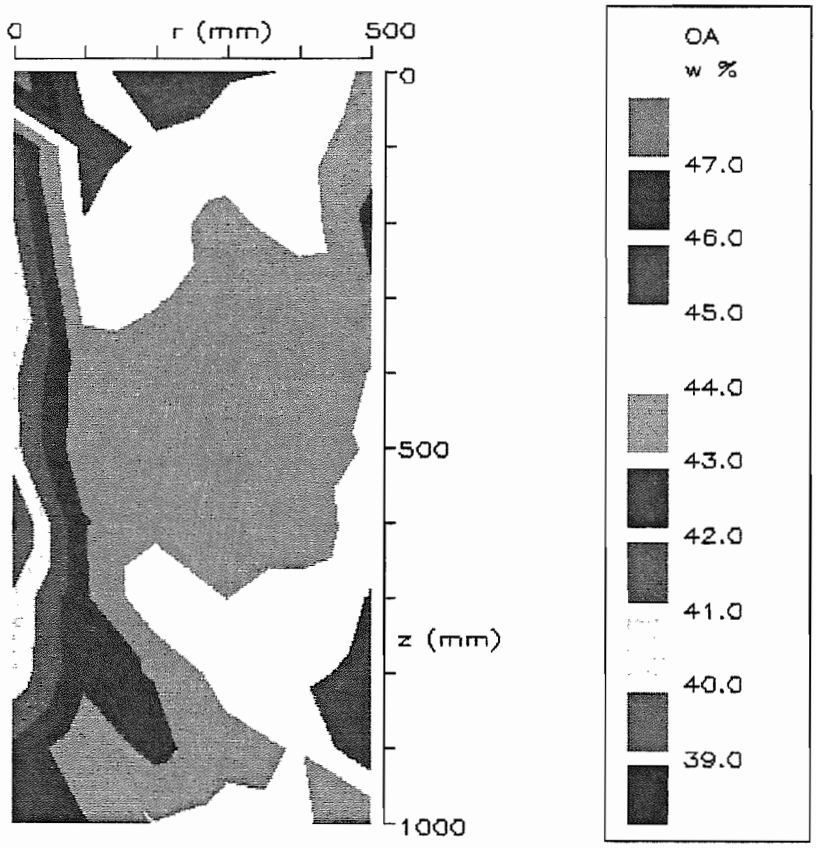


Figure 4.6 Sample OCDX a) Water content contour plot, and b) Vane undrained strength contour plot.

a)



b)

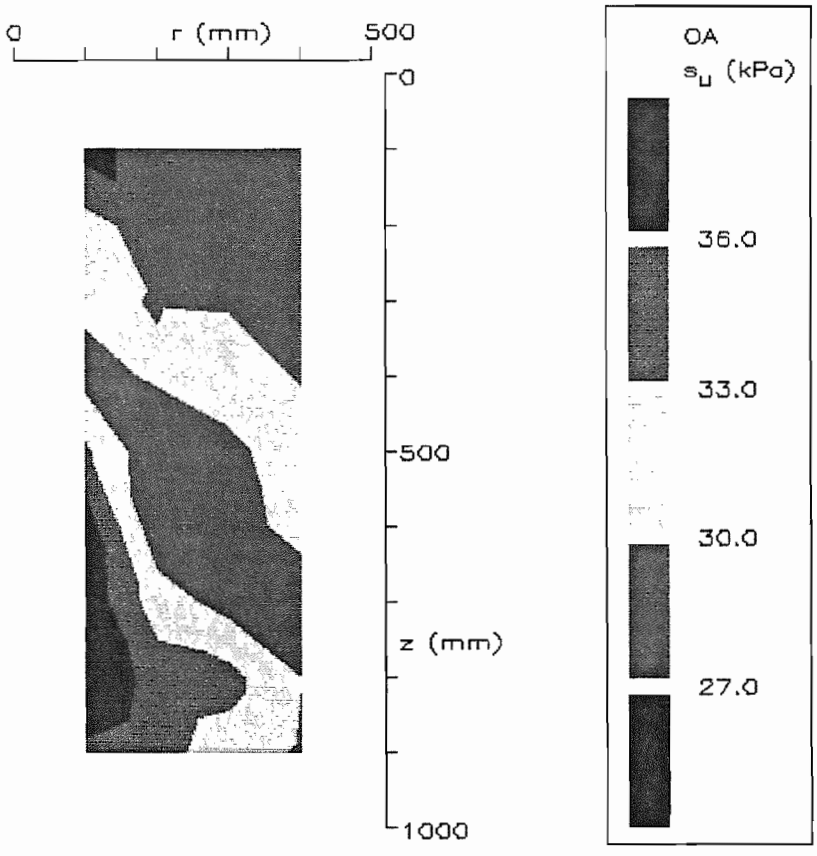
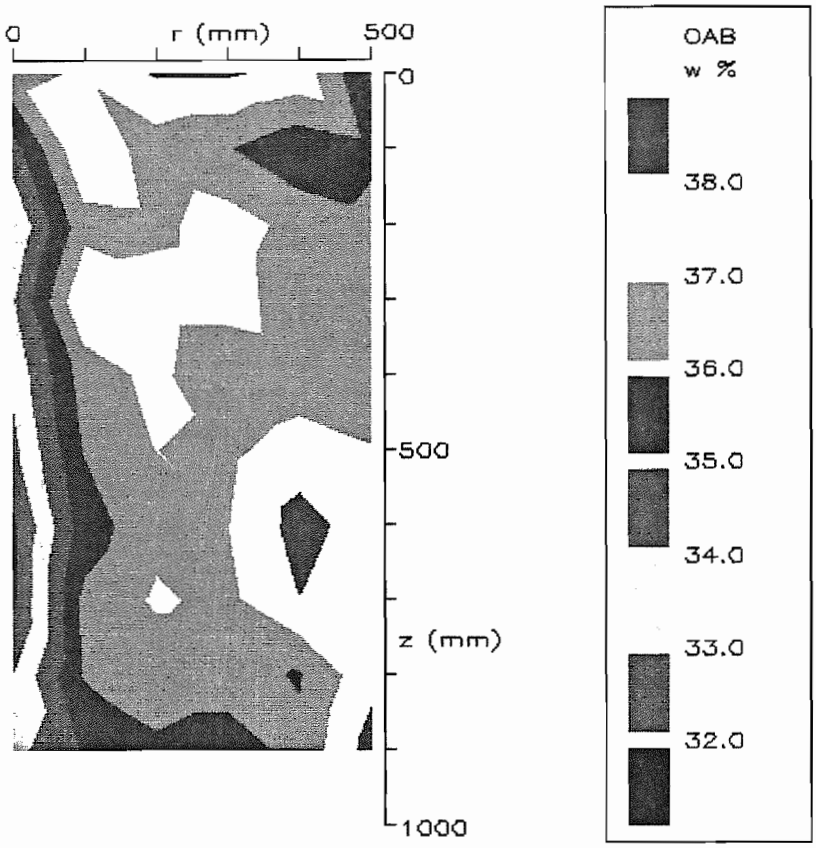


Figure 4.7 Sample OA a) Water content contour plot, and
b) Vane undrained strength contour plot.

a)



b)

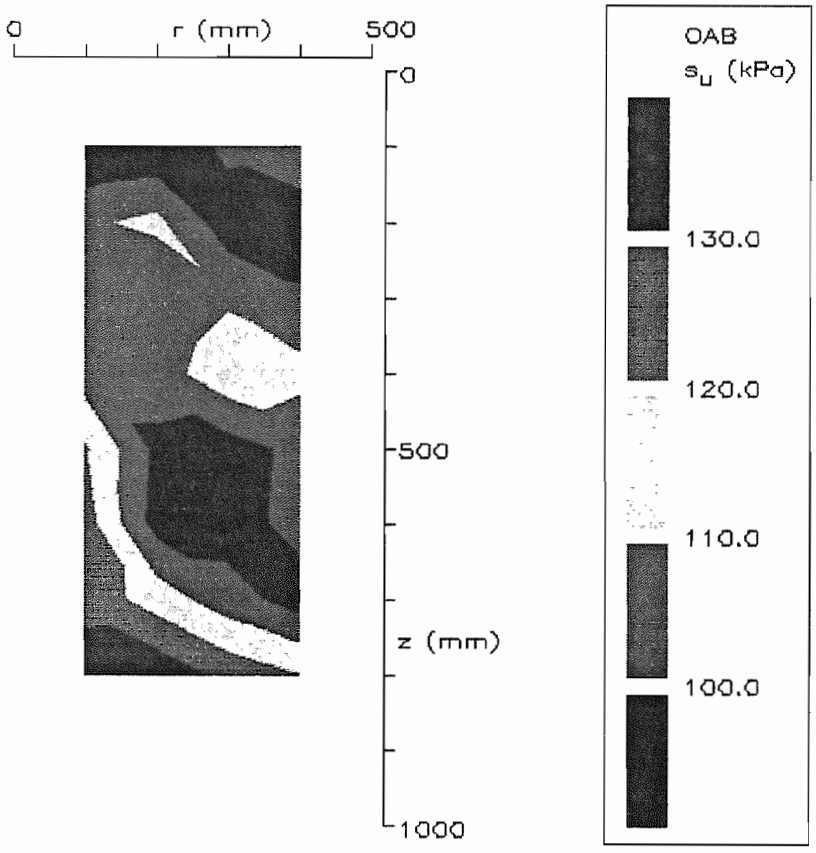
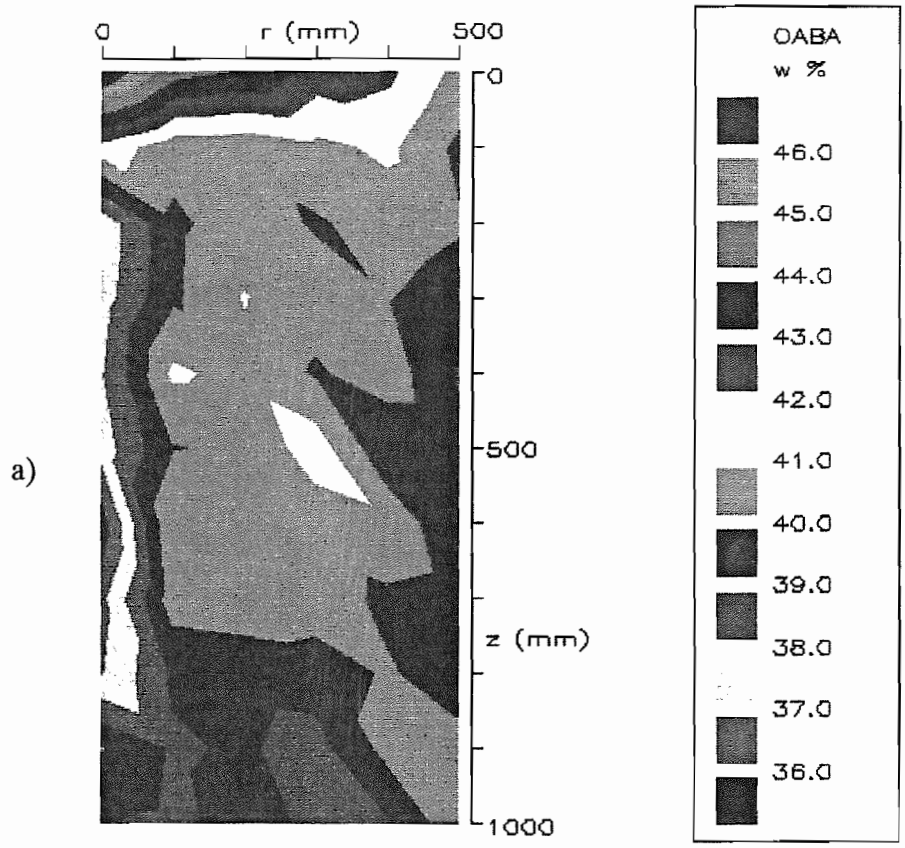


Figure 4.8 Sample OAB a) Water content contour plot, and
b) Vane undrained strength contour plot.



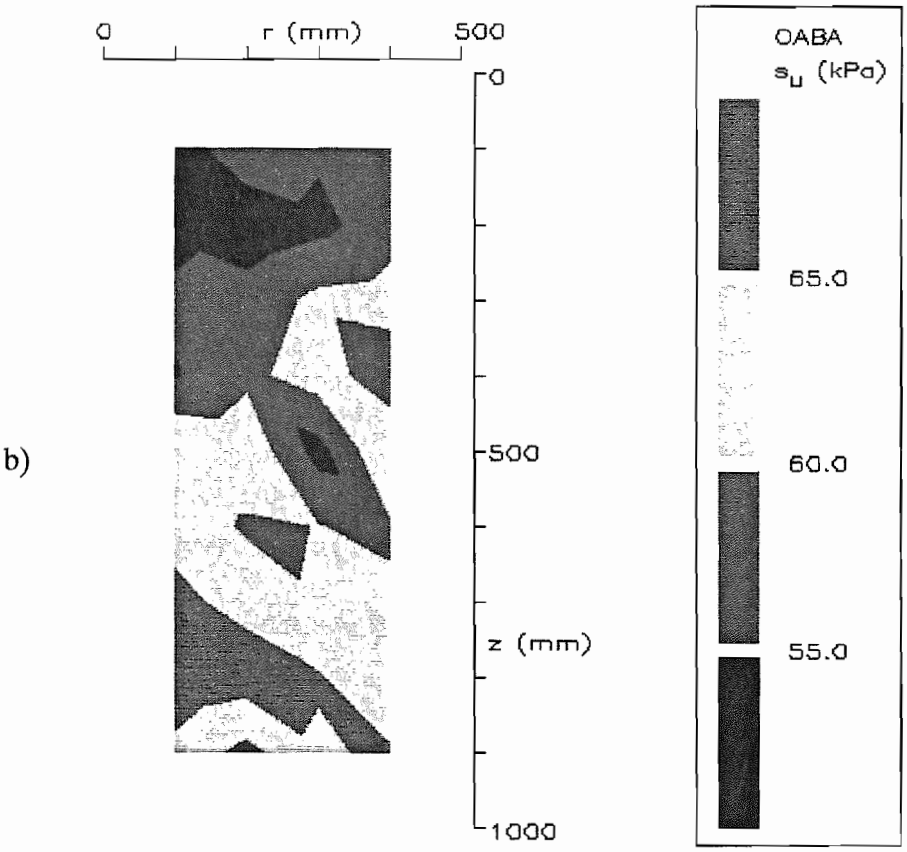
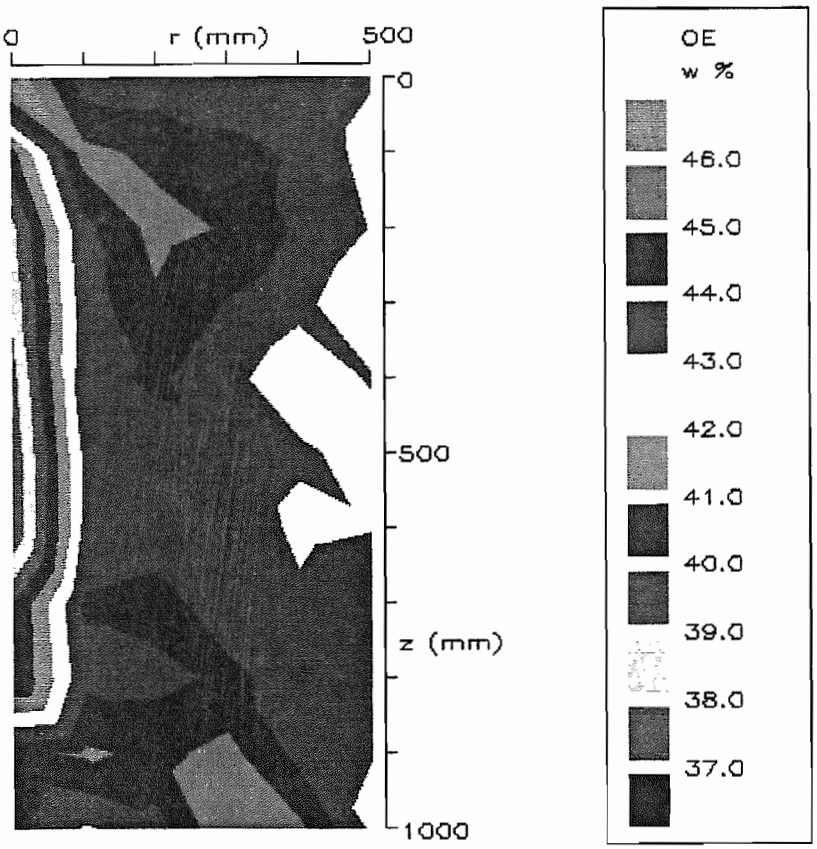


Figure 4.9 Sample OABA a) Water content contour plot, and
b) Vane undrained strength contour plot.

a)



b)

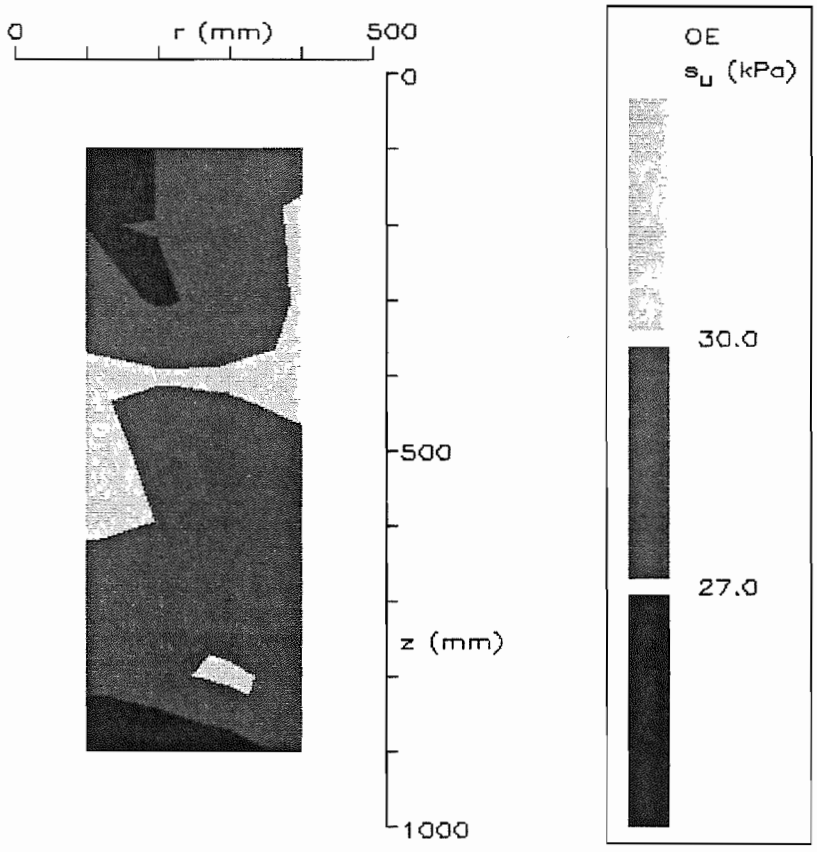
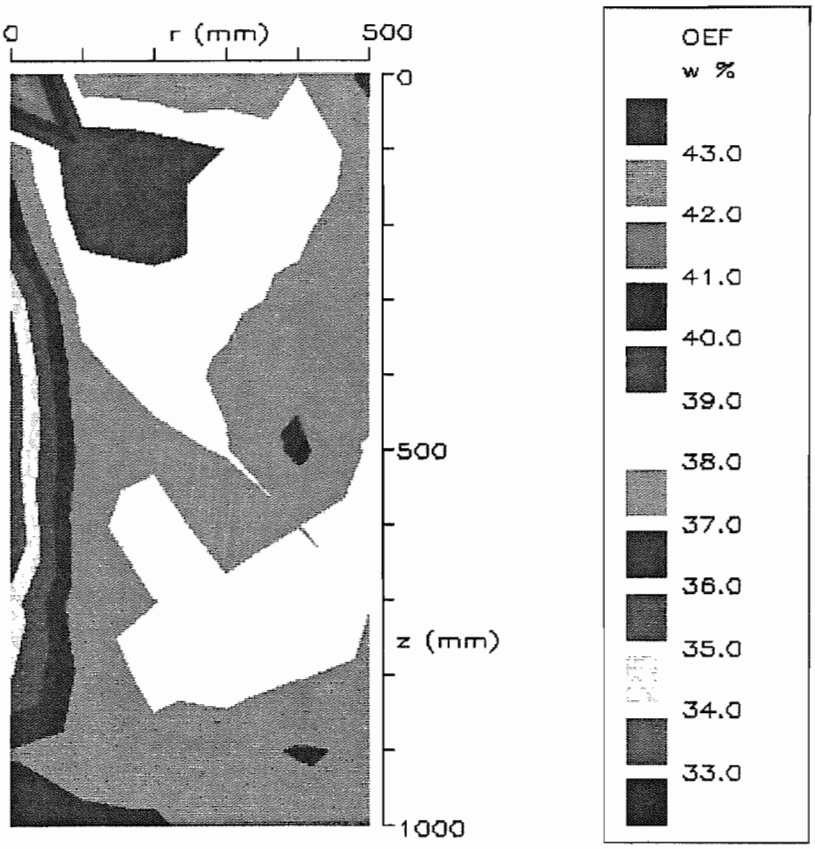


Figure 4.10 Sample OE a) Water content contour plot, and
b) Vane undrained strength contour plot.

a)



b)

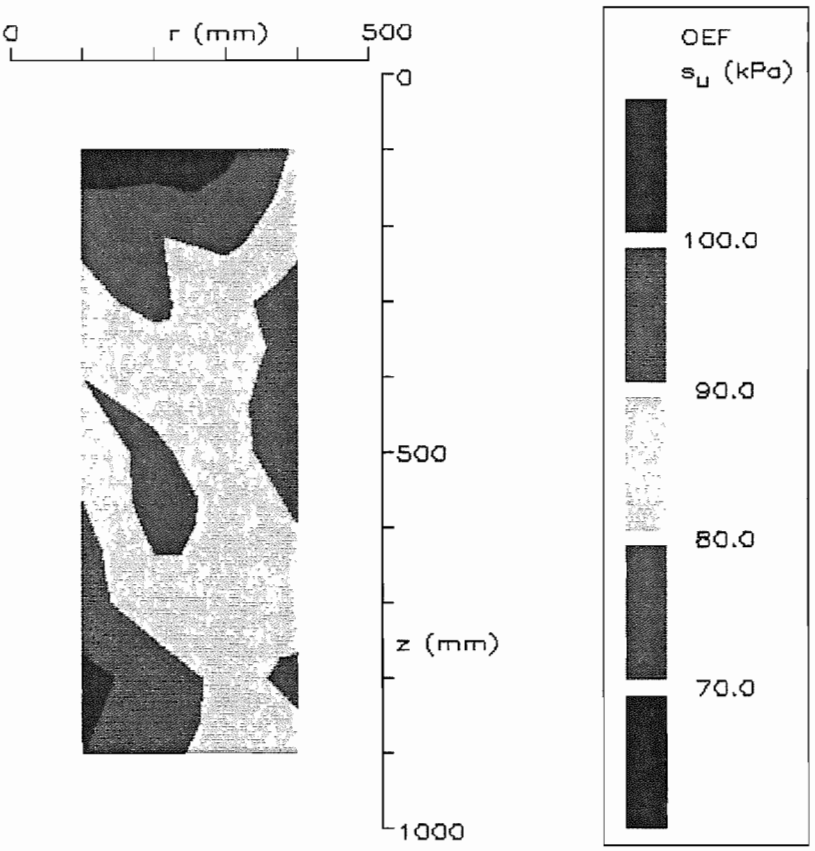


Figure 4.11 Sample OEF a) Water content contour plot, and b) Vane undrained strength contour plot.

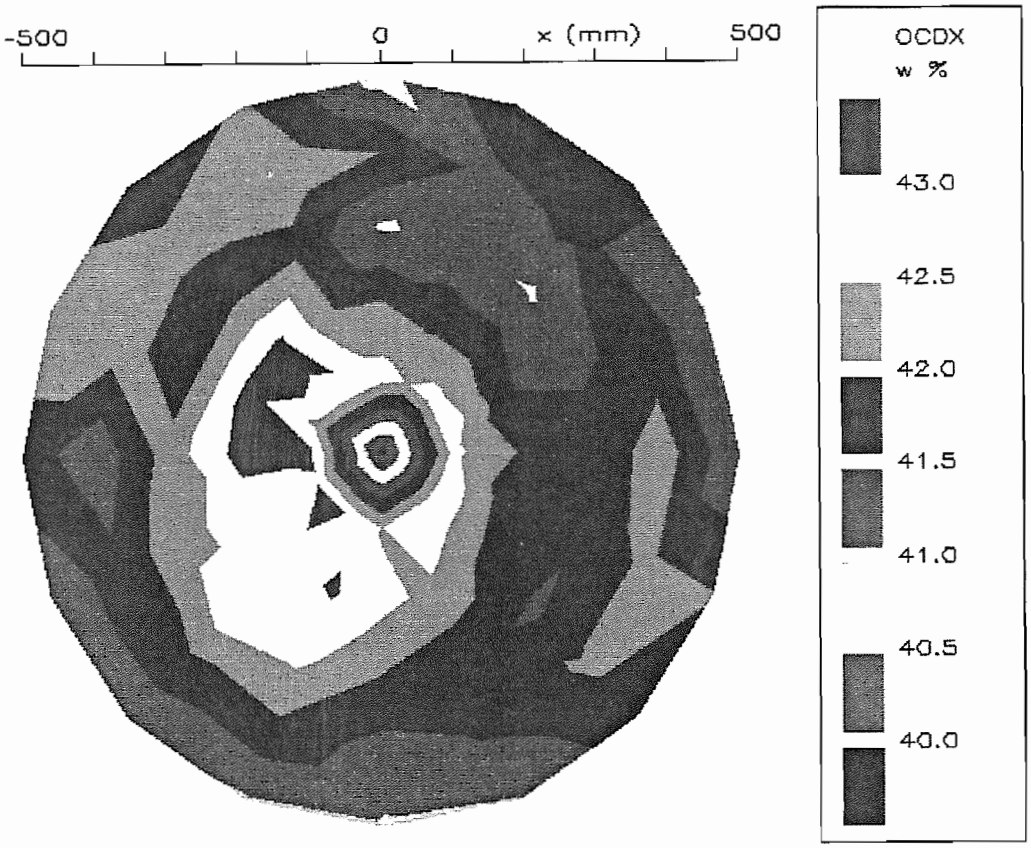


Figure 4.12 Contour plot of water content on plan section through bed OCDX at depth of 500mm.

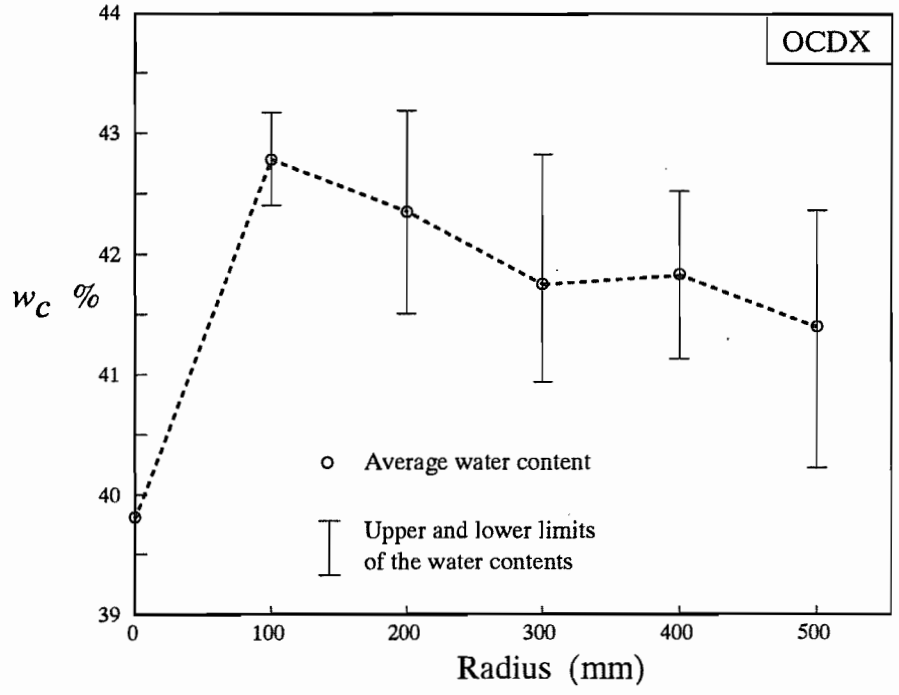


Figure 4.13 Variation of water content with radius for clay bed OCDX.

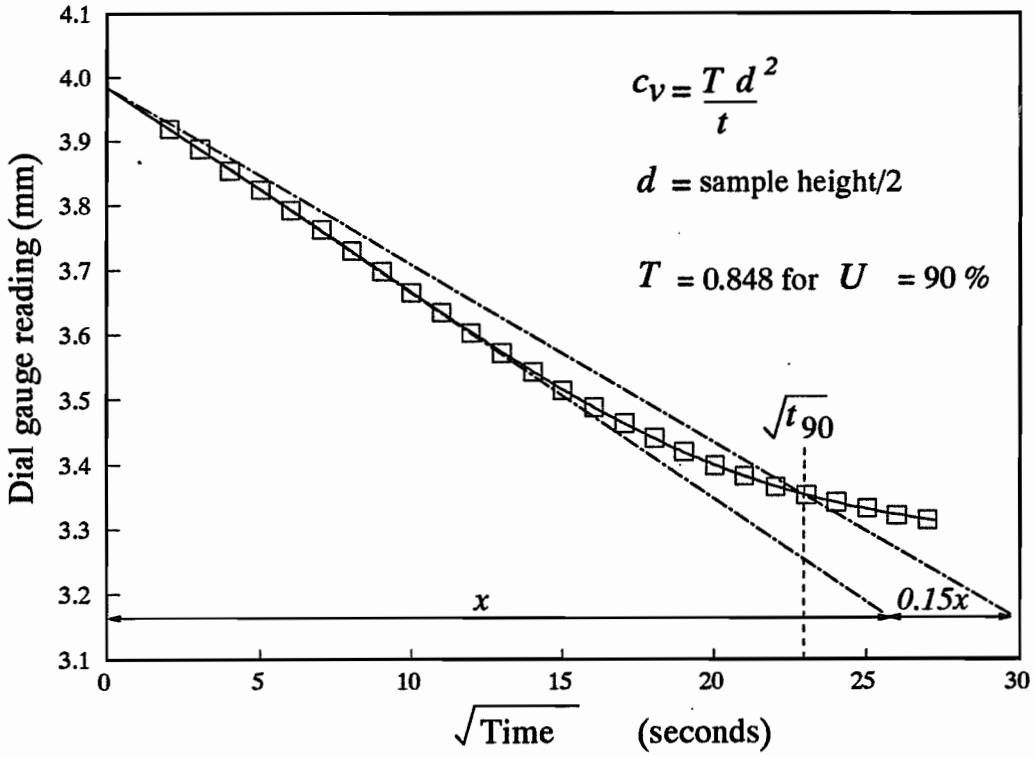


Figure 4.14 Displacement versus the square root of time for a typical oedometer test.

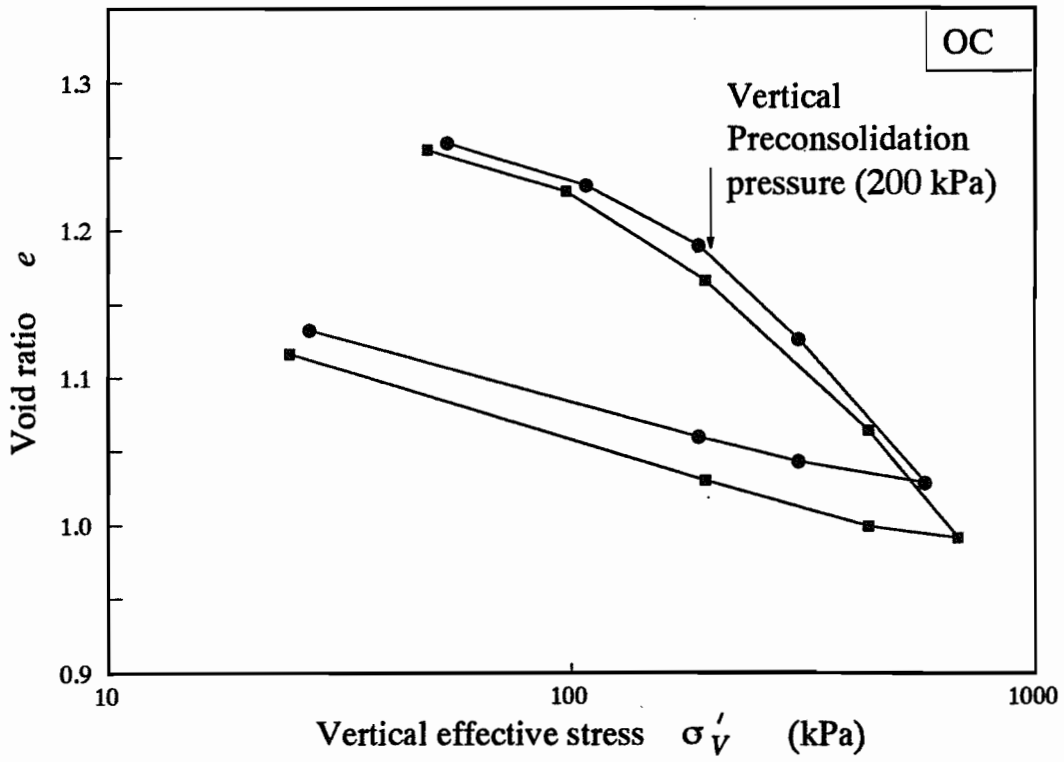


Figure 4.15 Void ratio versus vertical stress curve obtained from oedometer tests on two samples taken from clay bed OC.

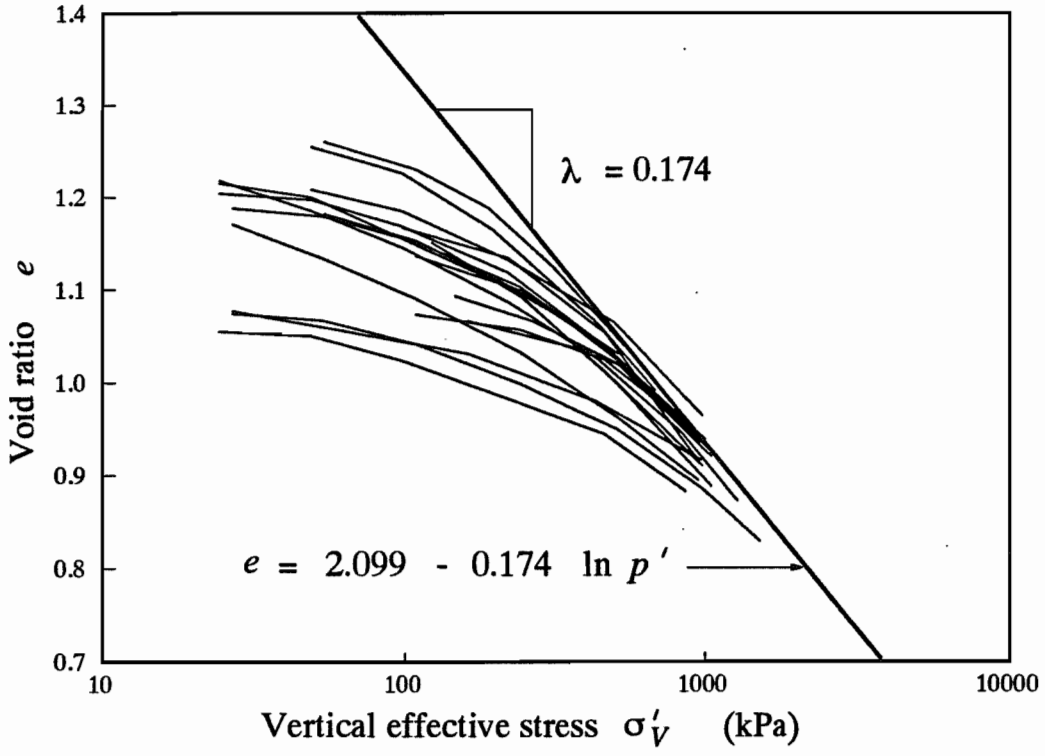


Figure 4.16 Void ratio versus vertical stress for loading portions of all oedometer tests.

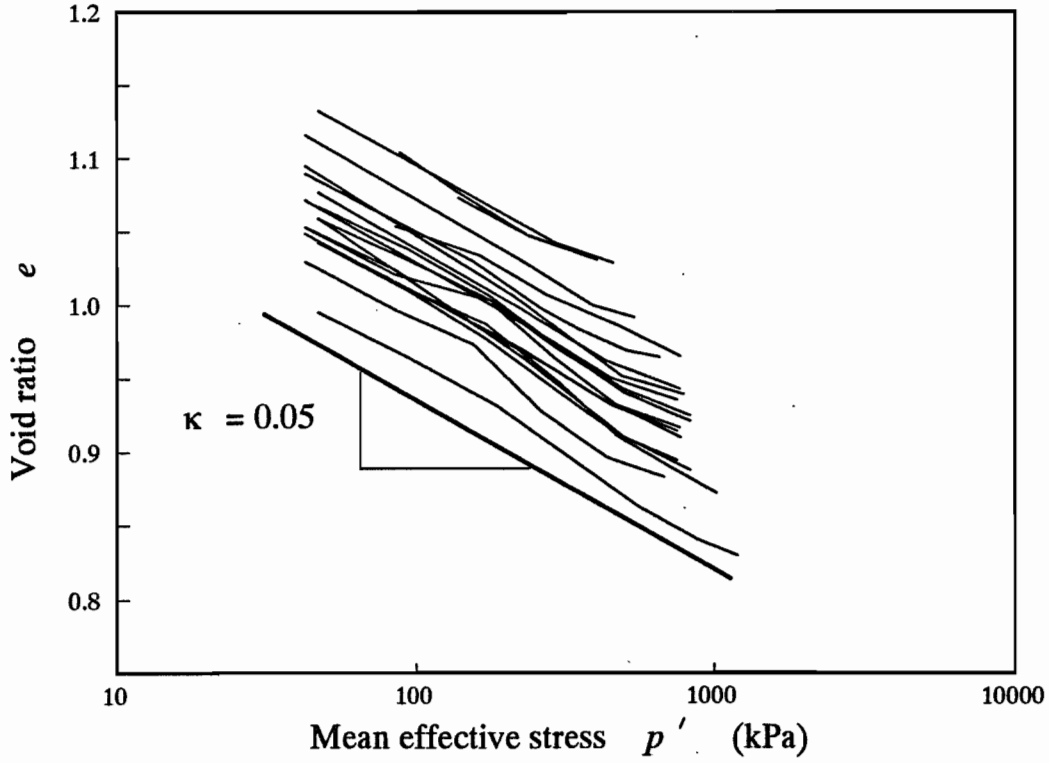


Figure 4.17 Void ratio versus mean stress for unloading portions of all oedometer tests.

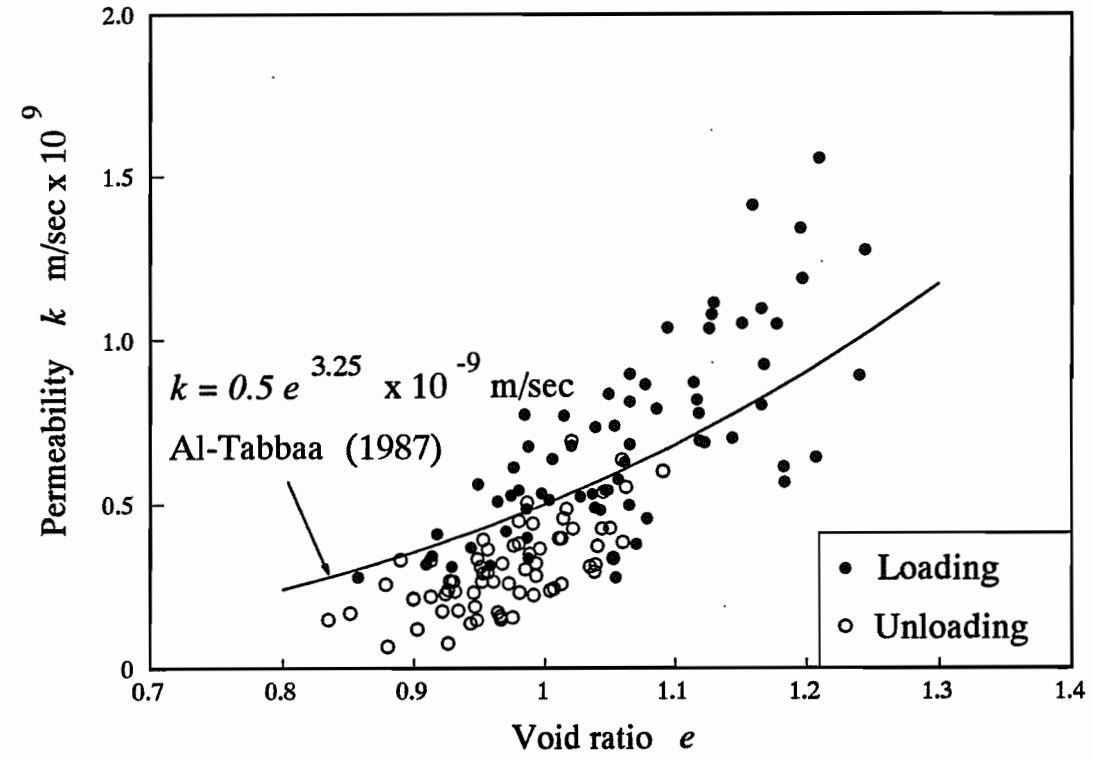


Figure 4.18 Void ratio and permeability derived from oedometer tests.

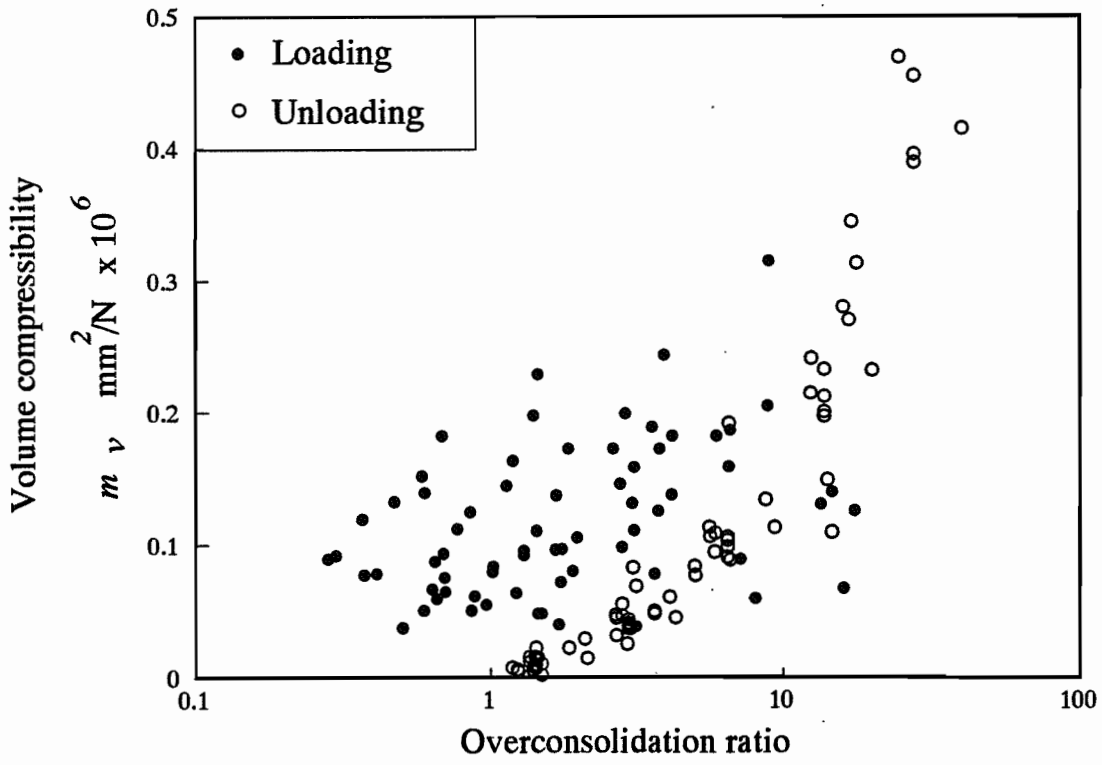


Figure 4.19 Coefficient of volume compressibility versus overconsolidation ratio.

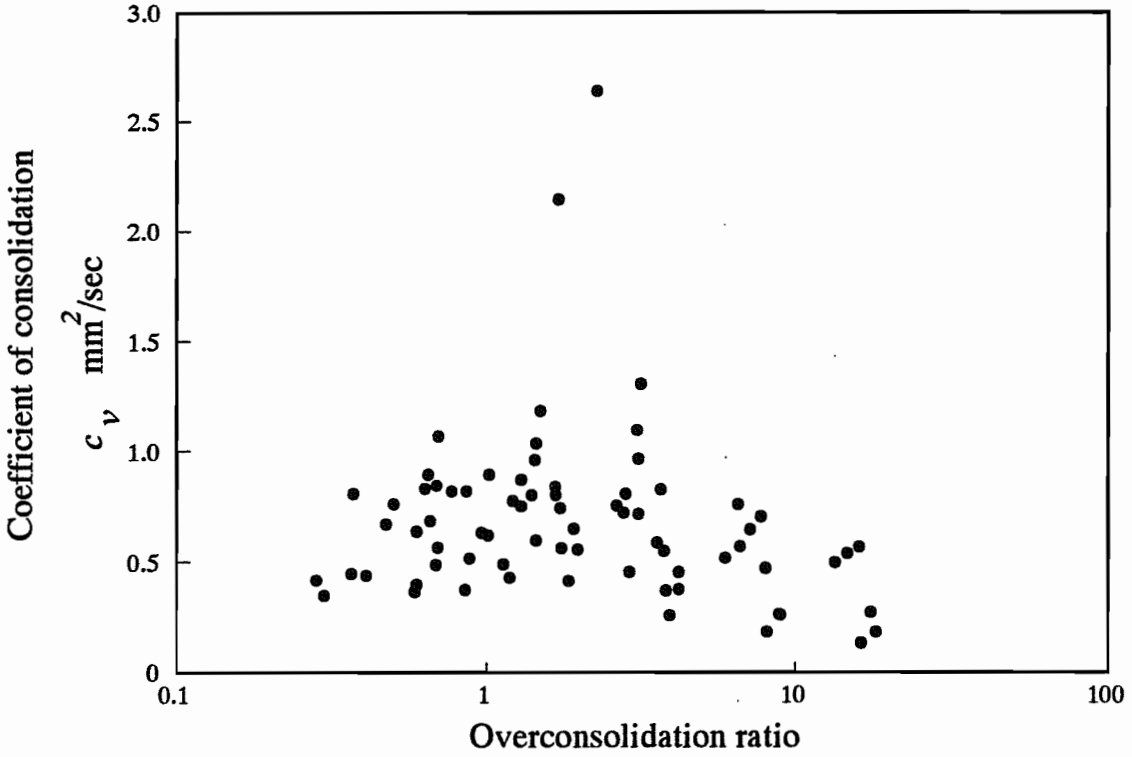


Figure 4.20 Coefficient of consolidation versus overconsolidation ratio.

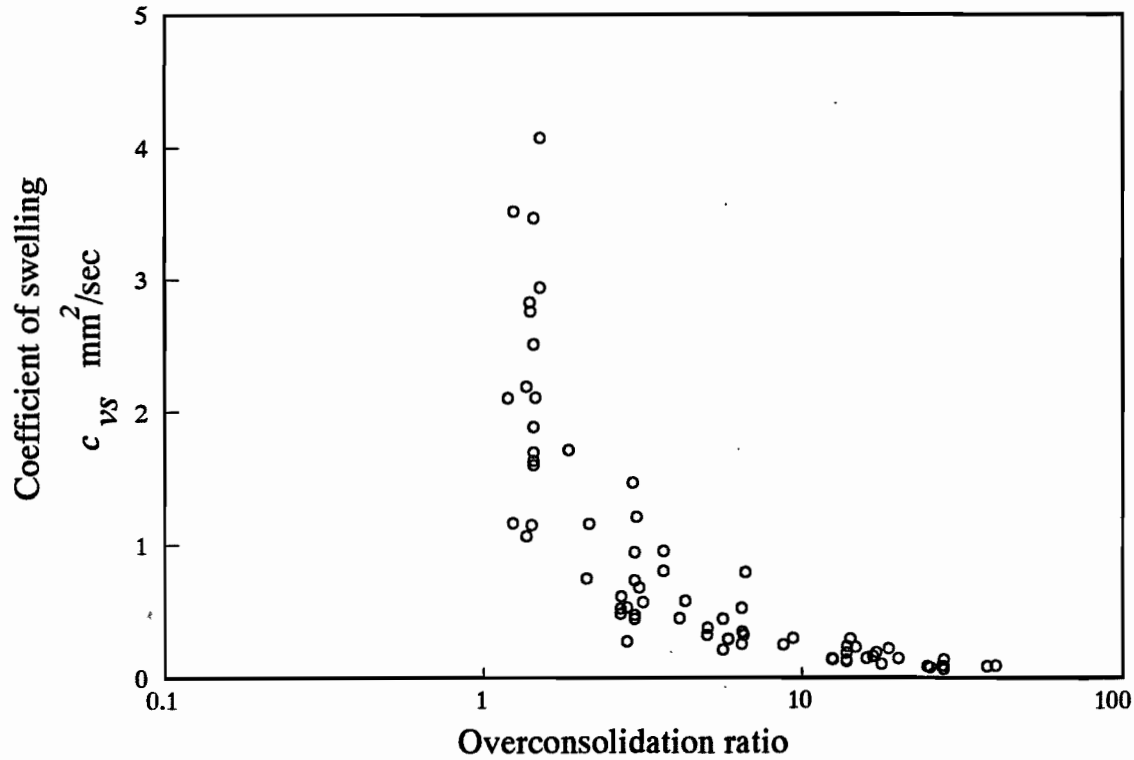


Figure 4.21 Coefficient of swelling versus overconsoldation ratio.

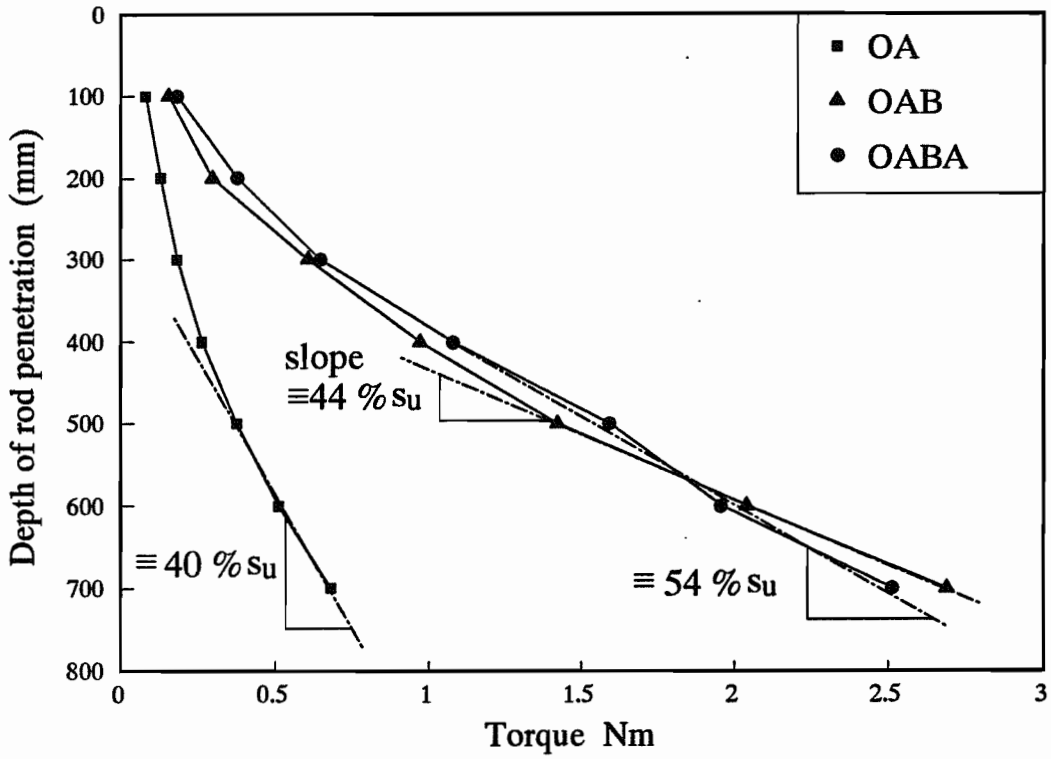


Figure 4.22 Rod friction measured in clay beds OA, OAB and OABA.

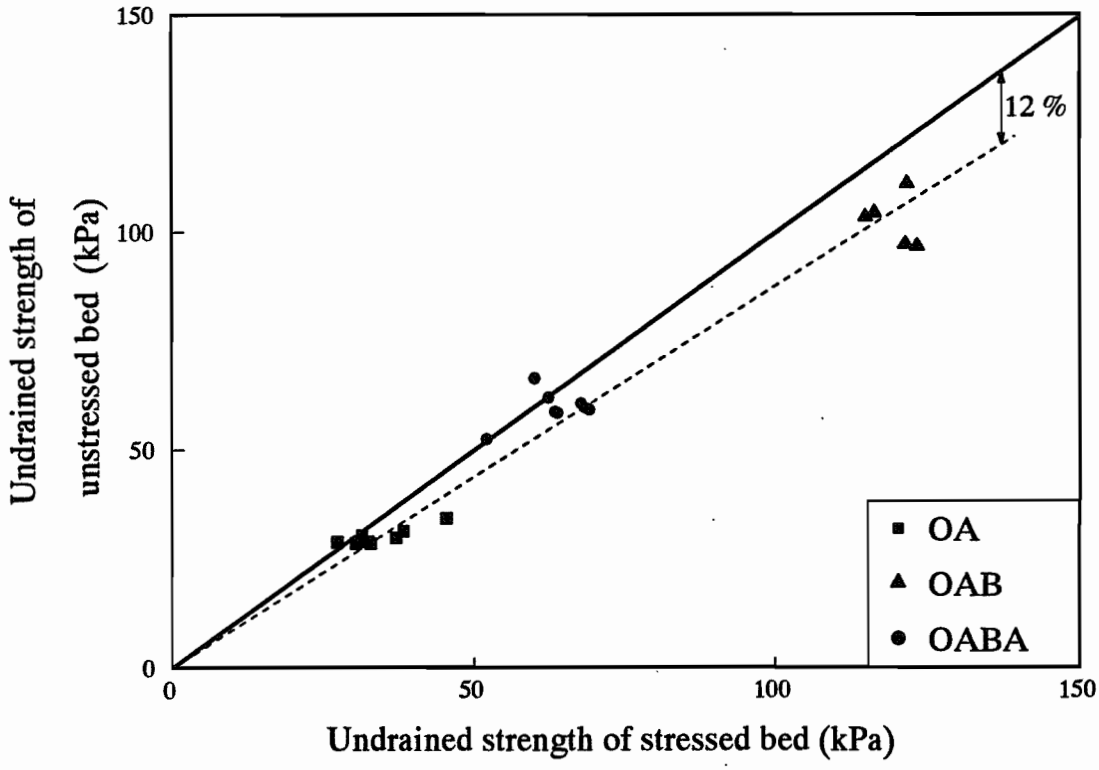


Figure 4.23 Undrained strengths measured with vane in stressed and unstressed clay beds.

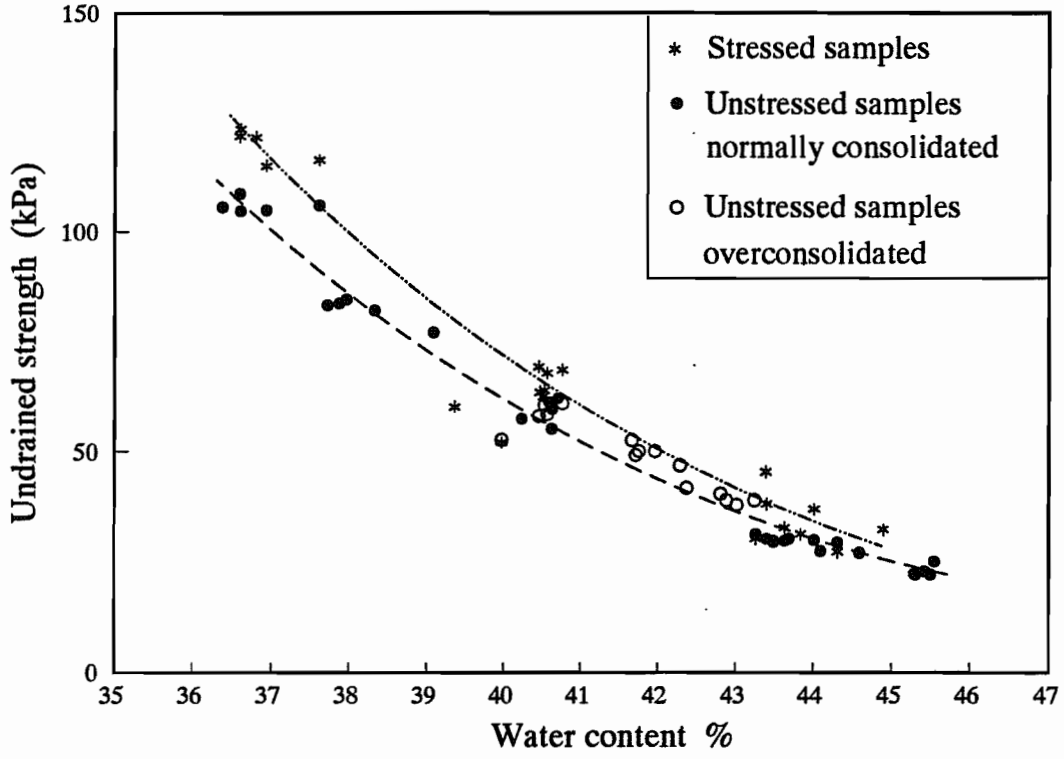


Figure 4.24 Vane undrained strengths versus water content.

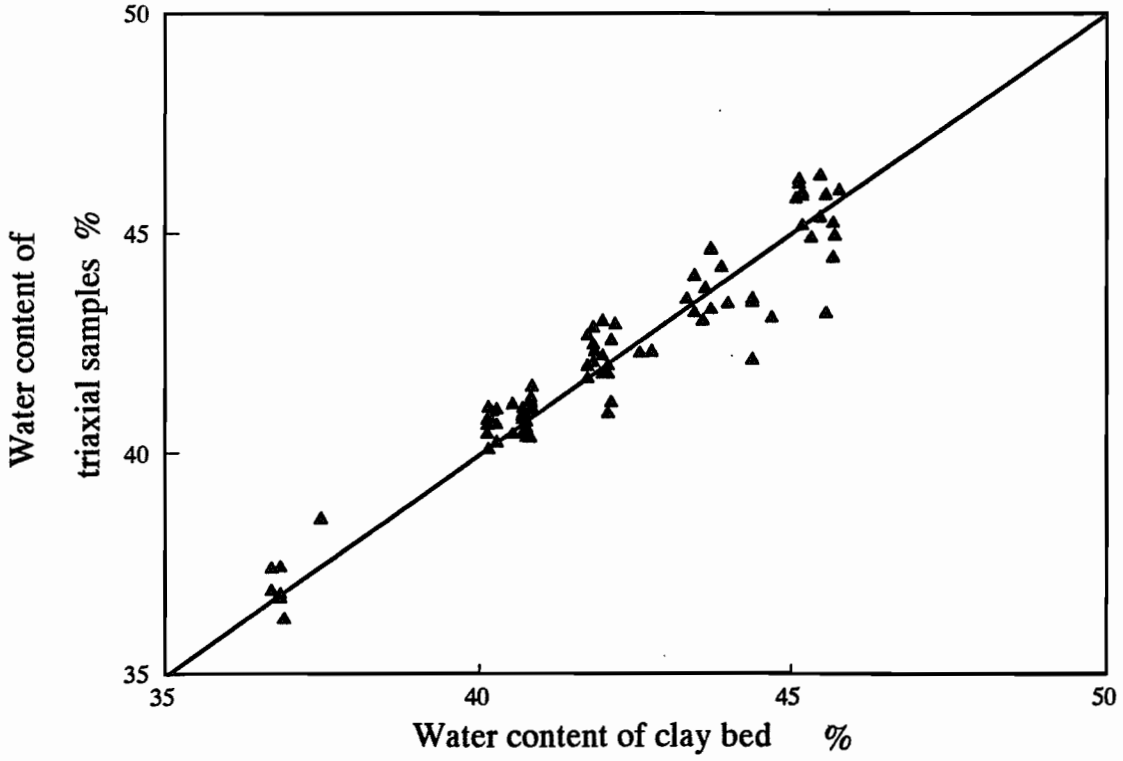


Figure 4.25 Comparison of water content of triaxial samples before and after storage.

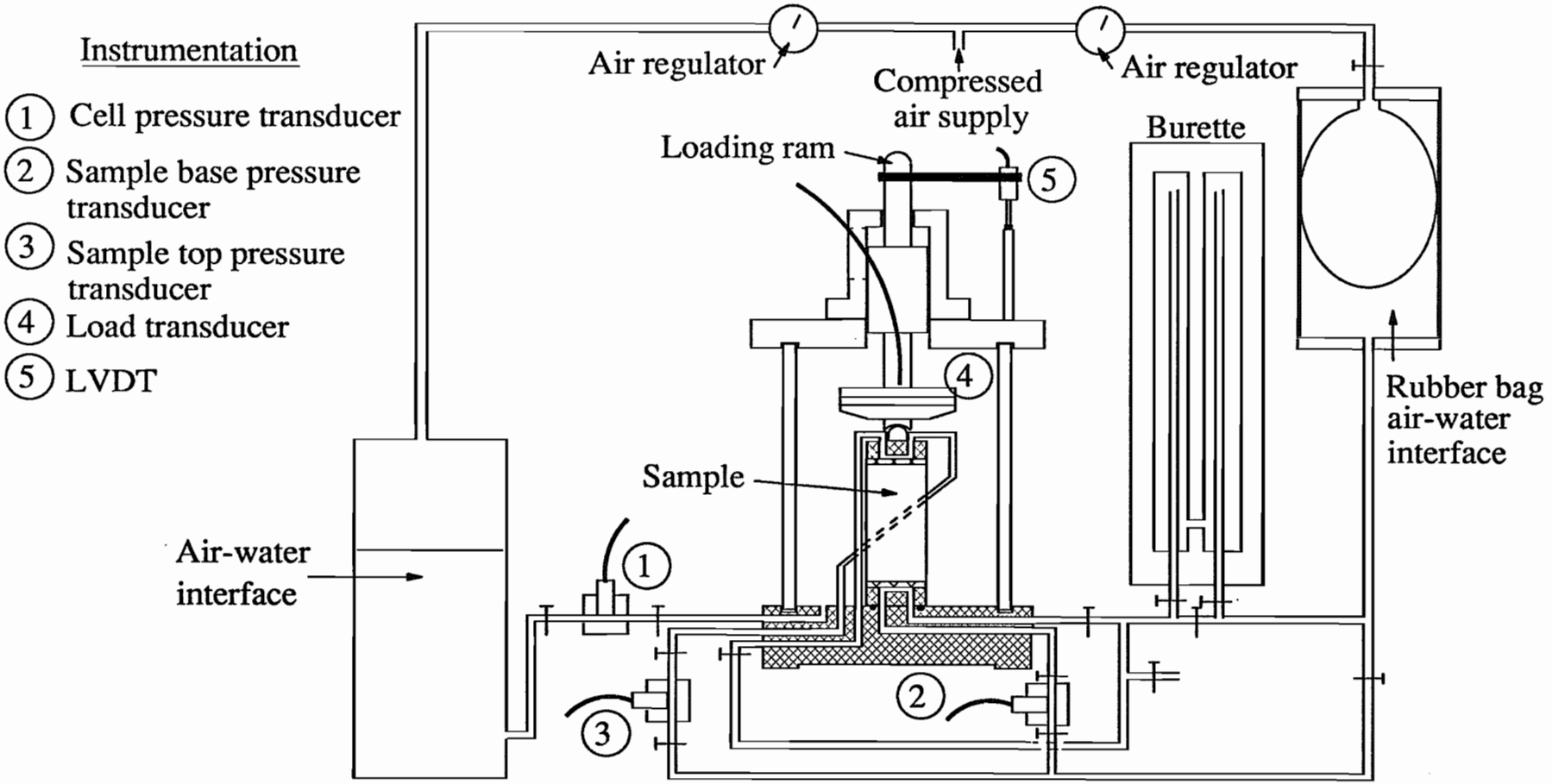


Figure 4.26 Triaxial testing apparatus

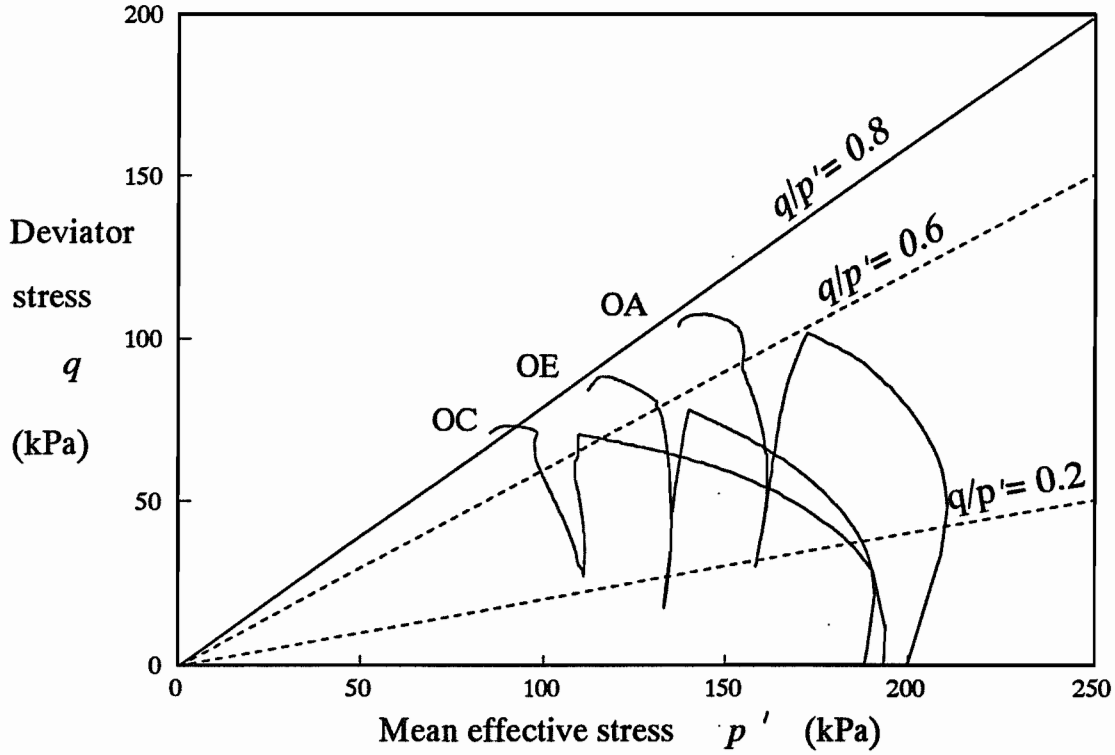


Figure 4.27 Stress paths from triaxial tests on samples taken from clay beds OA, OC and OE.

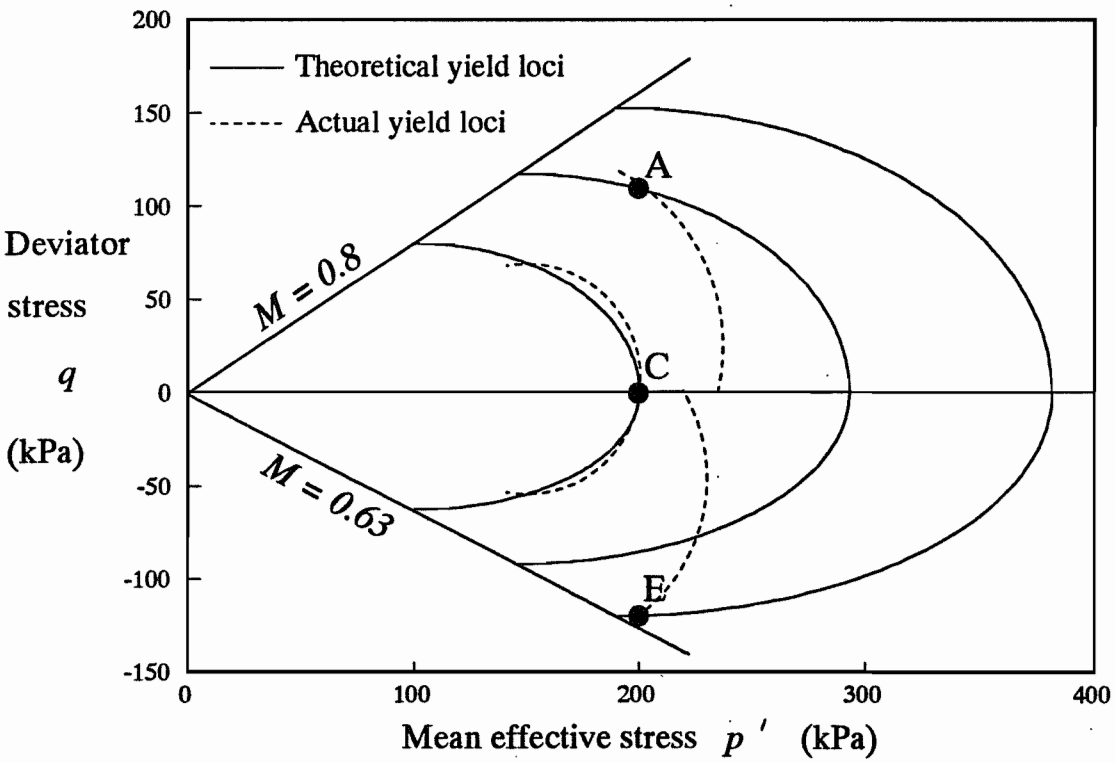


Figure 4.28 Comparison of actual and theoretical yield loci.

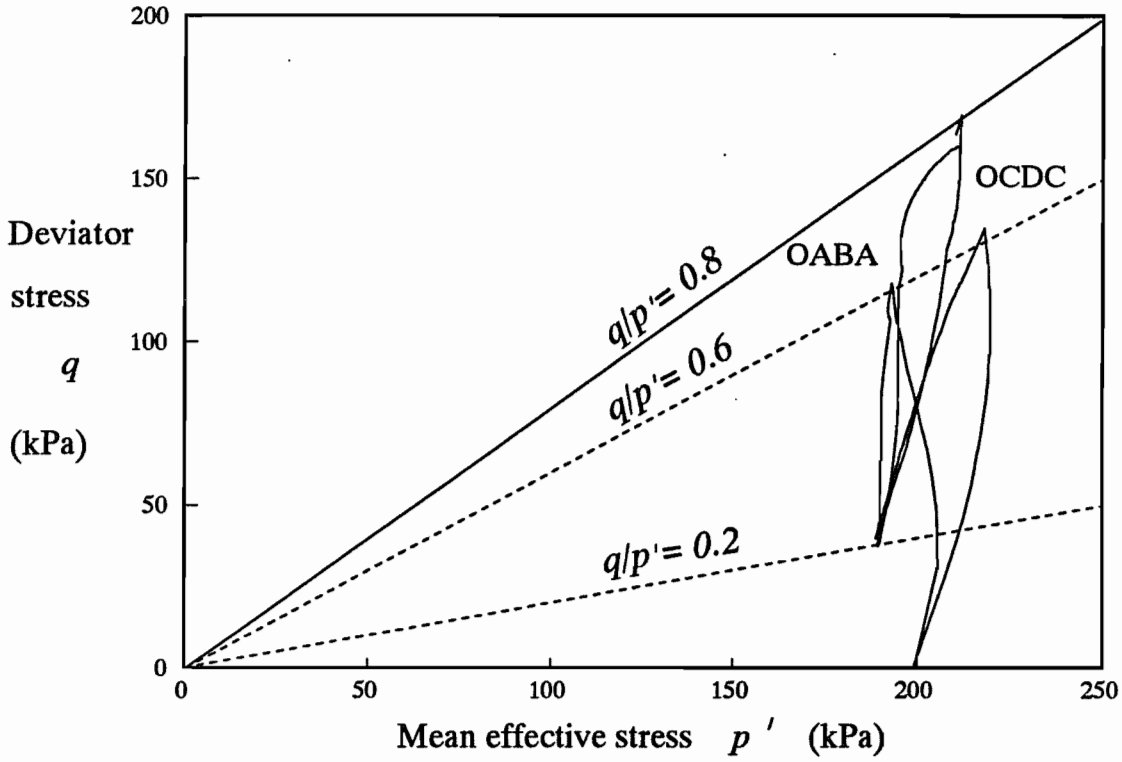


Figure 4.29 Stress paths from triaxial tests on samples taken from clay beds OCDC and OABA.

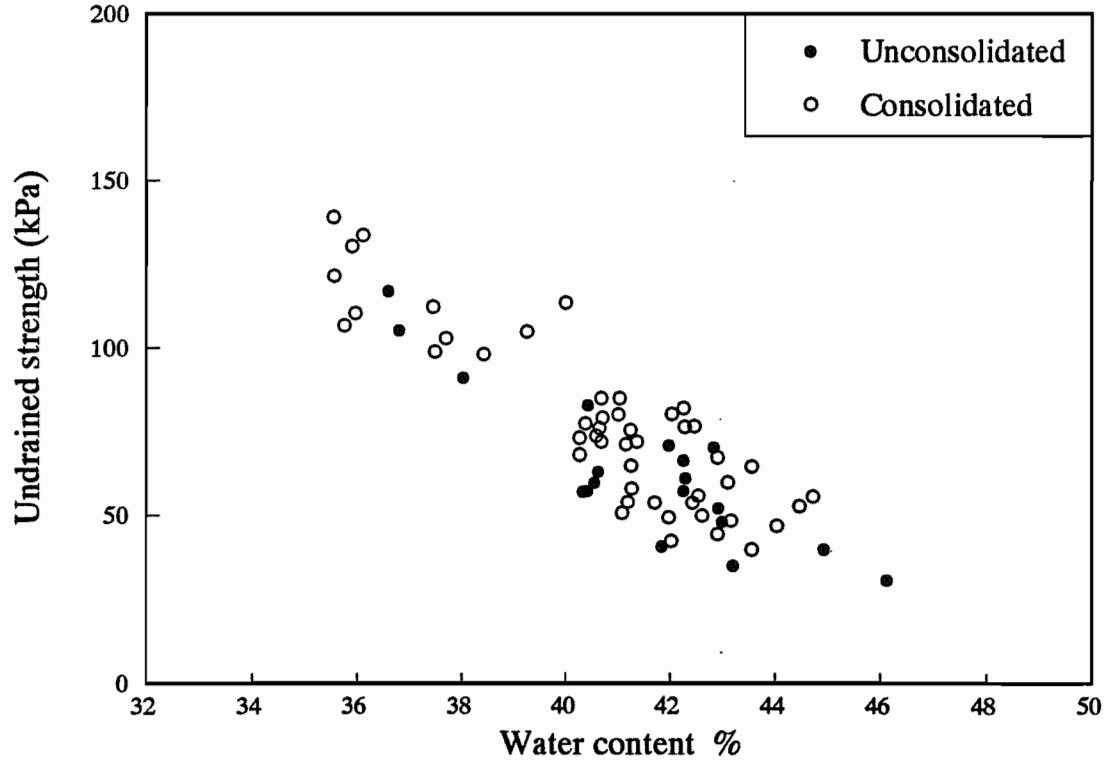


Figure 4.30 Undrained strength from unconsolidated and consolidated triaxial tests versus water content.

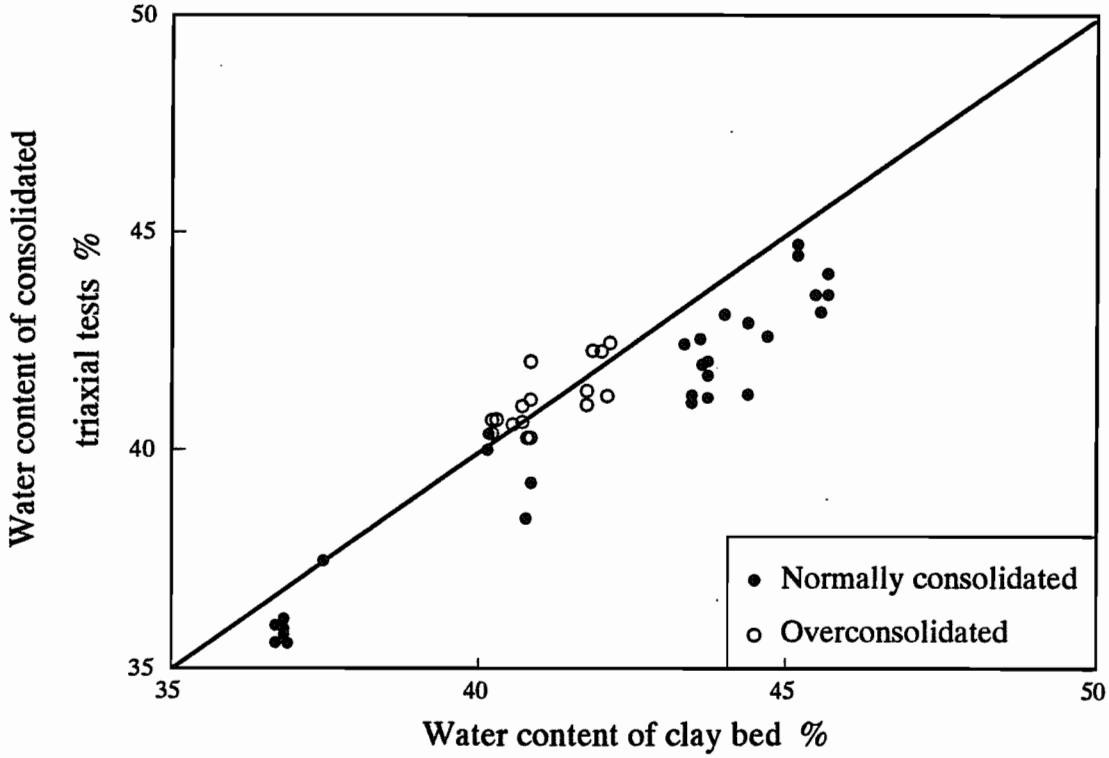


Figure 4.31 Reduction in water content during reconsolidation of triaxial samples.

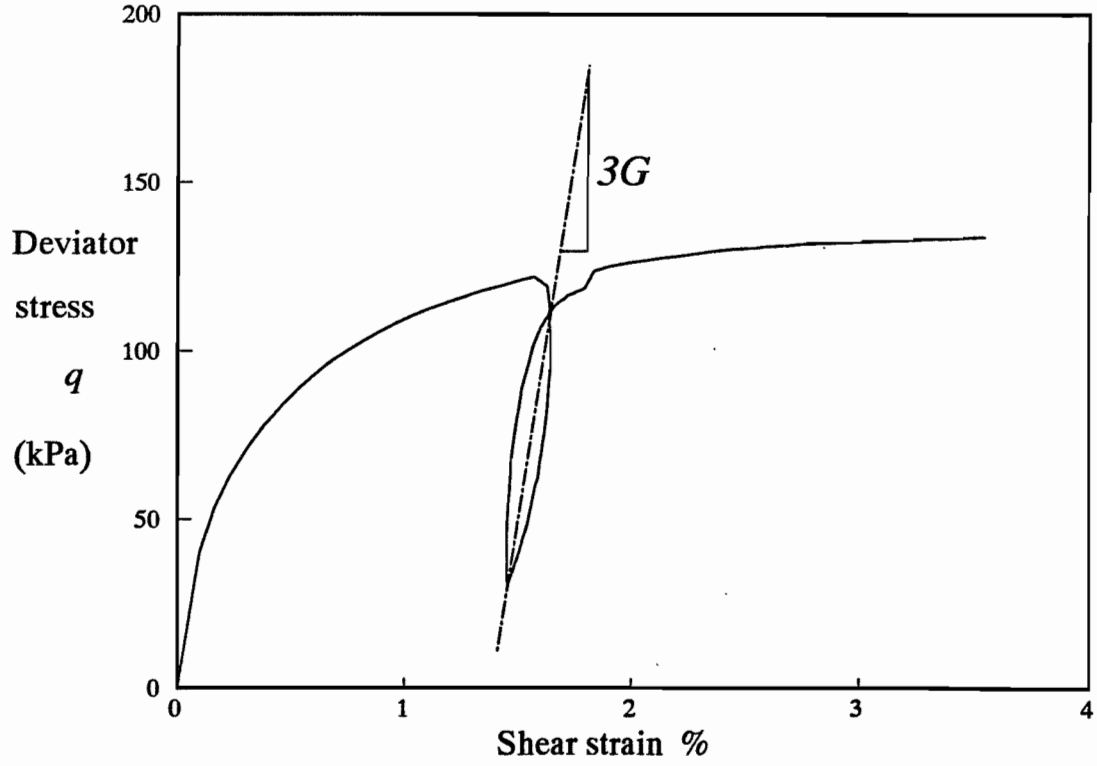


Figure 4.32 Shear stress-shear strain curve during triaxial test with an unload-reload loop.

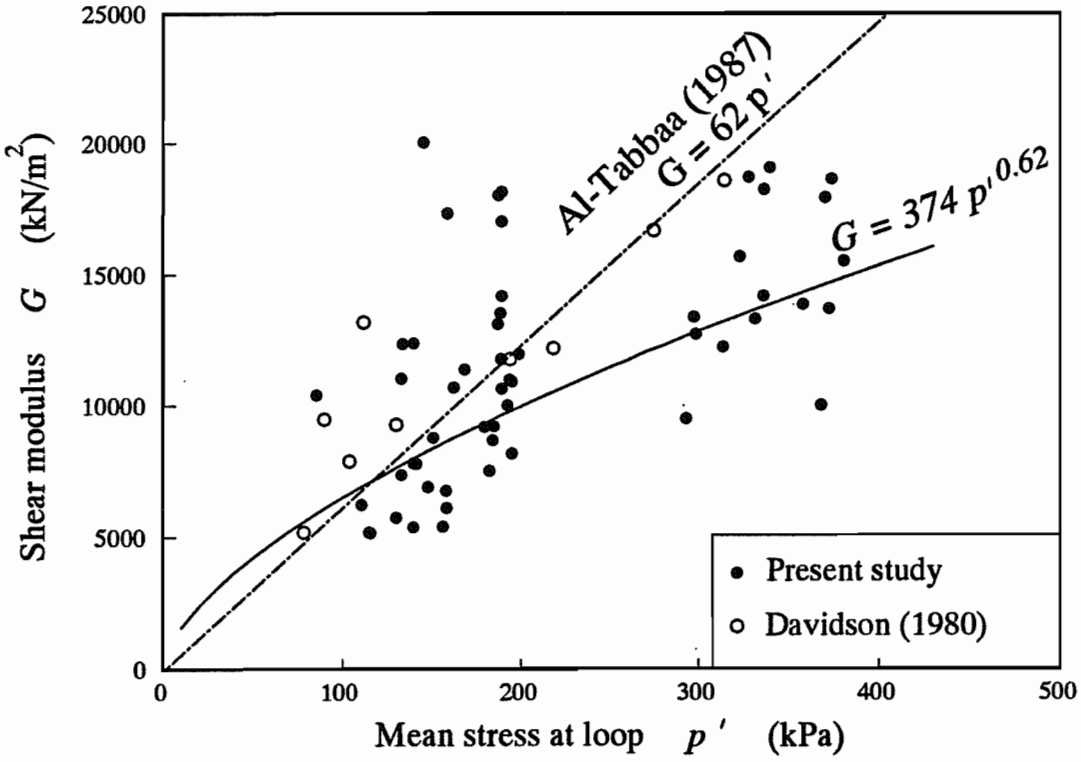


Figure 4.33 Shear modulus versus mean stress at unload-reload loop.

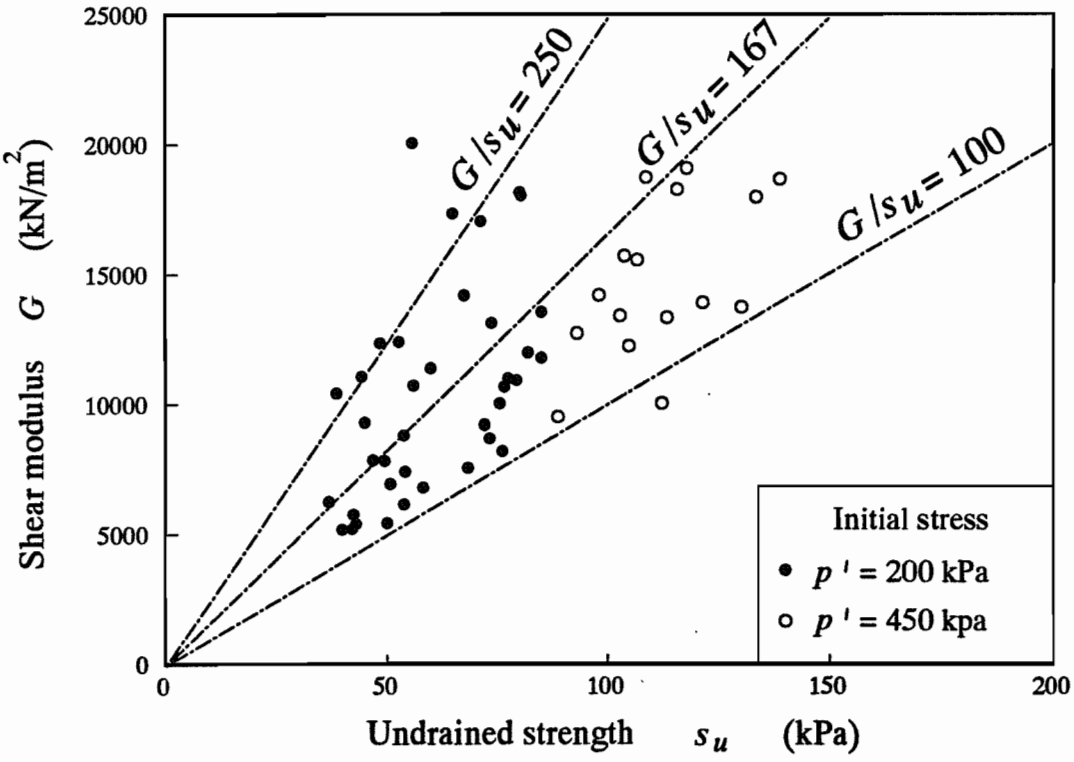


Figure 4.34 Shear modulus versus undrained strength.

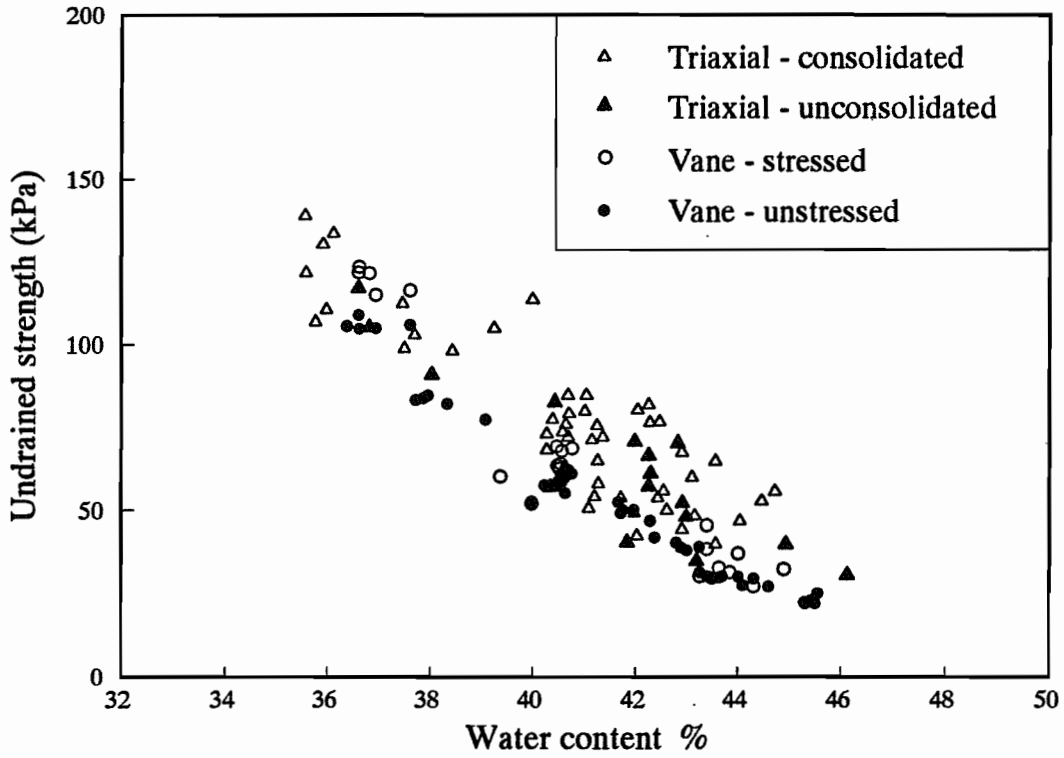


Figure 4.35 Summary of undrained strengths and the corresponding water content.

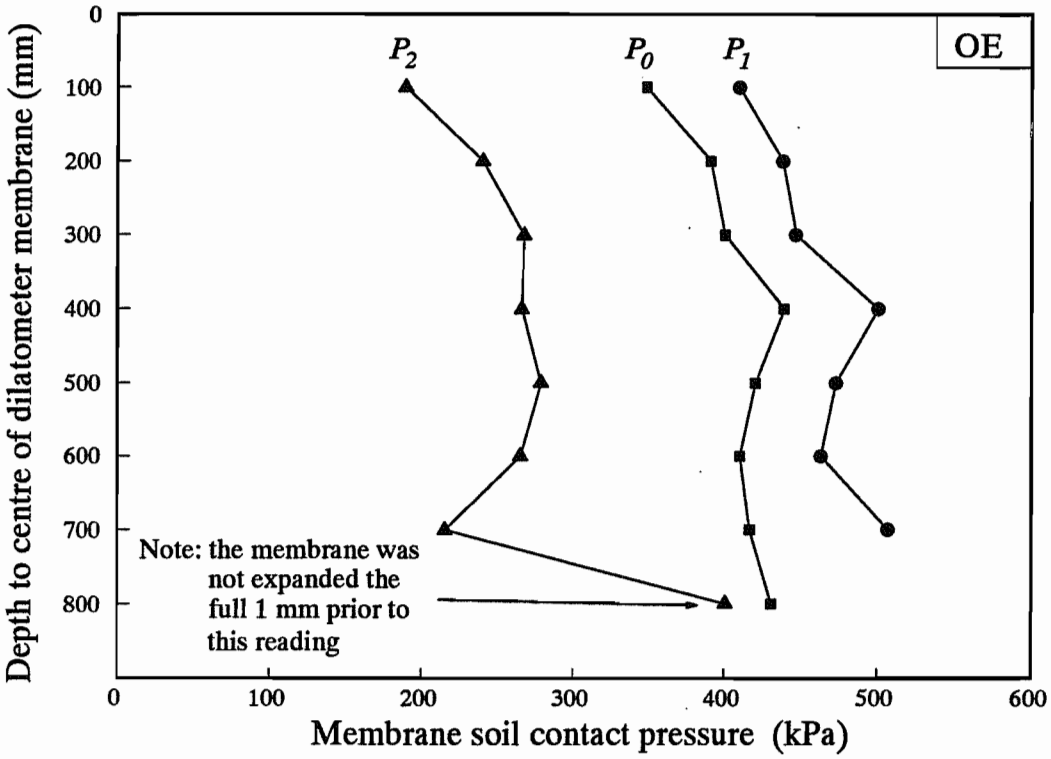


Figure 5.1 Dilatometer readings in clay bed OE.

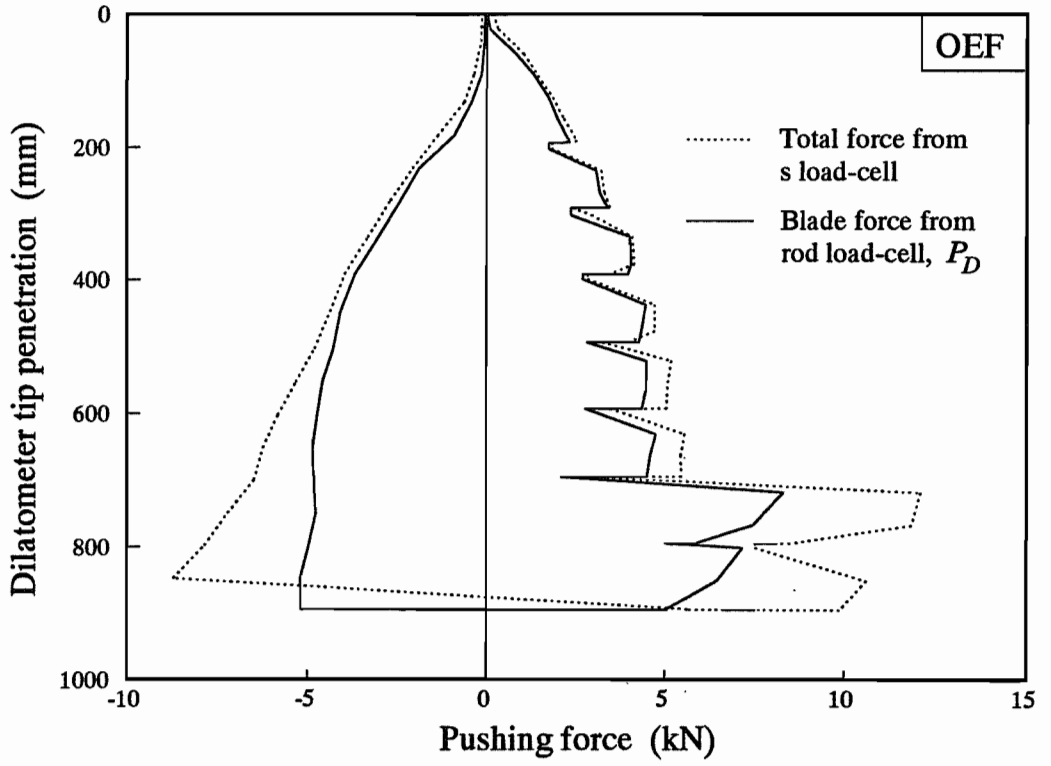


Figure 5.2 Thrust during penetration of clay bed OEF.

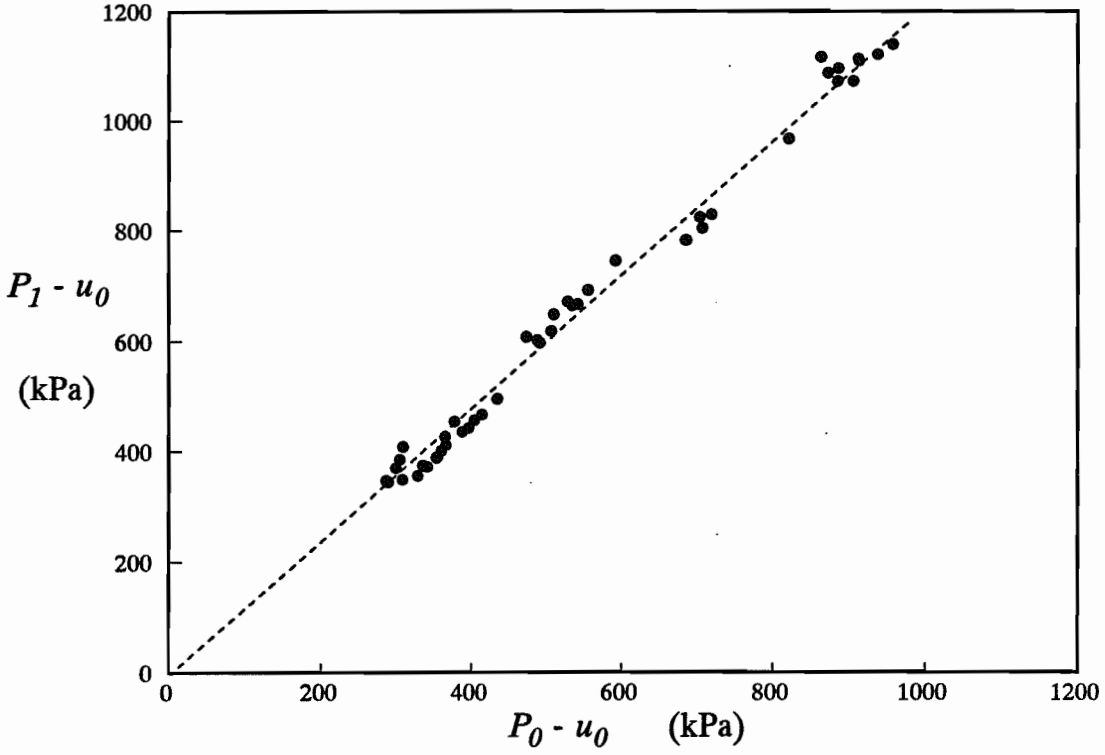


Figure 5.3 Comparison of dilatometer P_0 and P_1 readings.

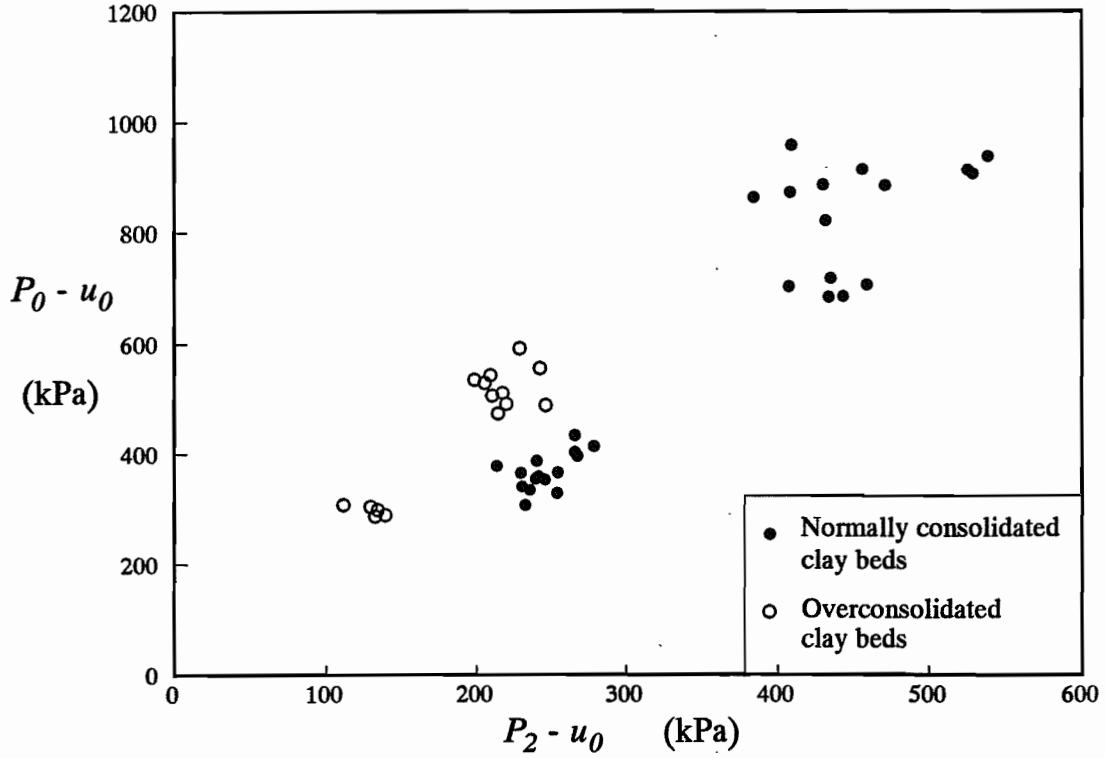


Figure 5.4 Comparison of dilatometer P_0 and P_2 readings.

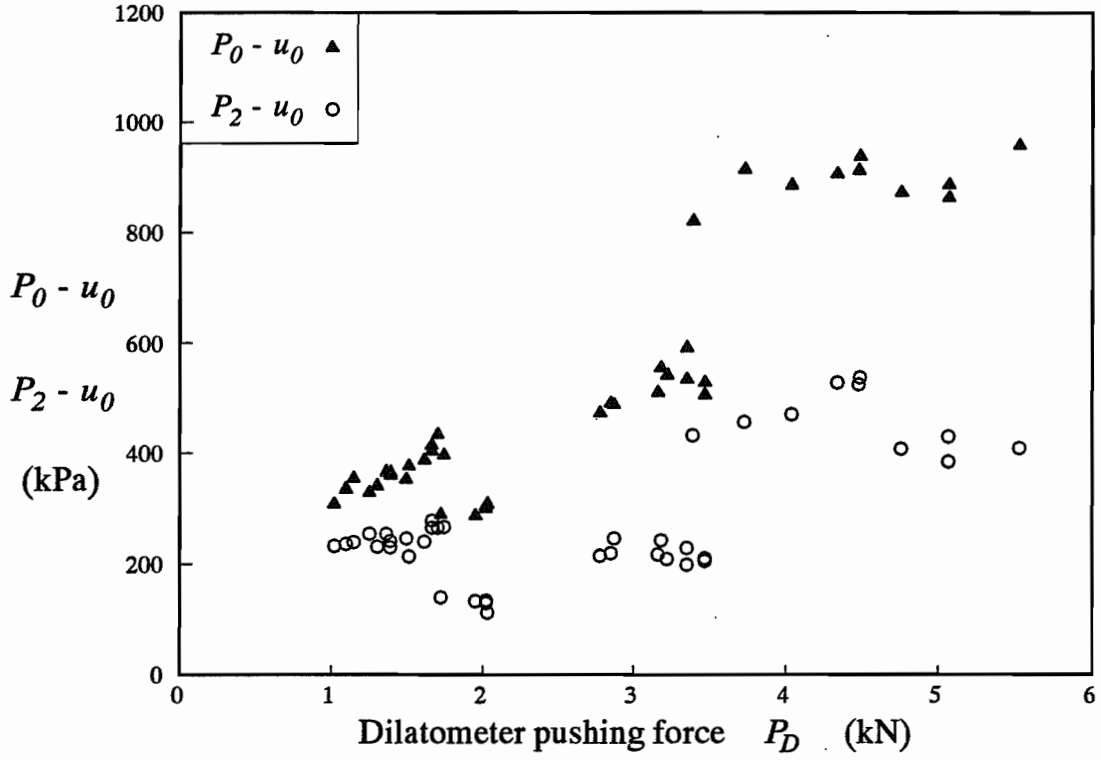


Figure 5.5 Comparison of P_0 and P_2 with the dilatometer thrust.

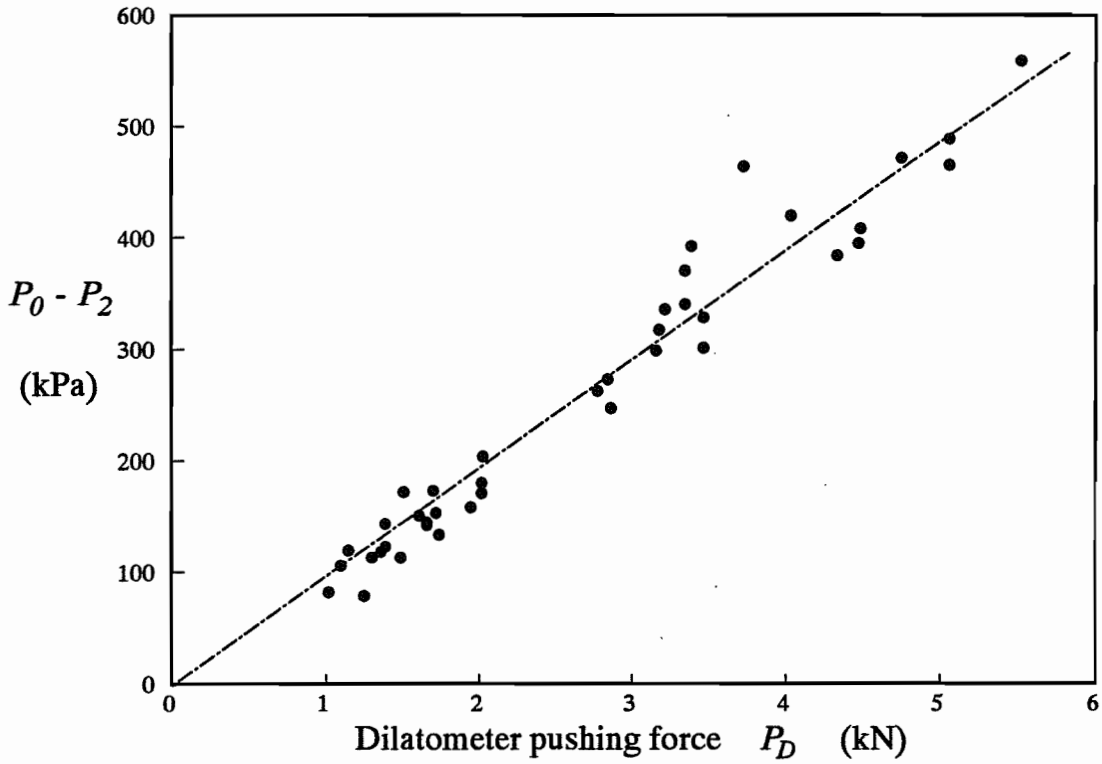


Figure 5.6 Comparison of P_0 - P_2 with the dilatometer thrust.

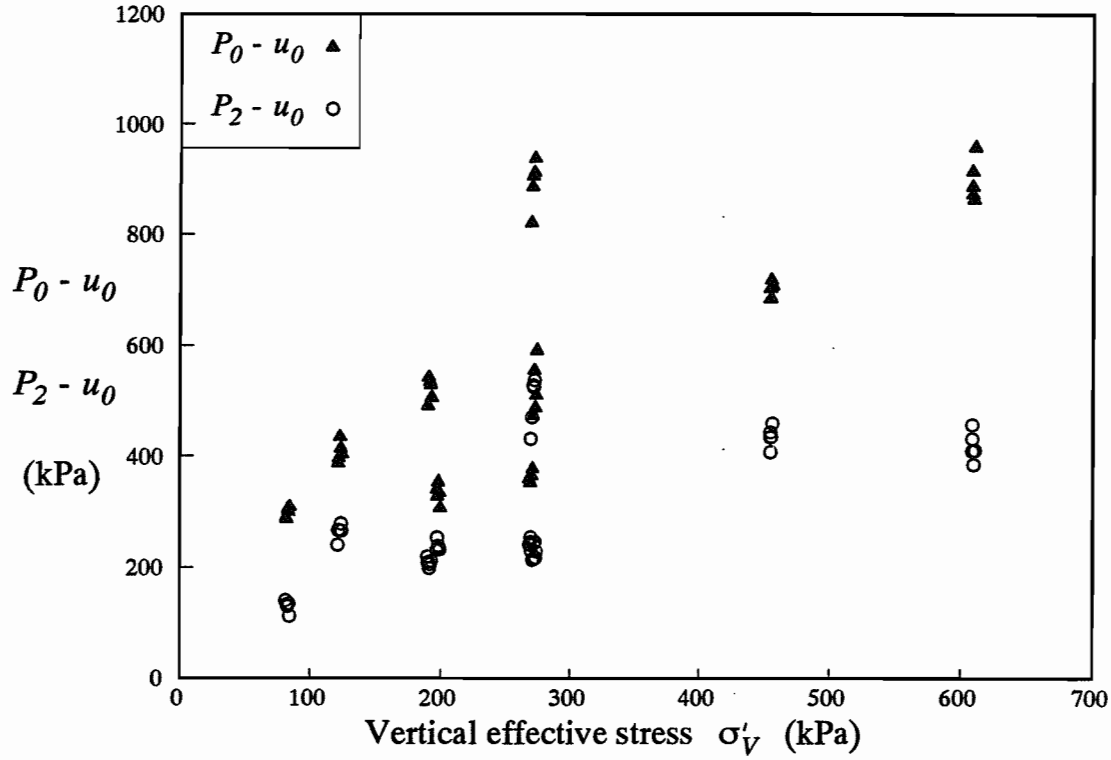


Figure 5.7 P_0 and P_2 versus the vertical effective stress.

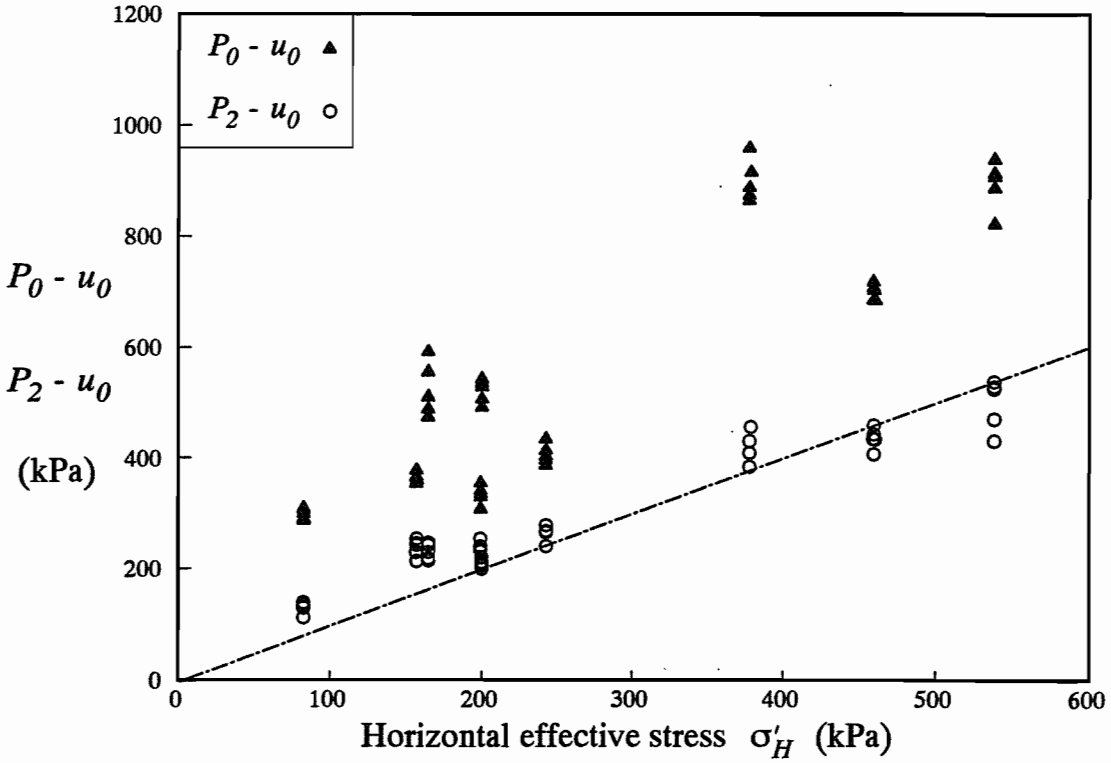


Figure 5.8 P_0 and P_2 versus the horizontal effective stress.

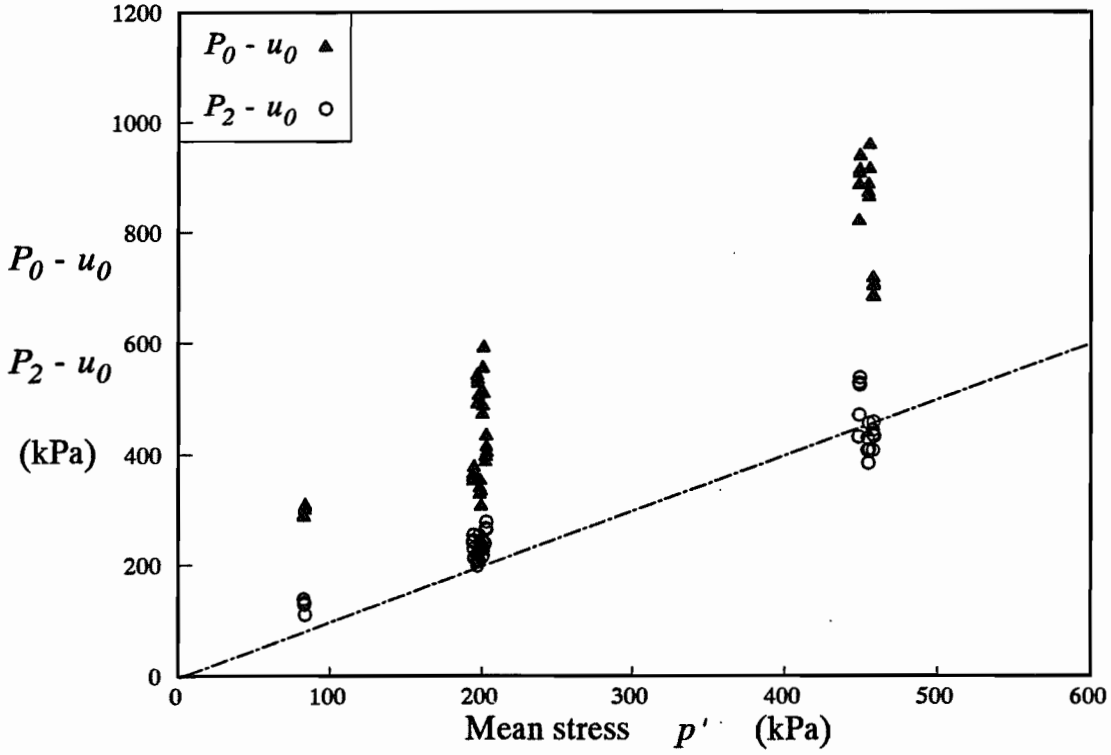


Figure 5.9 P_0 and P_2 versus the mean effective stress.

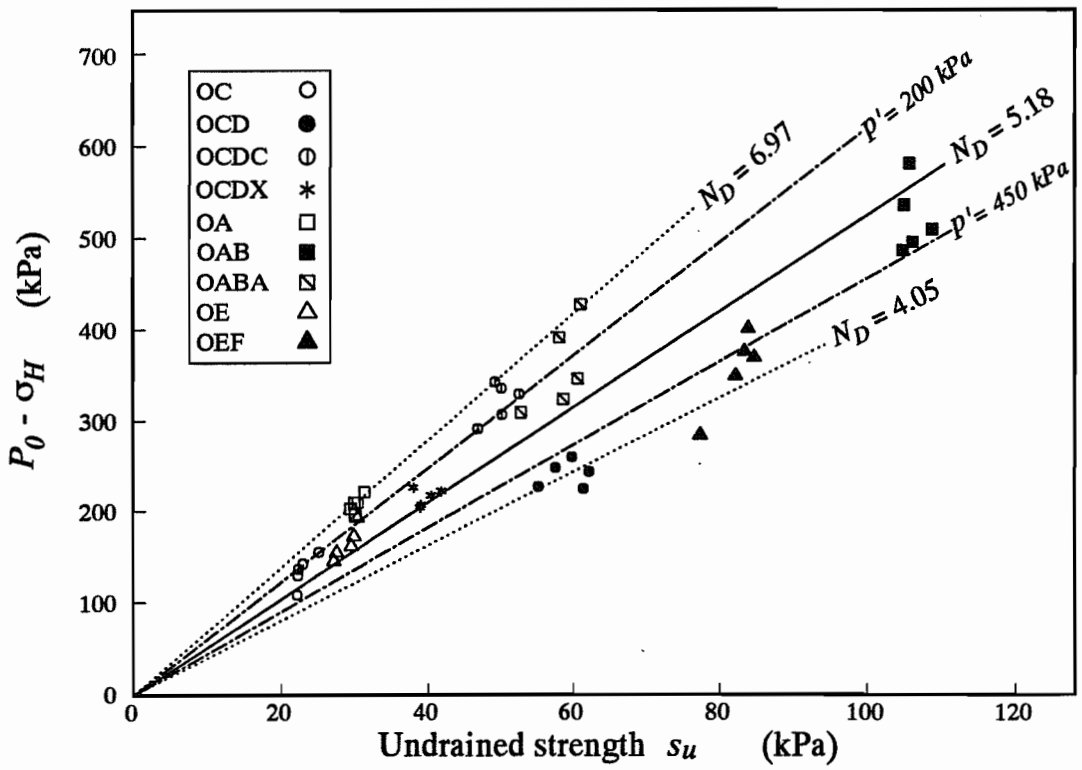


Figure 5.10 P_0 - σ_H versus the undrained strength.

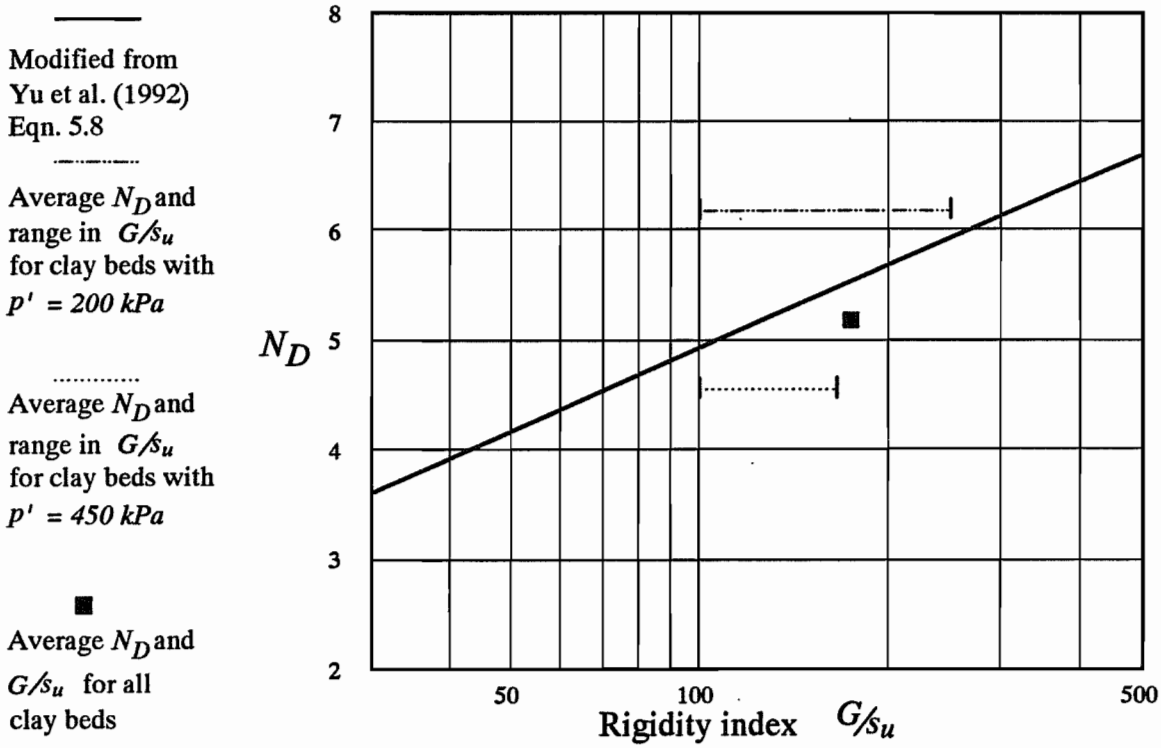


Figure 5.11 Experimental and numerical relationship between the rigidity index and the dilatometer factor, N_D.

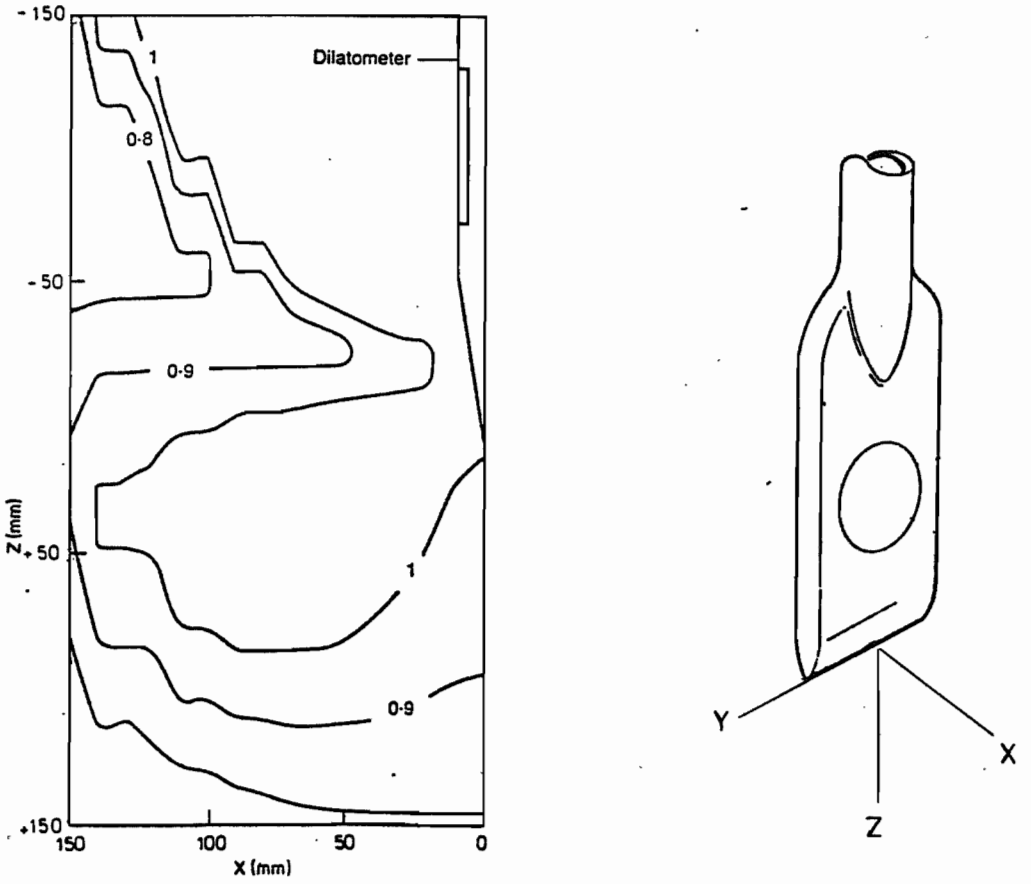


Figure 5.12 Numerical prediction of the stress ratios around a dilatometer, Finno (1993).

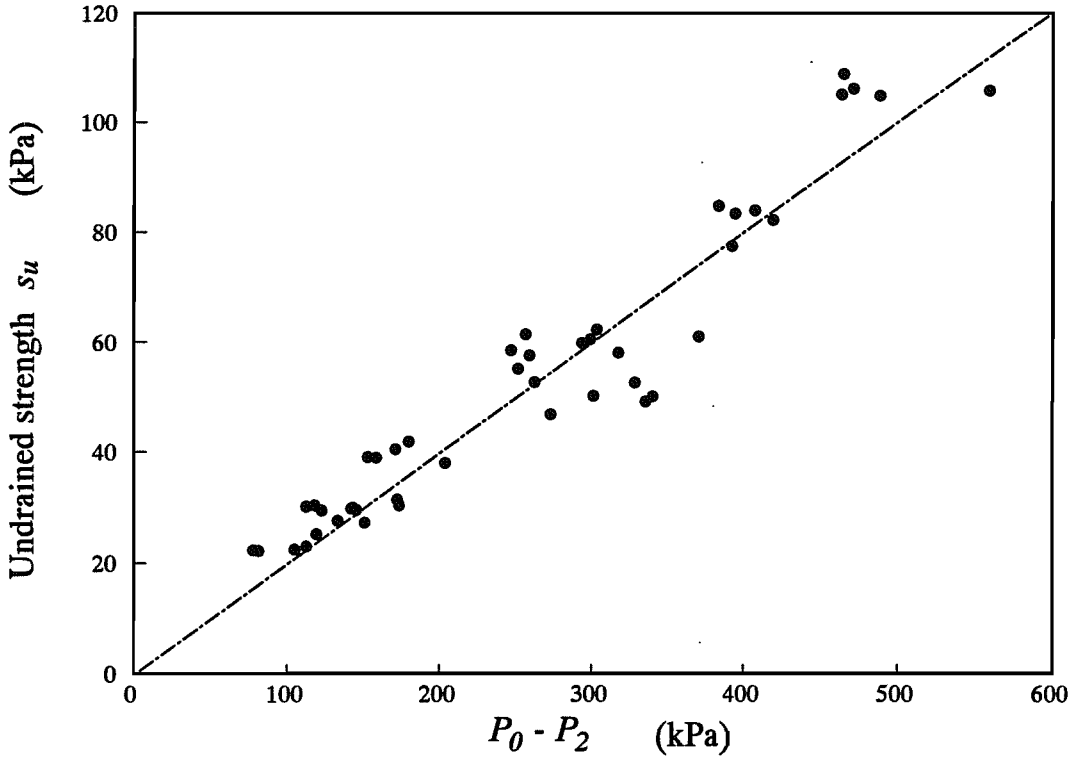


Figure 5.13 P_0 - P_2 versus the undrained strength.

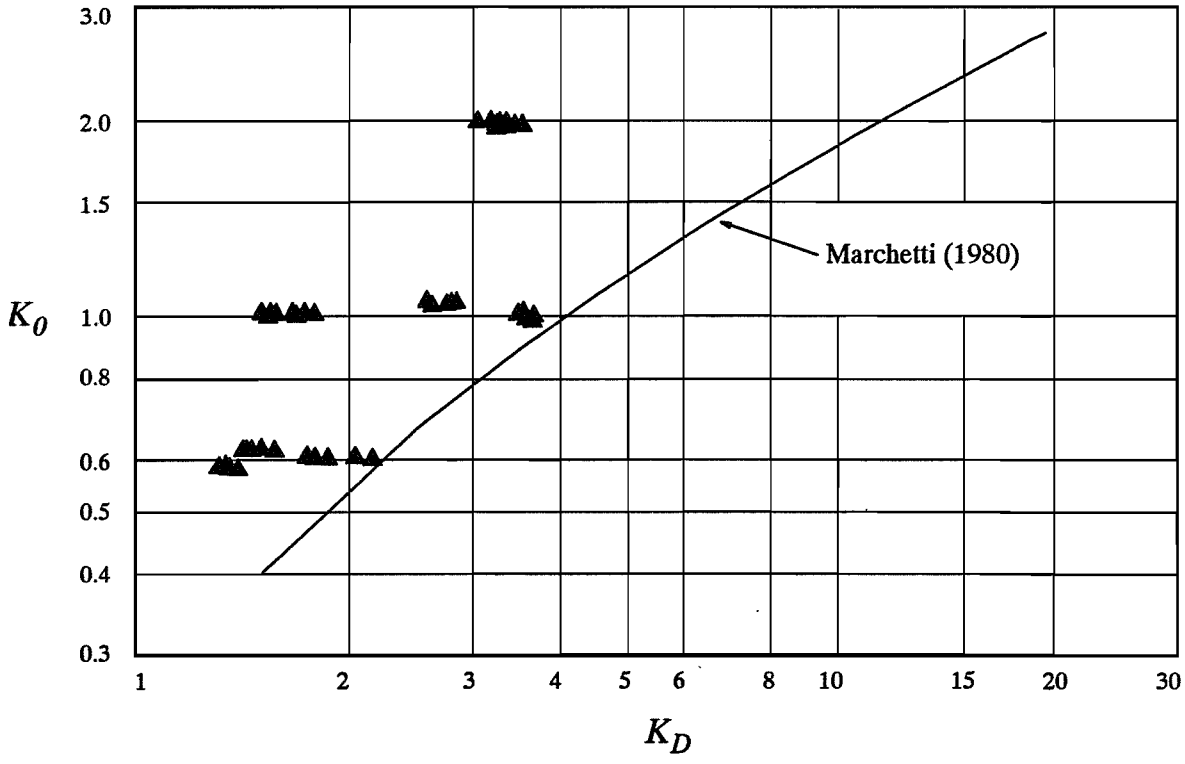


Figure 5.14 Experimental K_0 and K_D in comparison with Marchetti (1980).

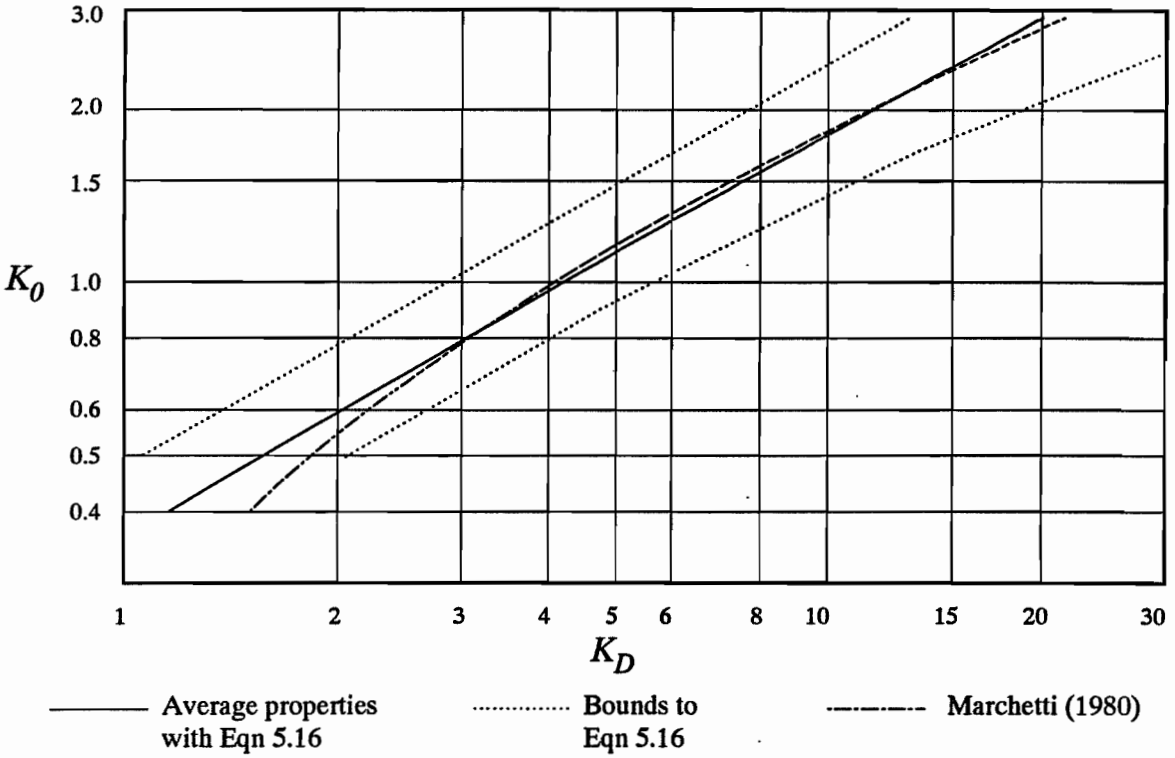


Figure 5.15 Comparison of experimental-empirical correlation (Eqn 5.16) and Marchetti (1980).

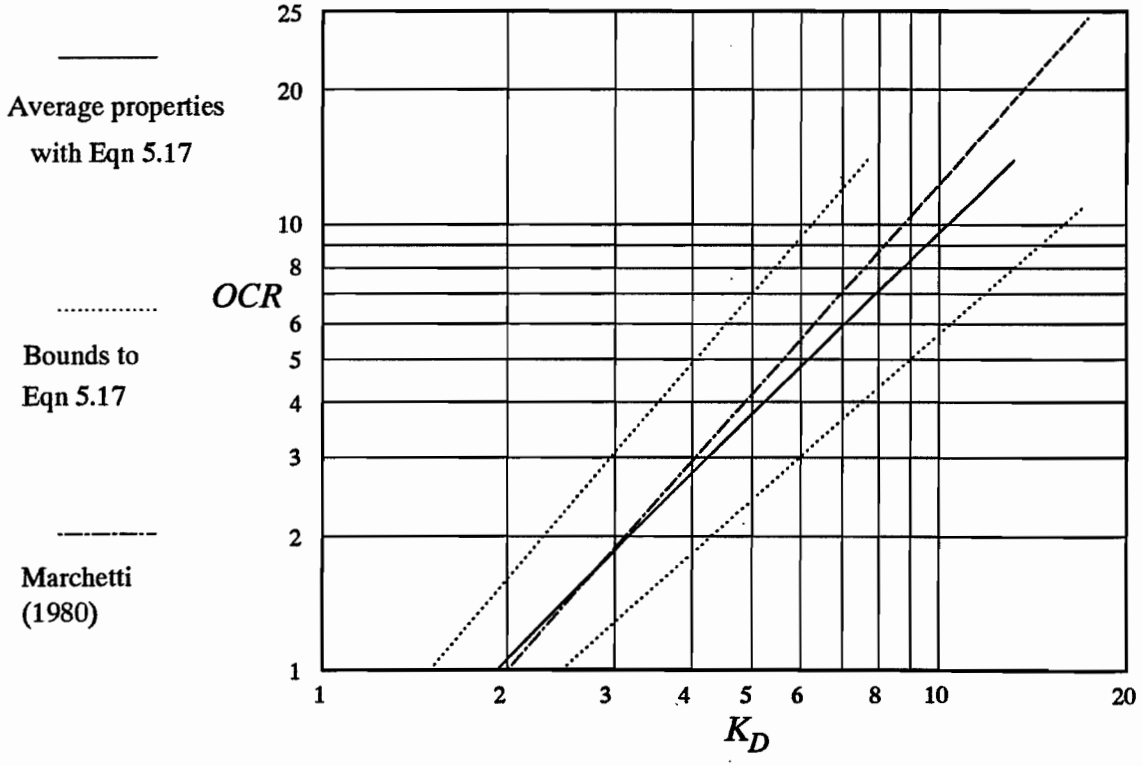


Figure 5.16 Comparison of experimental-empirical correlation (Eqn 5.17) and Marchetti (1980).

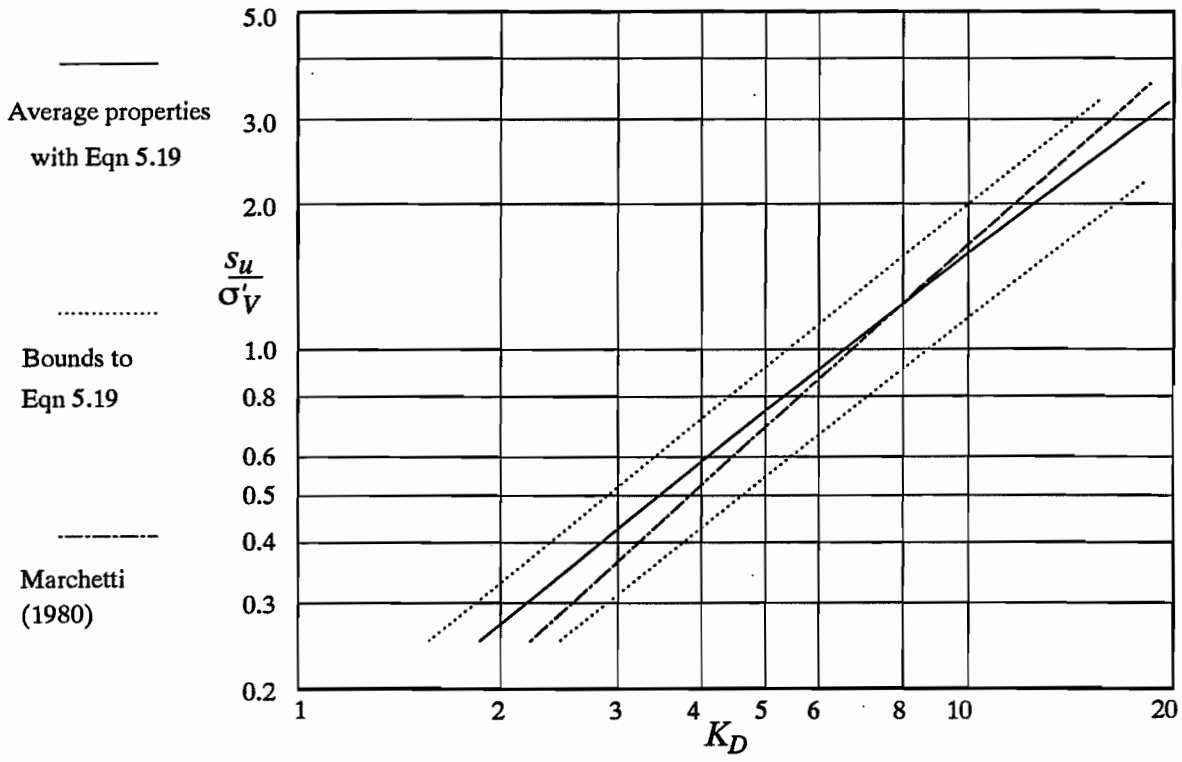


Figure 5.17 Comparison of experimental-empirical correlation (Eqn 5.19) and Marchetti (1980).

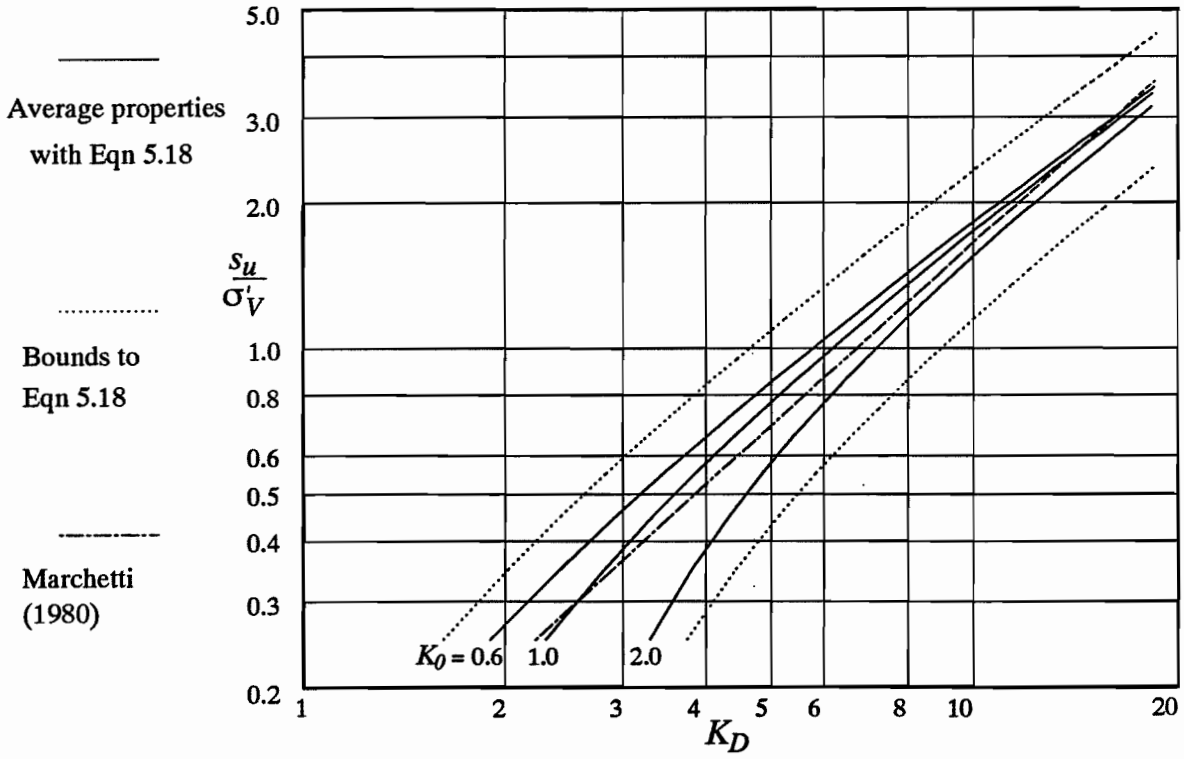


Figure 5.18 Comparison of experimental-empirical correlation (Eqn 5.18) and Marchetti (1980)

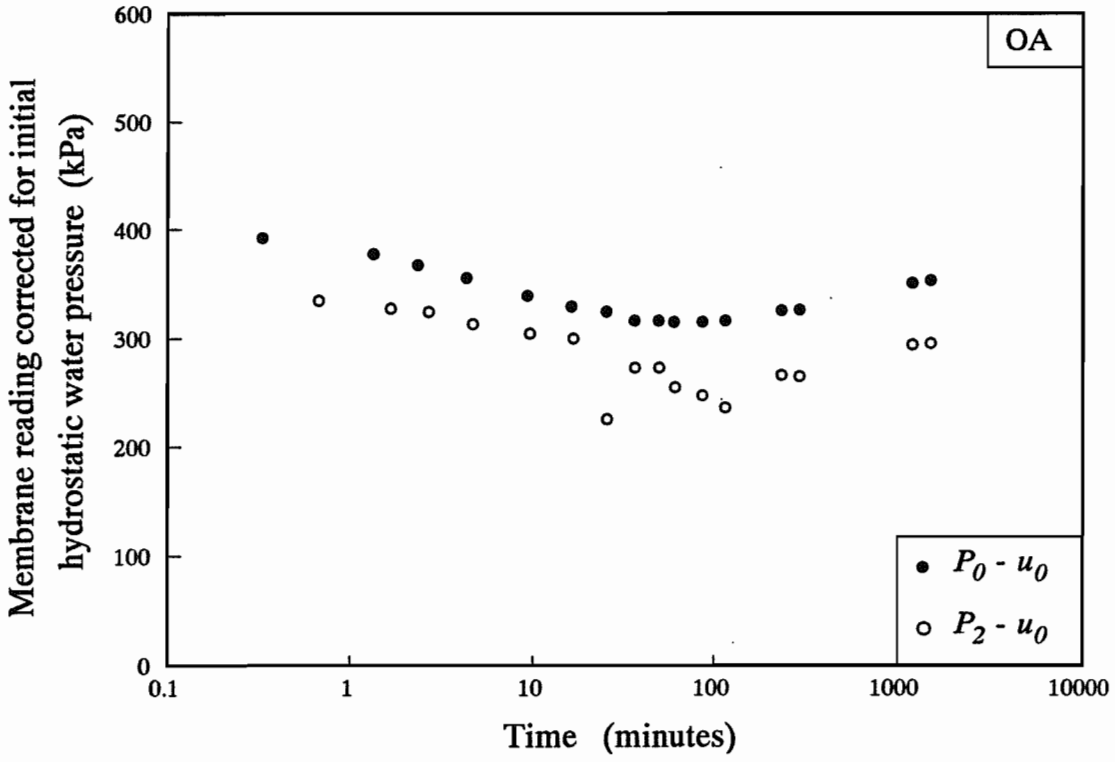


Figure 5.19 Results of P_0; P_2 dissipation test in clay bed OA.

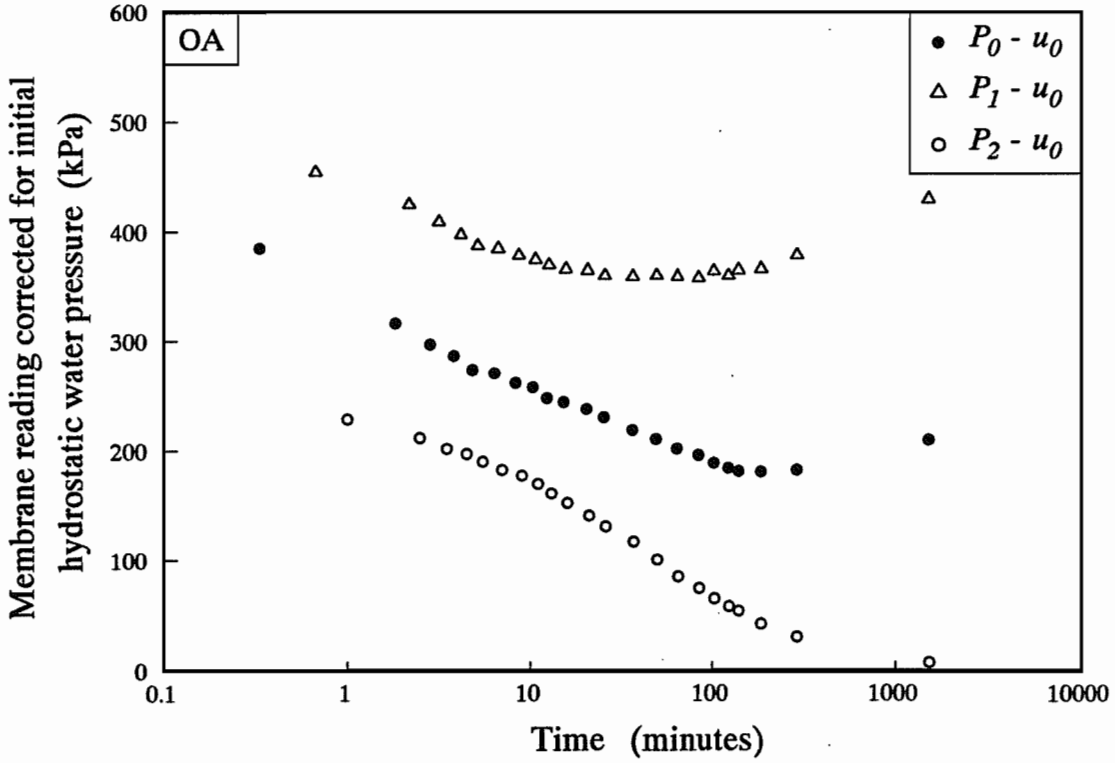


Figure 5.20 Results of P_0; P_1; P_2 test in clay bed OA.

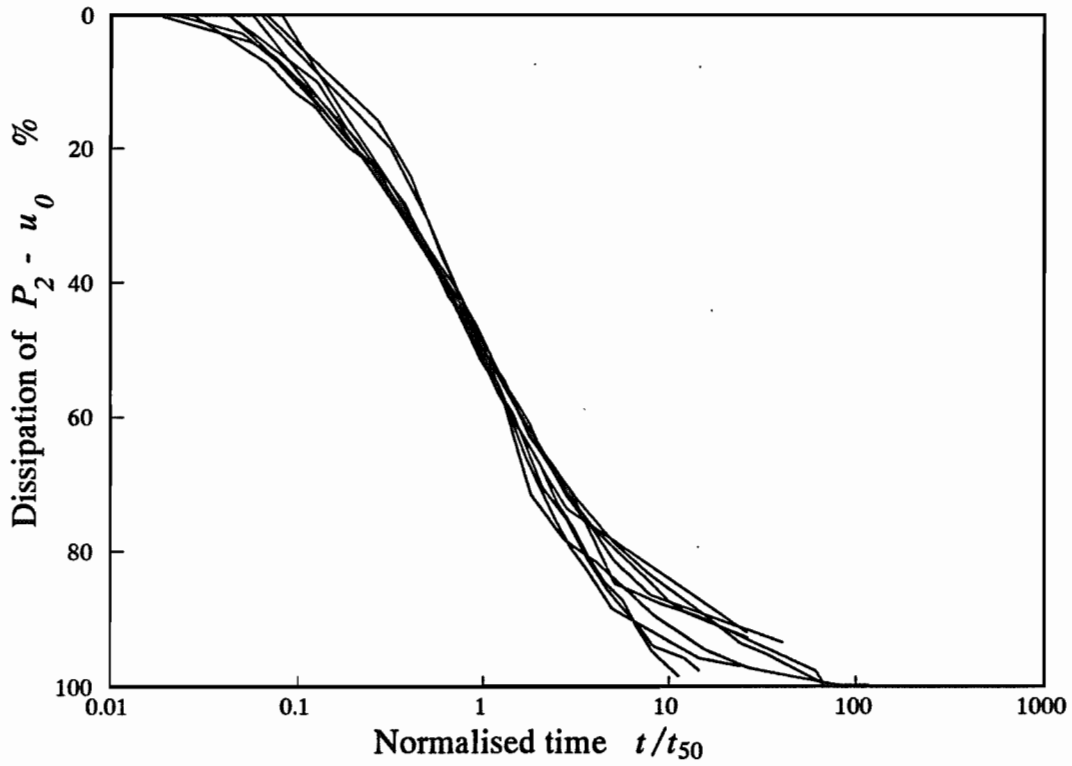


Figure 5.21 Normalised P_2 dissipation curves.

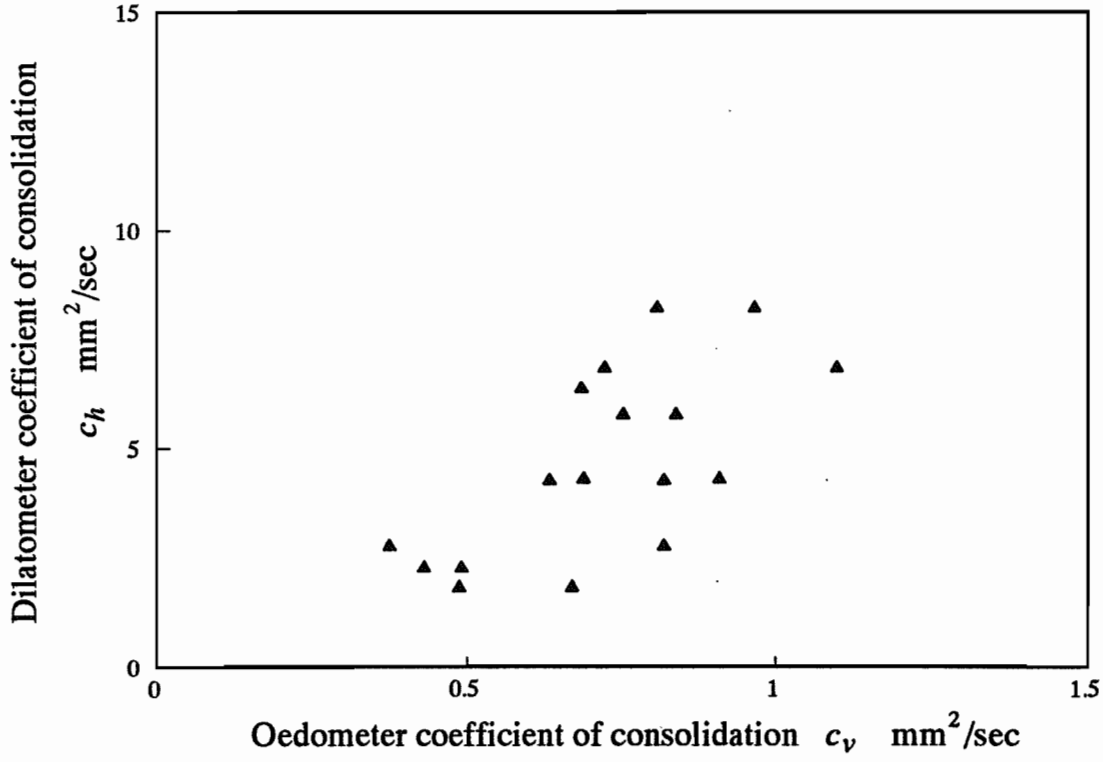


Figure 5.22 Coefficients of consolidation for each clay bed determined from dilatometer and oedometer tests.

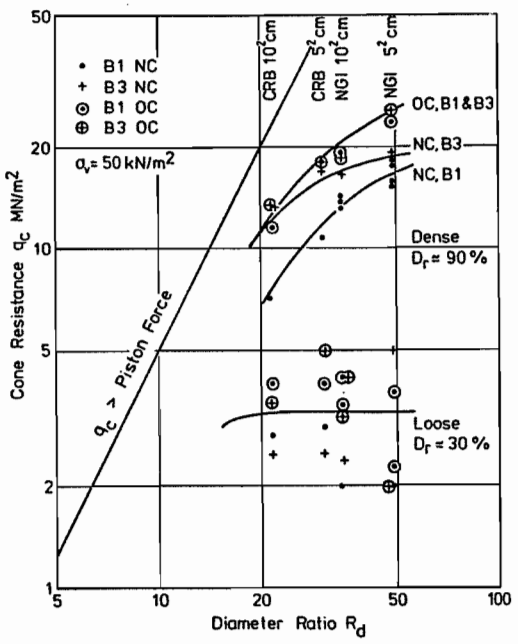


Figure 6.1 Chamber size effects on q_c, Parkin & Lunne (1982)

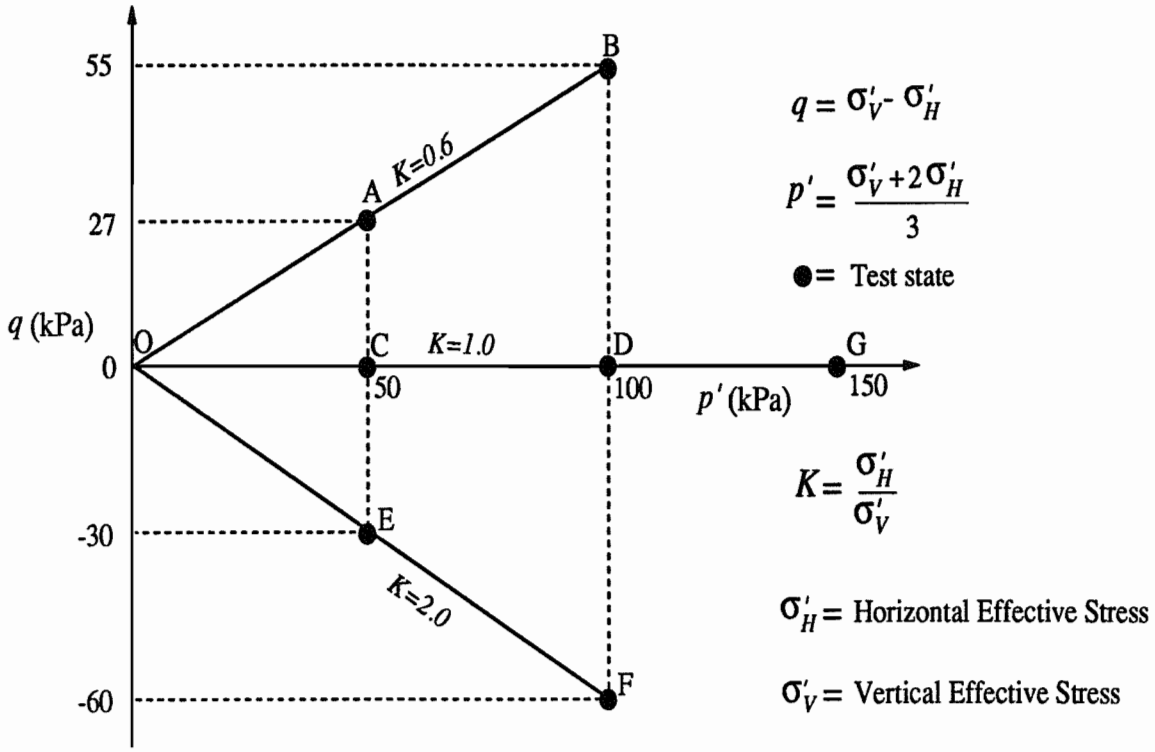


Figure 6.2 Stress states for dilatometer tests in sand.

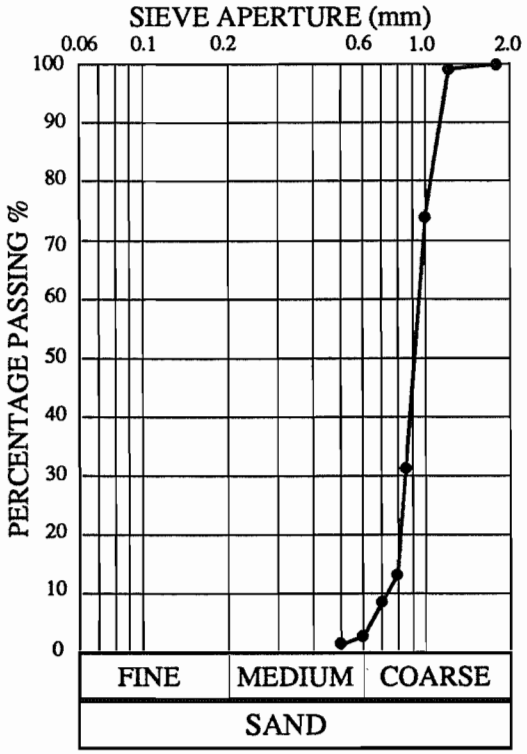


Figure 6.3 Grading analysis for Leighton Buzzard sand.

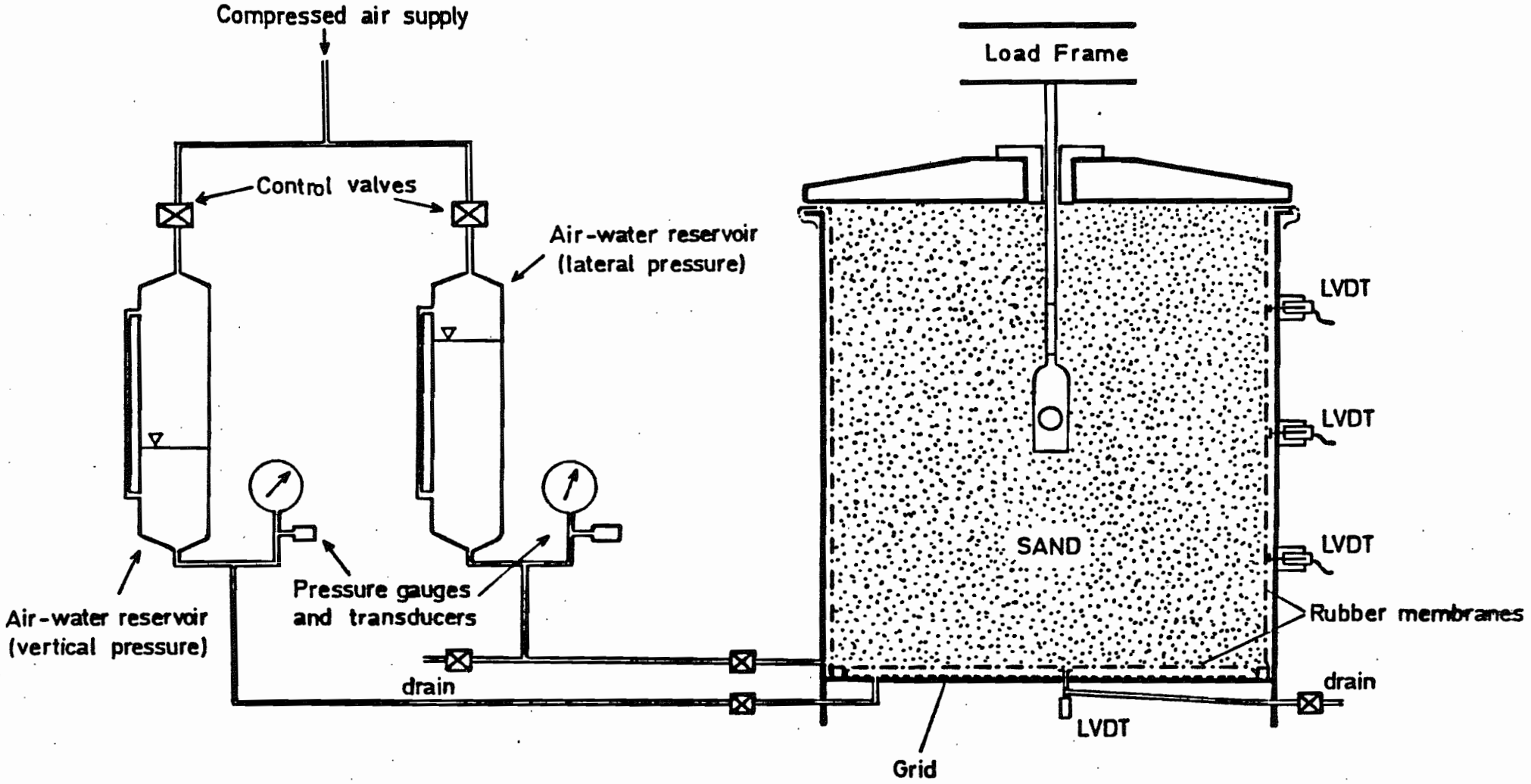


Figure 6.4 Oxford University calibration chamber for sand.

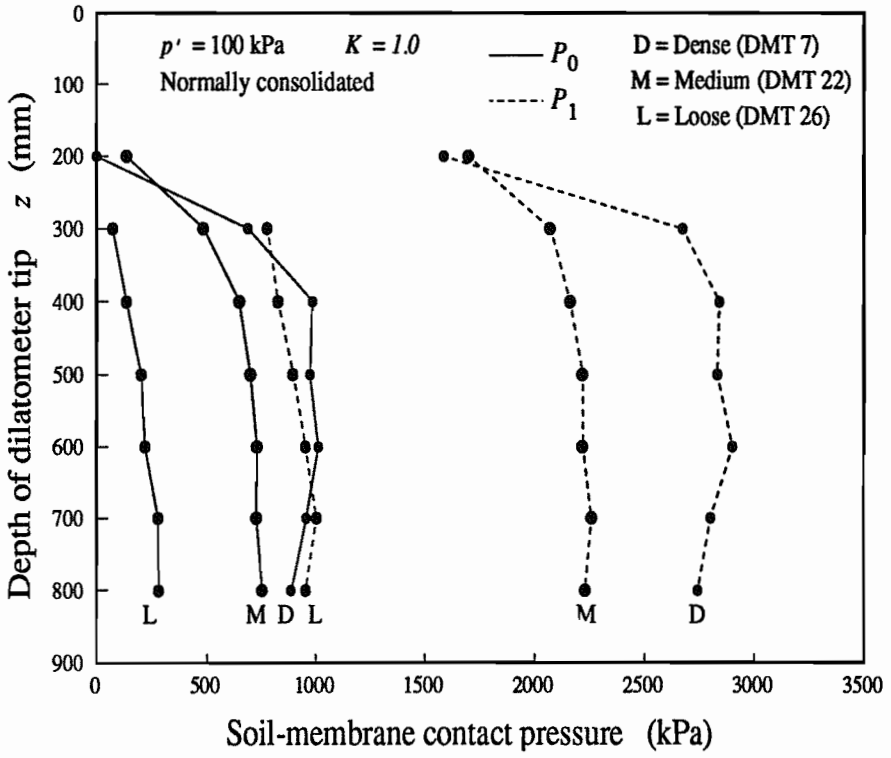


Figure 6.5 P_0 and P_1 profiles in similarly stressed dense, medium and loose samples.

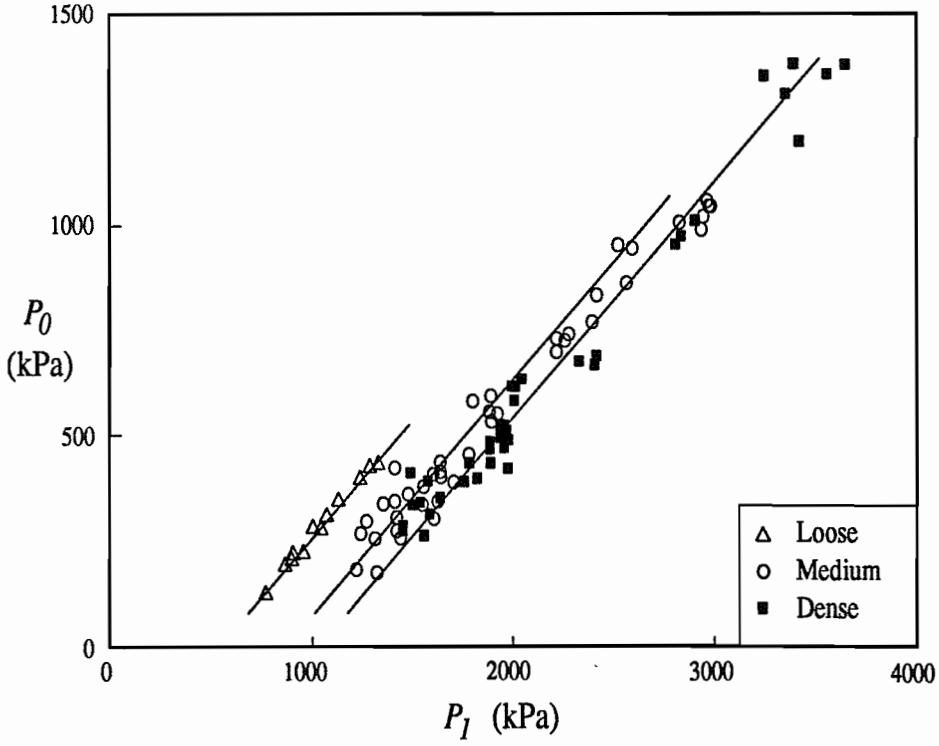


Figure 6.6 P_0 versus P_1.

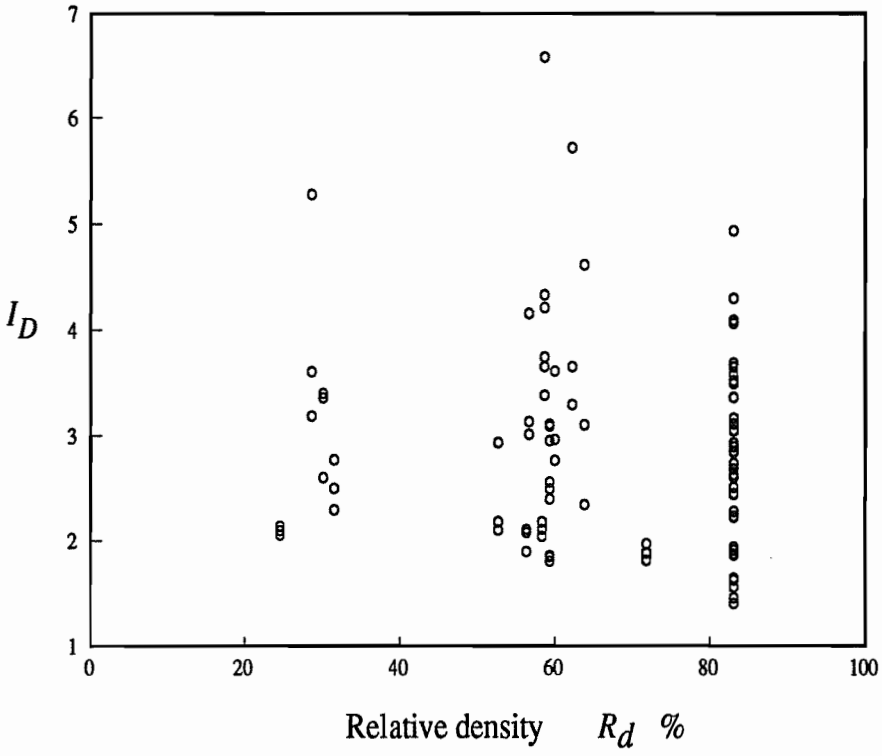


Figure 6.7 Material index I_D, versus relative density.

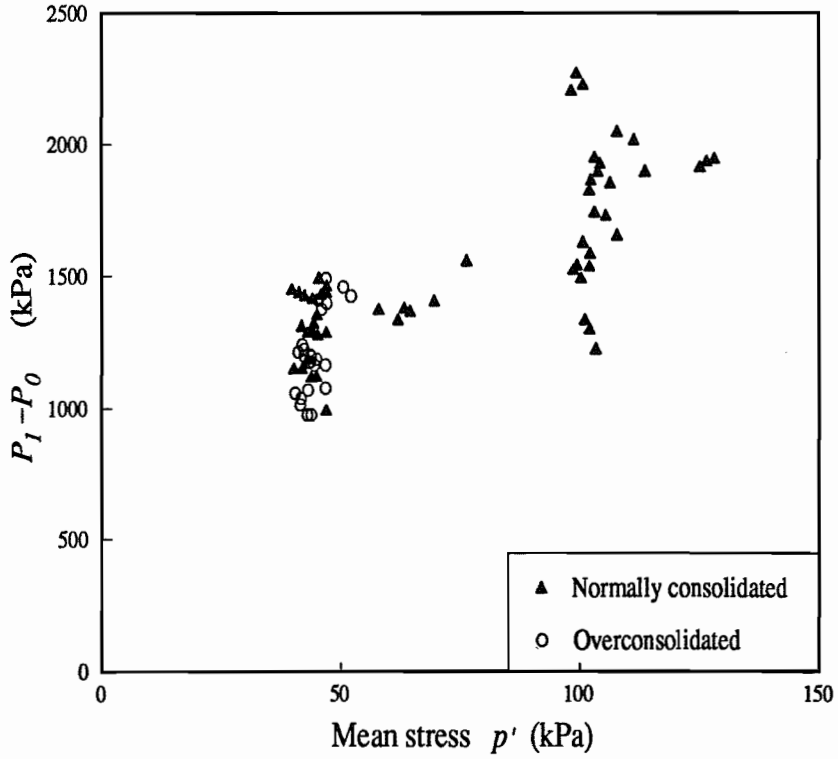


Figure 6.8 P_1-P_0 versus mean stress for dense and medium tests.

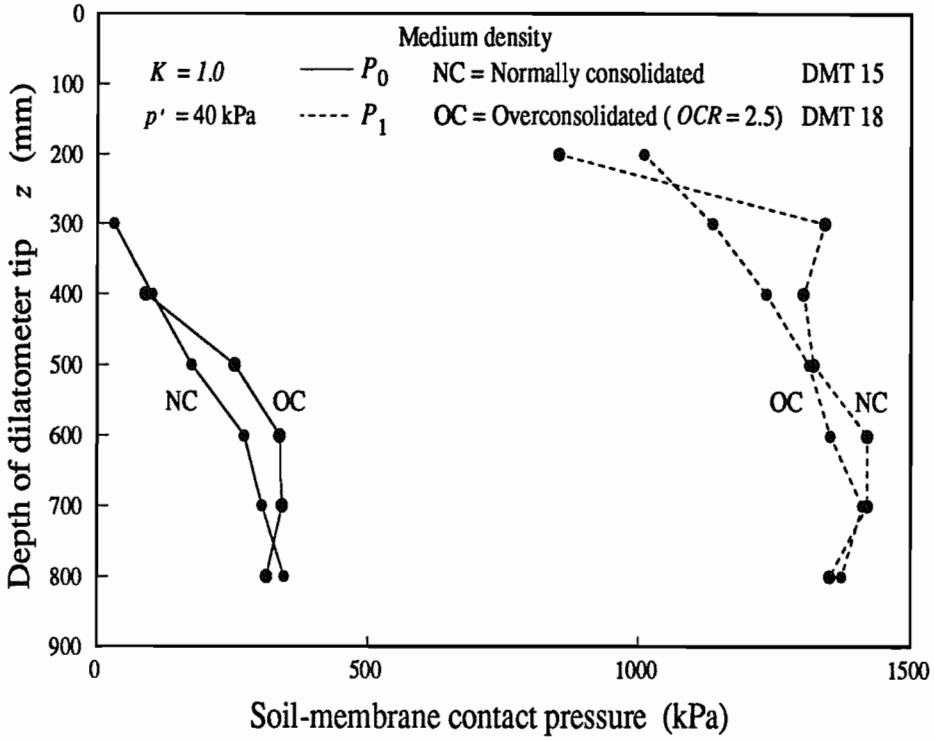


Figure 6.9 P_0 and P_1 profiles in similarly stressed medium density overconsolidated and normally consolidated samples.

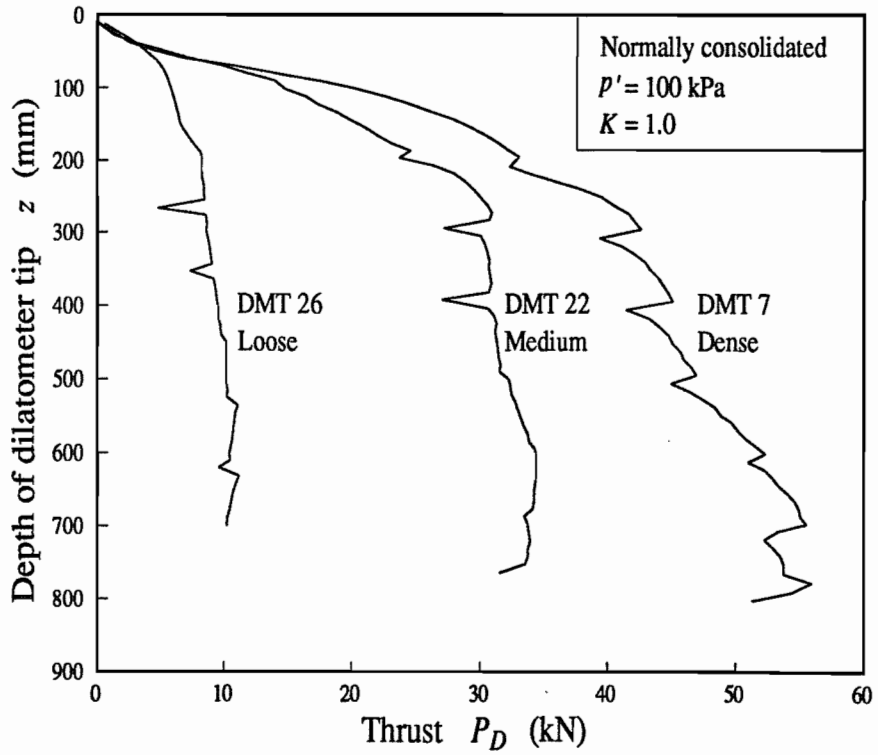


Figure 6.10 Penetration resistance for dilatometer soundings in dense, medium and loose samples.

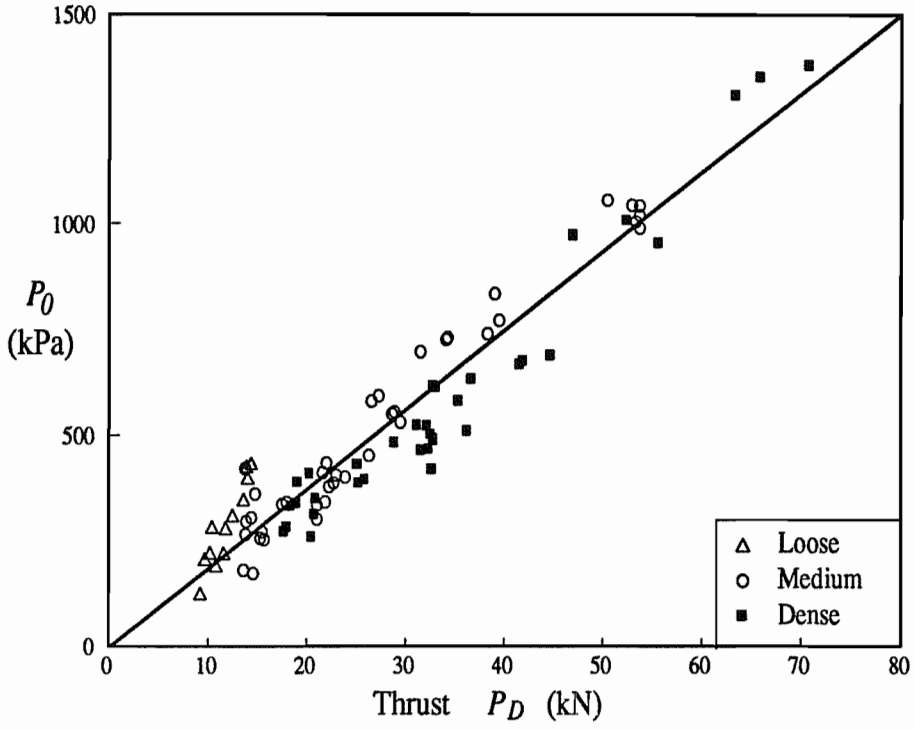


Figure 6.11 P_0 versus dilatometer thrust P_D.

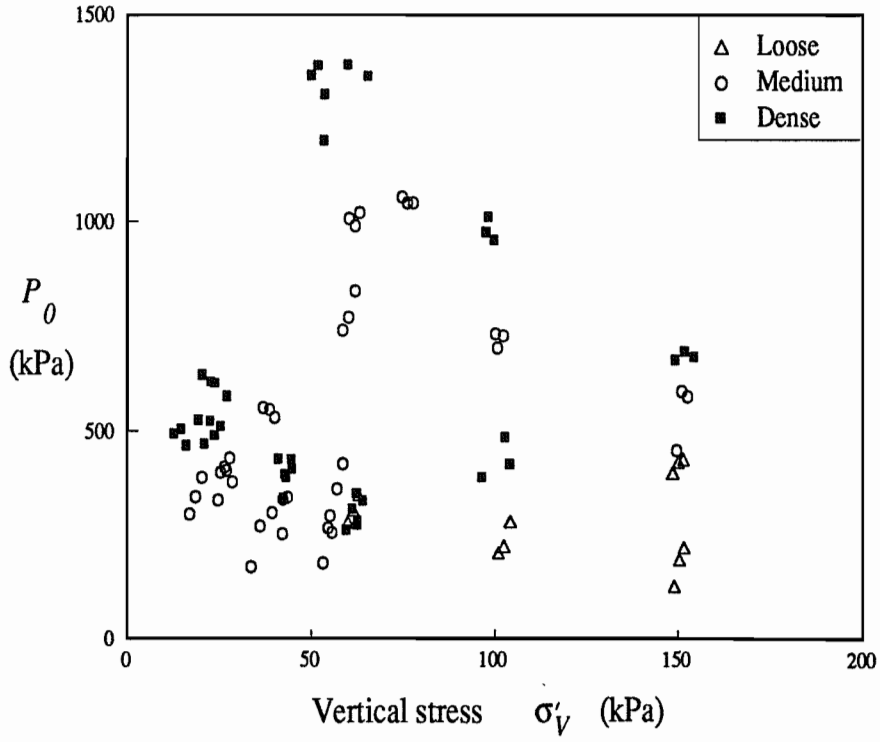


Figure 6.12 Dilatometer P_0 versus applied vertical stress.

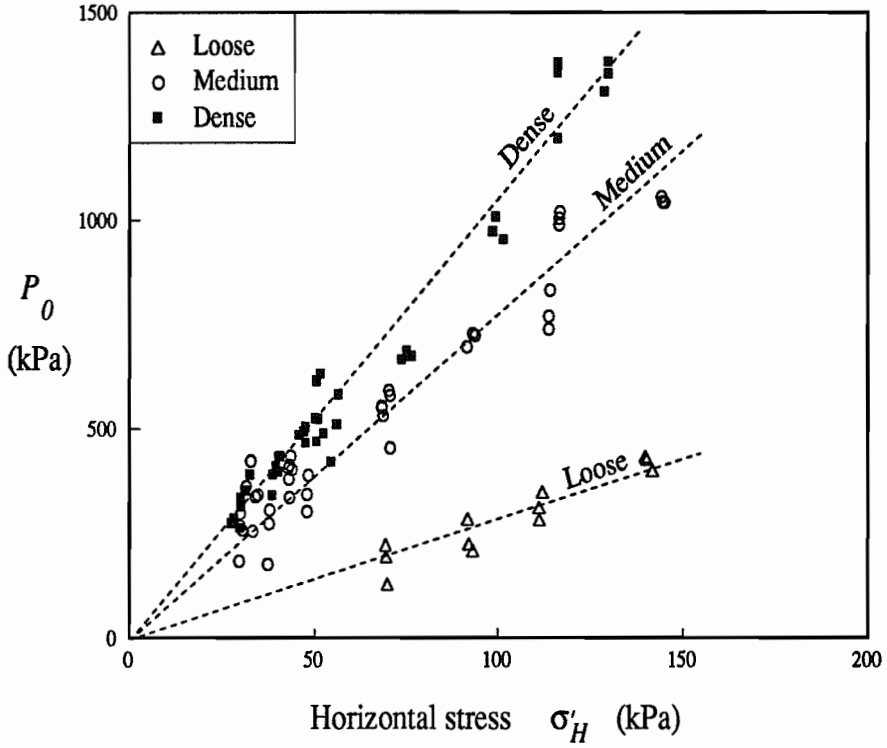


Figure 6.13 Dilatometer P_0 versus applied horizontal stress.

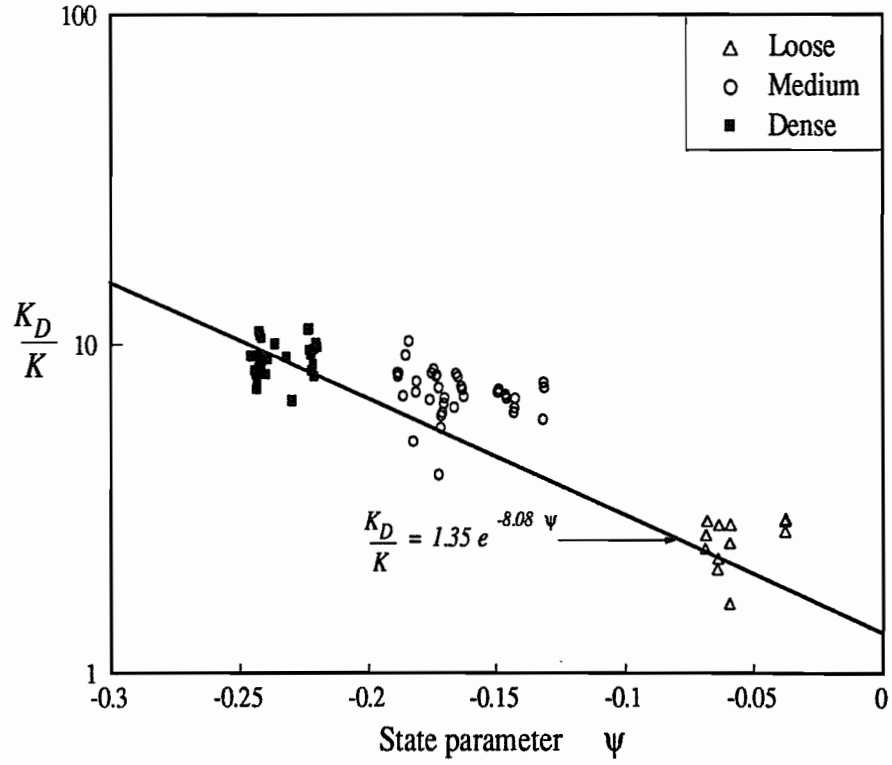


Figure 6.14 Amplification factor, K_D/K, versus state parameter, ψ.

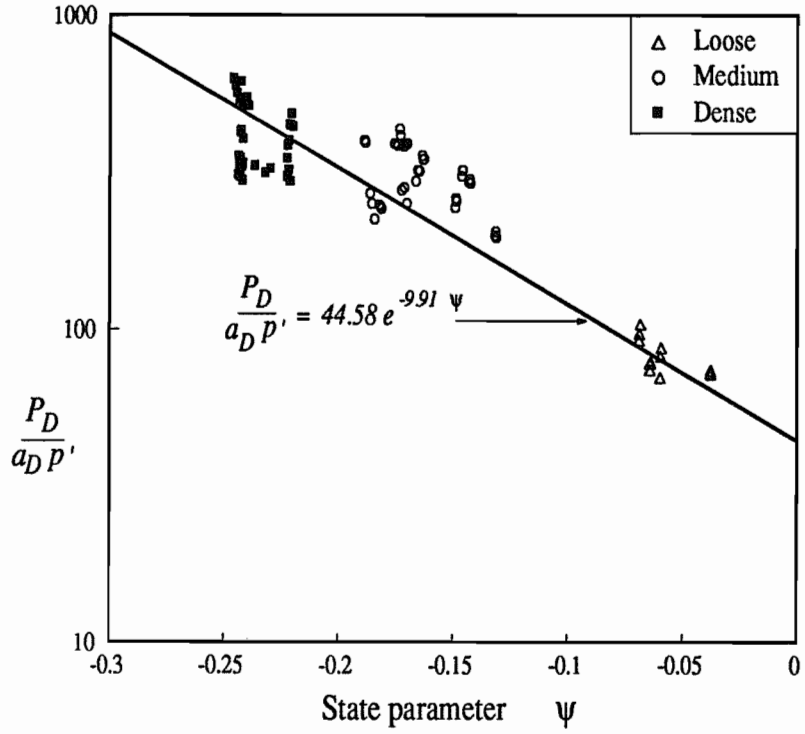


Figure 6.15 Normalised dilatometer bearing stress versus state parameter, ψ.

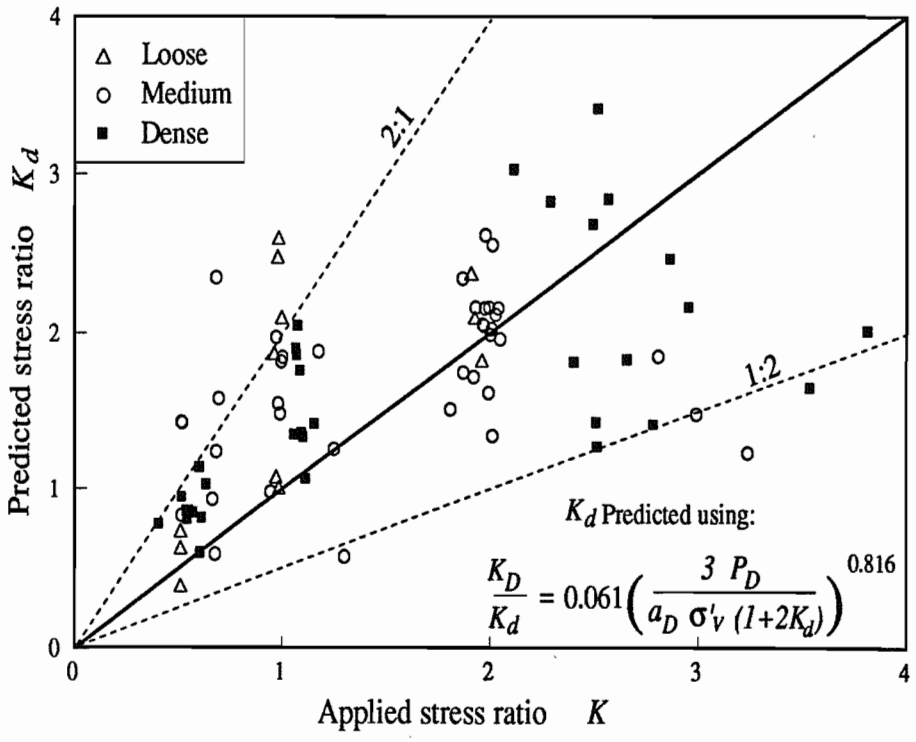


Figure 6.16 Predicted stress ratio, K_d, versus applied stress ratio.

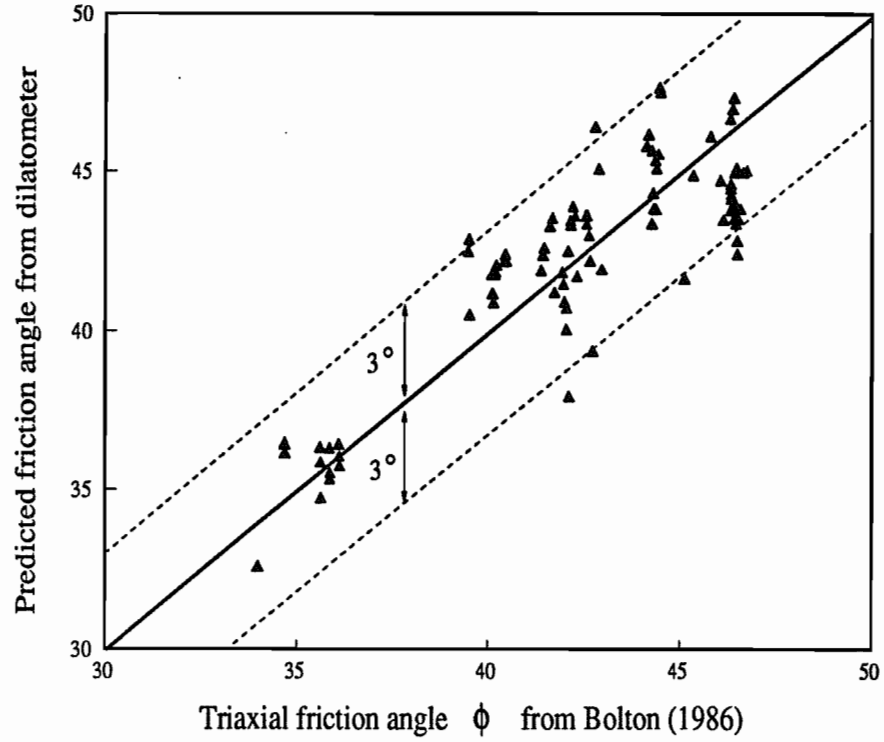


Figure 6.17 Predicted friction angle versus Bolton's friction angle.

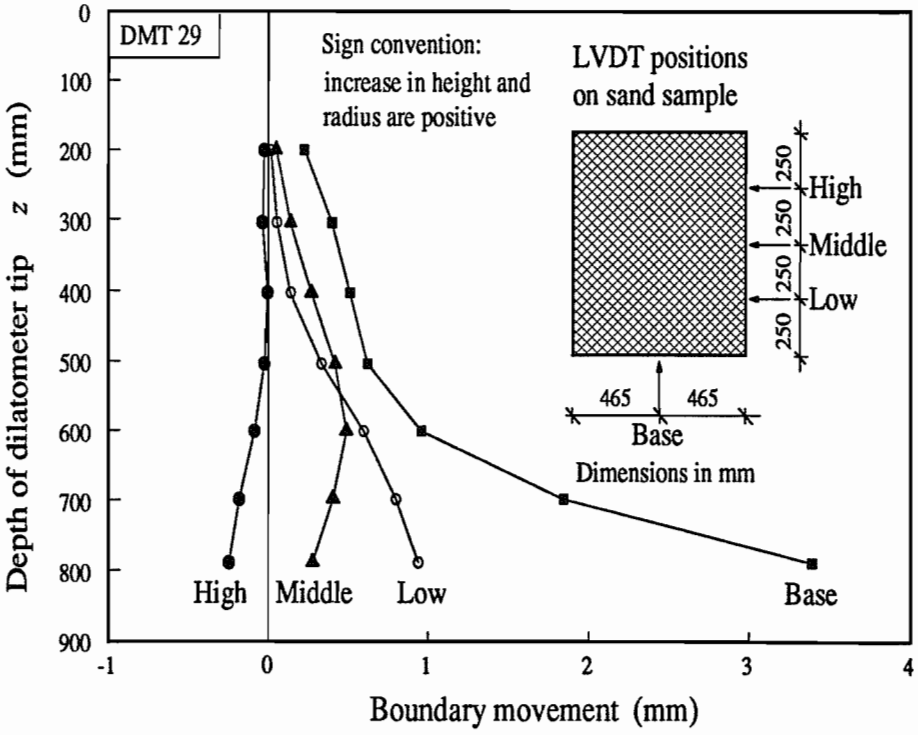


Figure 6.18 Boundary movements for medium sample, DMT 29.

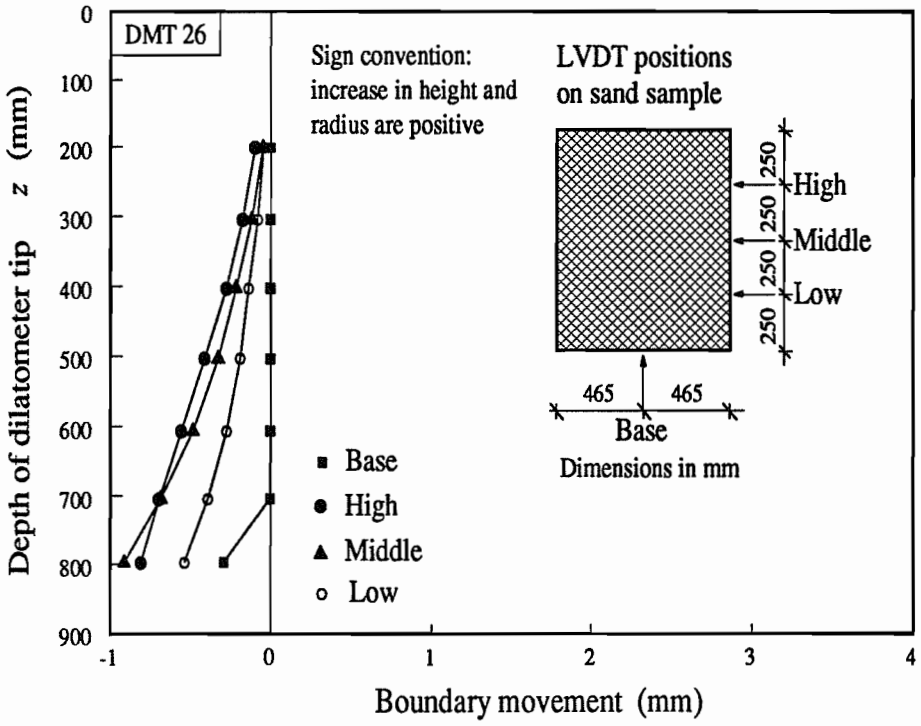


Figure 6.19 Boundary movements for loose sample, DMT 26.

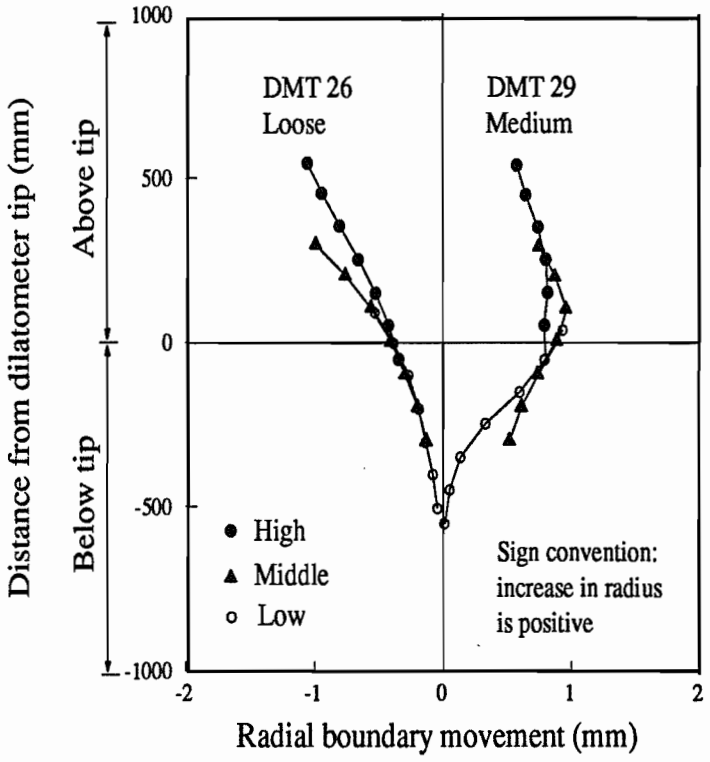


Figure 6.20 Inferred boundary movement profile in loose and medium tests.

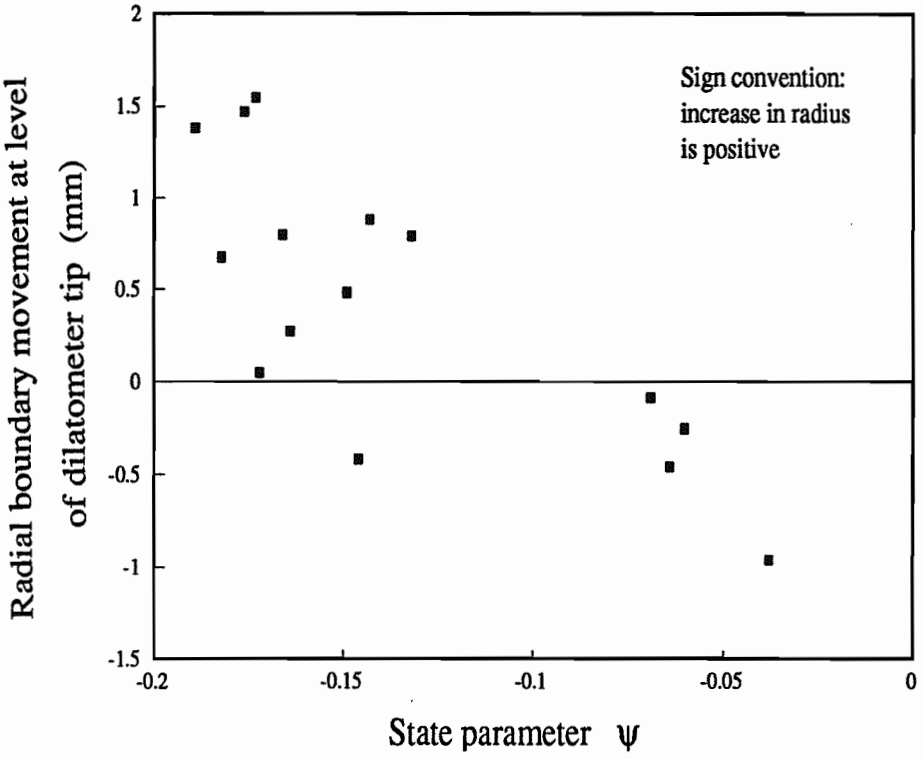


Figure 6.21 Radial boundary movement versus state parameter.

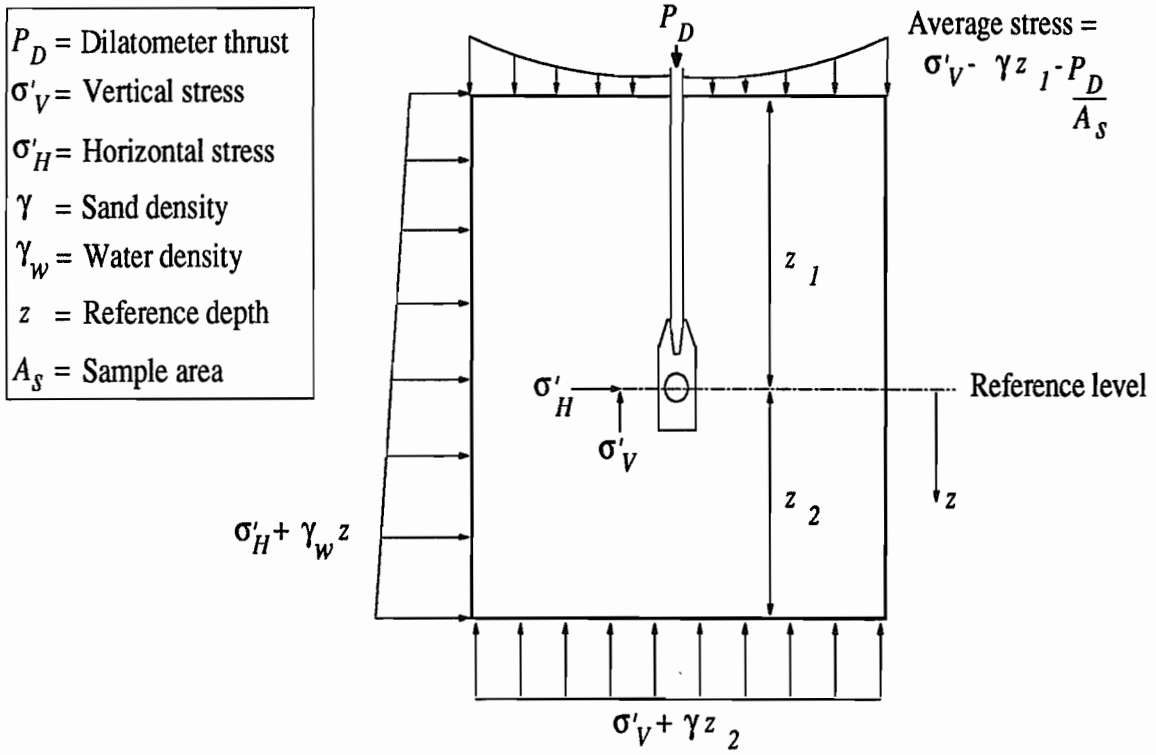


Figure 6.22 Equilibrium forces on sand sample inside calibration chamber.